Cyprus University of Technology

Faculty of Engineering and Technology

Engineering and Informatics

A probability control and statistical modeling study for the feasibility of large-scale implementation of Seebeck-Peltier modules in ship cladding

DOCTORAL DISSERTATION

PhD Candidate: **Ioannis P. Armenakis**

Academic Supervisor: **Prof. Sotirios Chatzis**

Academic Committee:
Prof. Sot. Chatzis CUT
Prof. Chr. Damianou CUT
Prof. Ioannis Prousalidis NTUA

2022

To my father,
who taught me that every ship has a soul,
to my mother
for making me what I am,
to my daughters
for giving me a reason to live,
and to Despina
for making my life worth living.

«Λίθος, ὃν ἀπεδοκίμασαν οἱ οἰκοδομοῦντες, οὗτος ἐγενήθη εἰς κεφαλὴν γωνίας»

Ψαλμός 117:22

«The stone the builders rejected, has become the cornerstone»

Psalm 117:22

List of relevant publications by the Author et al.

- **Armenakis Yiannis P., Chatzis Sotirios**, "Waste heat recovery and electrical power production on vessels by means of TEG arrays attached on the hull plates below the waterline" As presented in the ESTS 2019 International Conference, Washington USA, 15/08/2019.
- **Armenakis Yiannis P.,** "Exploitation of Waste Heat of Marine Diesel Engines using Seebeck Elements", International Journal of Innovative Research in Science, Engineering and Technology, Volume 11, Issue 7, July 2022, DOI:10.15680/IJIRSET.2022.1107002

Table of Contents

ABSTRACT

Regaining a part of the heat lost during industrial or commercial activities has become a modern Holy Grail quest ever since the 1st Industrial Revolution. Since energy in general and heat in particular, are both the strategic and financial support beam of modern society, a continuous scientific and technical struggle is constantly running towards the rationalization of energy usage and the minimization of its losses. To achieve the above, several technologies have been and are being developed. In this research, the installation of large-scale Thermoelectric (TEG) elements arrays onboard ships was be examined. This venture was attempted several times in the past with limited success due to the immense need of cooling the elements. The goal of this research was the investigation whether or not the recovery of waste heat would be possible by TEG, if effective cooling was possible by attaching them on the inner side of the vessel's hull plates. Towards this, several design approaches have been attempted, numerus simulations have been run, the international bibliography was thoroughly investigated, whilst architectural, structural, mechanical, and electrical data from an actual modern real, large vessel have been evaluated. What was proven to be extremely important was the statistical investigation of the impact of the vessel's routing during its regular voyages on the effectiveness of the system due to the seawater temperature alterations. Although a thorough study of the thermoelectric theory was the cornerstone of this research, it was proven to be a rather interdisciplinary task.

During the research, the need for extensive knowledge of thermodynamics, electrical power management, 2D and 3D CAD drawing, FEA and CFD analyses, MATLAB® SIMULINK®, PLC and SCADA as well as of several statistics software has been proven necessary.

The conclusions of this research indicated that the installation and effective operation of a system of TEG arrays cooled by their attachment on the inner side of the vessel's hull plates, is feasible. The simulations run, have shown that the amount of energy that can be recovered is quite significant and its financial benefit for the ship's operators is indeed impressive. The amount of energy recovered per square meter of arrays was calculated to be 92KWh per 24hrs, thus saving some 17,5 Kg of Diesel Oil which otherwise would have been burned in the vessel's Generator sets. This would save some 68 Kg of CO_2 let alone other GHGs otherwise diffused in the environment.

The conclusions of this research can hardly be considered as a fulfillment of the whole task. In the author's opinion, they are rather the starting point of further discussion and investigation regarding the technical approaches to be followed for the completion of the final goal which was from the very beginning the improvement of the effectiveness and the reduction of the eco-footprint of Marine transportation.

Keywords and Phrases: Seebeck, TEG, Hull plates, Exhaust gas, Waste Heat, Eco Footprint, Back-pressure,

CHAPTER 1: INTRODUCTION

Heat is the fundamental energy form since the beginning of human civilization. Man's efforts to exploit heat is lost back in centuries. Yet, since the first Industrial Revolution, heat becomes the moving power of society through the various inventions that changed the route of human history. Steam engines powered knitting machines to make dressing affordable, steam grain mills helped feed people, while trains and steamships made the world look smaller.

Energy was cheap at the time. Coal and oil were plenty and easily accessible from industrially developed countries, due to the much different than today's political conditions and coalitions. Yet it was soon understood that the power over fossil fuel energy sources would be synonymous with world domination. World Wars and numerous local conflicts broke and the need for energy sparing emerged imperative[1].

Together with the struggle to make the thermal engines of the early years more effective, several technologies were developed aiming to harvest the largest part possible of the heat escaping to the environment[2]. Heat is known to have what is commonly called an "entropic character" depicting its natural tendency to diffuse to (the colder) environment hence making its further use hard or even impossible[3].

The subject of the Ph.D. research is the examination of the probability to regain a significant part of the heat of the exhausted gases produced in large naval engines which is now wasted in the environment using a large-scale system of Seebeck module arrays mounted on the internal side of a vessels hull plates, below the waterline.

Today's marine internal combustion engines, although significantly improved the recent years, can barely use 45 to 50 % of the energy offered, the rest being wasted in the environment as dissipated heat[4]. Though exhaust gases are used for auxiliary uses[5]

after exiting the engine, they still carry a very important amount of energy when exiting the vessel's funnel[6]. A promising way for the further use of exhaust gas heat is the use of thermoelectric materials. These materials have the ability to convert directly the heat they receive into electricity, without the mediation of any intermediate mechanical means[7].

Thermoelectric technology is considered one of the three more rapidly developing in the world nowadays, following only LED and microprocessor technologies[8]. The use of Thermoelectric Generators (hereafter "TEG") is rapidly extended to several applications mainly having to do with energy supply in harsh environments such as satellite or waste heat recovery. As the power supplied per area unit and the degree of the temperature gradient between the hot and cold side of a typical TEG chip increases, the problem of sufficient cooling of the cold side becomes the most important of all, limiting its application to a significant degree. On ships where the heat waste is still vast, this problem was not solved yet, as the traditional approach of cooling the TEG chip by seawater demanded too much power, thus turning the use of TEG meaningless. The new technique examined by this Ph.D. research follows a different approach. Instead of leading the cooling media to the TEG chip being attached to the waste heat recovery surface, it leads the heat media (namely the exhaust gases) to the TEG chips now being attached to the cool inner side of the wet plates of the vessel's hull[9]. Experiments have shown this approach to perform effectively so far[10], yet thorough research on the subject is being run.

A number of problems arose from this new approach:

- The exhaust gas back pressure built has to be carefully calculated as it would lead to increased emissions, increased fuel consumption, and will negatively affect the engine's performance. This of course depends solely on the topology of the ducting system to be chosen, the size[11] of the ducting network, and on its structural characteristics.
- The exhaust Gas Dew Point consideration and neutralization of the Sulphuric content of the gases is necessary.

- Matching the Load through plc control (when and if this is possible) is required.
- Inverting the power from DC to AC, when required[12].

In this dissertation, a thorough theoretical approach to the Seebeck phenomenon will be presented as well as all the issues and subjects of the research will be discussed. Several technical details having to do with thermodynamics and fluid dynamics will also be examined to the extent that the engineers to implement the system in real-life applications become prepared to fully comprehend it. The basic question of the research will be approached here on a theoretical basis in conjunction with the feasible experimental and practical approach. The problems arising from the initial concept of the application will be presented and proposals on their possible solutions will be discussed. It has to be stressed at this point, that the elaboration of a general solution for the implementation of the proposed technology in every vessel is impossible and out of the scope of this dissertation. This dissertation aims to estimate the feasibility of the application of this technology and to highlight the issues to be taken into consideration upon implementation in a real-world vessel.

Adequate knowledge of differential analysis, basic thermodynamics, fluid dynamics, technical drawing, and Finite Elements Analysis is rather prerequisite for the reader of this dissertation.

The Autor wishes to express his gratitude to several people for their support during this research:

1. Prof. John Prousalidis, head of the Laboratory Unit of Marine Electrotechnical Applications, School of Naval Architecture and Marine Engineering, National Technical University of Athens, for his relentless concern and vital importance suggestions,
2. Dr. Yiannis Kokkarakis, Gen. Technical Director, Bureau Veritas Greece, for his overall mentoring.
3. Dr. Nikos Trilizas, I&F Manager, Bureau Veritas Greece, for making me part of the Marine community of Piraeus.

4. Dr. Panos Zachariades, Gen. Technical Director, Atlantic Bulk Carrier Management Ltd, who embraced the idea and supplied all the necessary data from the Company's fleet.
5. Mr. Nikos Frangakis, Superintendent Chief Engineer Atlantic Bulk Carrier Management Ltd for his real world, "line of fire" technical support.
6. Mr. Nasos Biniaris, Marine Engineer, School of Naval Architecture and Marine Engineering, National Technical University of Athens, for his assistance in catching up with contemporary computing methods.

The whole project would not be feasible without the encouragement, contribution, guidance, and continuous supervision of Dr. S. Chatzis of the Department of Electrical Engineering, Computer Engineering and Informatics at The Cyprus University of Technology.

Finally, the Author wishes to express his eternal thanks and gratitude to his family for their support, encouragement, and faith they showed, all the endless hours of absence. Embracing someone else's dream, at their own cost, takes love, and devotion. And that they have showed they had plenty of these five years.

CHAPTER 2: RELATED WORK

2.1 THE THERMOELECTRICAL PHENOMENA

The study of thermoelectrical phenomena started in 1822 when the German physicist *Thomas Johan Seebeck (1770-1831)* in his article ‘’The Magnetic Polarization of Metals and Ores Produced by Temperature Difference (Magnetische Polarisation der Metalle und Erze Durch Temperatur-Differenz)’’ which was published in the annual records of the Royal Prussian Academy of Sciences (*Königlich-Preußische Akademie der Wissenschaften)* mentioned that an electrical circuit consisted of two different metals causes a deflection of the magnetic compass needle if their contacts are kept in different temperatures. He also noted that the deflection of the compass needle is proportional to the temperature difference and the magnetic flux created changes for other pairs of metals at the same temperature difference. He experimented with several materials including some semiconductors and he listed them according to the product α*σ, where “σ” is the electrical conductivity of the material. The proportional factor “α” is known as the Seebeck Coefficient.

Seebeck thought that the thermal difference causes a magnetic field ignoring the electrical origin of the phenomenon. However, *Hans Oersted* (1777-1851) soon defined that the temperature difference causes electrical voltage which, in a closed circuit creates a current proportional to the temperature gradient. This current creates then the magnetic field observed by Seebeck. Oersted named the phenomenon “thermoelectrical” while Seebeck insisted on using the term “thermomagnetism”.

Twelve years later, in 1834, a French watchmaker *Jean Charles Athanase Peltier (1785-1845)* observed that the thermoelectric phenomenon could work vice-versa, that

is if a voltage is applied in a circuit consisted of two different metals in contact it creates a temperature gradient between the contacts.

Similarly to Seebeck, Peltier had not completely understood the nature of the phenomenon claiming that the Joule-Lenz law for the thermal results of current flow does not apply for low currents. Some four years later *Heinrich Friedrich Emil Lenz (1804-1865)* a Russian physicist of German origin born in Estonia, shown that it is actually an autonomous phenomenon causing the absorption or release of heat, additional to that of the Joule's heat and the heating or cooling of each bi-metal contact depends on the current's direction. A significant boost to the explanation of the two phenomena was given by *William Thomson -later 1st Baron Kelvin (1824-1907)* an Irish-Scottish mathematician and Physicist in 1851. Thomson gave a physically adequate explanation and foresaw the existence of a third phenomenon known today as the Thomson phenomenon. Finally, in two separate publications in 1905 and 1911, the German physicist *Edmund Altenkirch* has shown that the materials suitable for an efficient implementation of the thermoelectric phenomena should have a high Seebeck coefficient while having a low thermal conductivity and a high electrical conductivity[13]. These characteristics were consolidated in the "Z" parameter where:

$$Z_T = \frac{\sigma S^2 T}{k} \quad (1)$$

which contains the Seebeck coefficient S, thermal conductivity κ, electrical conductivity σ, and temperature T. The Z_T is called *the thermoelectric material's figure of merit* and is a dimensionless number.

By the late '30s, the development of synthetic semiconductors produced thermoelectric materials with a Seebeck Coefficient of 10 times compared to the metals and alloys studied by then and the world's scientific interest in the thermoelectric elements grew. In 1947, *Maria Telkes (1900-1995)* manufactured the first TEG using Solar Power with an efficiency of 3%. In 1949, *Abram Fedorovich Ioffe (1880-1960)* developed the

theory for semiconducting thermocouples in use today[14]. His work on composite semiconductors mainly oriented to transistor applications led to new materials with much improved thermoelectrical properties. At the time due to the military needs dictated by the Cold War an intensive research began leading to the discovery (rather say "manufacture") of materials with Z_T close to 1,5.

Since the end of the 19th century, the TEGs have not been able to compete with traditional electric generators based on the use of heat as the energy source. For this reason, the development of TMs was not being considered economically viable. This was mainly due to the following factors:

• The extremely low level of investment slowed down
the development of TMs.

• The use of the Thermoelectric Figure of Merit during the last decades as the main tool for the evaluation of the TM performance favored the creation of a great number of useless materials. It is probably for this reason that, currently, there are still few TMs of industrial interest.

Nevertheless, current conditions for the development of useful TMs are much better than those of the 19th century. Significant progress has been achieved in material science and material processing technology. Advanced equipment for the research of materials has been developed. In addition, modern research teams consist of highly qualified specialists and studies of TMs are focused on a few promising areas. Therefore, it is very likely that future research in these areas will lead to tremendous and unprecedented success[15]. The current international TEG market disposal is shown in the table below[16]:

Table 1: Current international TEG market disposal

Segments	Volume, %
Military and Aerospace	96
Other industrial areas	2
Other non-consumer	2
All segments	100

The thermoelectric phenomenon itself is the direct transformation of Temperature gradient to electrical voltage and vice-versa. A Thermoelectric device produces a voltage when its sides have different temperatures and respectively when voltage is applied a temperature gradient is developed (known as the Peltier phenomenon). If examined on the atomic scale an applied temperature gradient impels the electrically charged subatomic particles (electrons or holes) bearing electrical charge, to the hot or cold side, much likely as a typical gas expanding by temperature. This happens because the electron energy levels shift differently in the different metals, creating a voltage between the junctions which in turn creates an electrical current through the wires, and -by own means- a magnetic field around the wires[17]. The electricity generators based on the Seebeck effect do not depend on the nature of consumable heat and, therefore, they can be used in different areas. It is important to note that the initial device built by Seebeck can be used not only for conversion of the heat into electricity but also for the inverse process. When current is supplied to this device, it produces the difference in temperatures between its two sides (the Peltier effect, as mentioned above was discovered in 1834). In this case, the device is called Thermo-Electric Cooler (TEC).

2.2 The Seebeck effect

The Seebeck effect appears when two different thermoelectric materials forming electrical conductors and attached at their ends, have their junctions in different temperatures. In such a case potential difference is built at the junctions, depending on the temperature gradient between the junctions[18]. In general terms, this potential difference can be stated as:

$$E_{emf} = -S\nabla T \quad (2)$$

where S is the Seebeck coefficient and ∇T is the temperature gradient. Given that there are two materials (say, A and B) involved, the full expression would be:

$$E_{emf} = (S_A - S_B)\left(T_{High} - T_{Low}\right) \quad (3)$$

Seebeck coefficient of the relevant materials (S_A and S_B in eq. 3) is a non-linear function of the material temperature, however, in certain industrial applications and for a narrow range of temperature differences is considered relatively linear[19].

As mentioned above, Seebeck coefficients generally vary as a function of temperature and depend strongly on the chemical composition of the material. For ordinary materials at room temperature, the Seebeck coefficient may range in value from −100 μV/K to +1,000 μV/K.

In open electrical circuit cases, where the current created diminishes, the voltage produced is, then the voltage gradient is given simply by the emf: is given by Eq. (2). The voltage, in this case, does not refer to electric potential but rather the "voltmeter" voltage. This simple relationship, which does not depend on conductivity, is used in modern thermocouples to measure a temperature difference; an absolute temperature may be found by performing the voltage measurement at a known reference temperature. A metal of unknown composition can be classified by its thermoelectric effect if a metallic probe of known composition is kept at a constant temperature and held in contact with the unknown sample that is locally heated to the probe temperature.

It is used commercially to identify metal alloys. Thermocouples in series form a "Thermal Pile" or "Thermopile".

The heat flow needed on the hot side of the element can be calculated as follows:

$$\dot{Q}_{hot} = a(\hat{T}_{hot}) \cdot I \cdot \hat{T}_{hot} - \frac{\bar{\rho}}{2} \cdot I^2 + \bar{k}(\hat{T}_{hot)} - \bar{T}_{(cold)}) \quad (4)$$

The voltage occurring at the element is:

$$U = \alpha(\tilde{T}\,hot) \cdot \tilde{T}\,hot - \alpha(\tilde{T}\,cold) \cdot \tilde{T}\,cold - \bar{\rho} \cdot I \quad (5)$$

The electric power emitted by the element is:

$$P = U \cdot I$$

The effective temperatures are given by:

$$\tilde{T}_{hot} = T_{hot} - R_{th,\,hot} \cdot \dot{Q}_{hot}$$
$$\tilde{T}_{cold} = T_{cold} + R_{th,\,cold} \cdot (\dot{Q}_{hot} - P)$$

The mean value of the electric resistance is:

$$\bar{\rho} = \frac{\int_{\tilde{T}_{cold}}^{\tilde{T}_{hot}} \frac{\rho(T)}{\kappa(T)} \cdot dT}{\int_{\tilde{T}_{cold}}^{\tilde{T}_{hot}} \frac{1}{\kappa(T)} \cdot dT} \quad (6)$$

The mean value of the thermal conduction is:

$$\bar{\kappa} = \frac{\int_{\tilde{T}_{cold}}^{\tilde{T}_{hot}} \frac{1}{\kappa(T)} \cdot dT}{\int_{\tilde{T}_{cold}}^{\tilde{T}_{hot}} \frac{1}{\kappa(T)^2} \cdot dT} \quad (7)$$

Equations (1), (2), (3) and (4) are the main expressions explaining the behavior of the TEG elements. The explanation of the symbols used follows:

T_{hot}: absolute temperature applied at the hot side (heat source)

$R_{th,\,hot}$: thermal resistance on the hot side (ceramic plate, thermal compound, etc.)

$\tilde{T}_{hot}$: effective temperature on the hot side

T_{cold}: absolute temperature on the cold side (heat dissipation)

$R_{th,\,cold}$: thermal resistance on the cold side (ceramic plate, thermal compound, heat sink, etc.)

$\tilde{T}_{cold}$: effective temperature on the cold side

$\dot{Q}_{hot}$: heat flow needed on the hot side

U: voltage generated at the element

I: current flowing through the element

P: electric power emitted by the element

α(T): corrected thermal force

ρ(T): corrected electric resistance

κ(T): corrected thermal conduction

$\bar{\rho}$: effective electric resistance of the element

$\bar{\kappa}$: effective thermal conduction of the element [20]

A more concise and a fully detailed description of all Thermoelectric effects (Seebeck, Peltier Thomson and Joule) will be presented in the final Ph.D. dissertation.

2.3 Efficiency of Thermoelectric materials

According to Aldo Vieira da Rosa, the efficiency η of a single TM is defined by the equation:

$$\eta = \frac{(1+zT_m)^{0.5}-1}{(1+zT_m)^{0.5}+\frac{T_C}{T_H}} \cdot \frac{T_H - T_C}{T_H}$$

where:

T_H – temperature of the TM pair hot side

T_C – temperature of the TM pair cold side, and

$$T_m = \frac{T_H - T_C}{2}$$

The η of modern TMs is in the range from 5 to 15%. The laws of physics do not forbid the existence of materials with a greater value of η. Therefore, the development of new materials goes on. The recent technological advances show that modern TMs may significantly surpass photovoltaic cells in the "efficiency" of energy generation[21]. Taking into account the advances in the development of thermoelectric materials, the efficiency of TMs of the new generation may reach 25% within the next few years[22].

2.4 Practical TEGs

As already mentioned, the TEG technology development pace has become a frenzy, nowadays.[23] [24] Several companies, mainly in the microprocessor or Semiconductor manufacturing business have started building commercially oriented TEG modules since the early '90s. The fact that the reverse Seebeck phenomenon (Thermoelectric

cooling or “Peltier”) uses almost the same modules[25] for practical cooling implementations gave a significant boost to the relevant research by revealing a significant market interest. The research for semiconductors leading to higher figures of merit Z_T - hence improving the overall power factor of commercial TEG modules, gave room for more practical uses.

Now, TEGs producing a significant 16 to 19 W of power for 200-250 C temperature gradient at a 40x40x3 mm are commercially available at affordable prices which are dropping rapidly. As wasted heat is practically everywhere, the increasing use of TEGs for its harvesting appears to be the most possible guess.

TEHP1-12656-0.3 made by IEH was selected for the experimental part of this work. The chip has the following characteristics:

- Hot Side Temperature (˚C) 300 (average)
- Cold Side Temperature (˚C) 30 (average)
- Open Circuit Voltage (V) 8.4
- Matched Load Resistance (ohms) 0.9
- Matched load output voltage (V) 4.2
- Matched load output current (A) 4.6
- Matched load output power (W) 19.3
- Heat flow across the module(W) ≈ 306
- AC Resistance (ohms) Measured under 27 ˚C @ 1000 Hz 0.25 ~ 0.4

The element is a Bi-Te based thermoelectric module that can work at the temperature of as high as 330 ˚C (626 ˚F) heat source continuously, and up to 400 ˚C (752 ˚F) intermittently. The thermoelectric module will generate DC electricity as long as there is a temperature difference across the module. More power will be generated when the temperature difference across the module becomes larger, and the efficiency of converting heat energy into electricity will increase almost linearly. The module is sandwiched with two high thermal conductivity graphite sheets on both sides of the ceramic plates to provide low contact thermal resistance, hence there is no need to apply

thermal gel or other heat transfer compound when installing the module. The graphite sheet will withstand extremely high temperatures easily.[26] Nevertheless, for massive and real-world applications, a somewhat more expensive, robust, and durable choice can be used[27].

CHAPTER 3: THE PROPOSED APPROACH

3.1 THE POWER DEMANDS OF A MODERN VESSEL

Modern vessels are quite complicated structures incorporating almost all the new technologies available. As sea transportation bears more than 90% of the world trade[28] the necessity for building bigger and more energy-efficient ships became imperative. The electrical power needs of a modern ship have long ago passed the threshold of traditional uses for control, communication and accommodation needs, to the point of using electrical power for the propulsion of the Ships. Submarines were the first to use electrical power for propulsion and the tendency is now being expanded to larger surface vessels such as Tugs and trawlers, Dredgers, Dynamic positioning vessels, Cable laying ships, Ice breakers, Research ships, Floating cranes, Vessels for offshore industries[29]. Though there are currently several technologies related to electric propulsion[30], they all end up in the use of one or more electric motors driving the propeller shaft(s). Given that the power needed to feed the electric motors has to be produced onboard, the whole subject can be summarized in two practical issues: The most cost-effective and efficient power production[31] and the overall rationalization of all secondary or tertiary power needs. The same applies to the vast majority of conventional ships who at the moment are powered by conventional thermal engines mainly two-stroke Diesels of various power outputs.

The demand for electrical power in modern vessels is large and varies from the primary needs for running the main propulsion system and its ancillaries (e.g. pumps, motors, control valves, burners, etc), power steering system and its ancillaries, to secondary needs such as ballast tanks and fire safety pumps and conducts network management,

communication and positioning systems supply, as well as needs having to do with accommodation, sanitation, and onboard welfare loads,(eg. Galleys, refrigerators, air-conditioners, and other equipment). The latter can be vast having in mind that Sea Cruise Industry, for example, holds a large percentage of international tourism, nowadays[32], leading to the building of larger Cruise ships. A modern large Cruise ship or a Warship has a power-producing capacity enough to supply a small town, a practice which was implemented several times in cases of natural disasters (e.g. earthquakes-fires)[33] or even permanent shore network inadequacies[34].

A cruise ship docking in a European harbor typically carries between 2,000 and 3,000 passengers plus 800-1,500 crew members. In recent years there has been a big increase in the size of these ships and this trend is expected to continue. Cruise ships carrying 4,000 passengers and more are now being built. The ships typically have an energy consumption of 7-11MW while they are in port. This is equal to the average electricity consumption of 27,000-42,000 European households in the same period. Every year, over 300 cruise ships visit a typical European capital harbor, with a total energy consumption of the order of 17GWh. This is equivalent to the annual consumption of around 7,500 average European households[35].

3.2 Power producing means and capacity of a modern vessel

Power production onboard is achieved using Diesel or MGO[36] engine-driven Generators which is one of the costliest and environmentally hazardous methods, second only to that of the use of coal. Despite the continuous optimization of the power factor of Diesel Engines the production of electricity using Diesel oil or even Gas from

hydrocarbons is a costly business itself, not to mention the extra costs coming from the necessary maintenance, service, and machinery downtime costs. An average cargo vessel has a power of 3 to 5 MW while for an oil carrier it can increase to 6 MW due to the pumping system needs[37].

As already stated for the onboard electric power production Diesel Engines are used. In the last decades, brushless, synchronous generators have vastly replaced the older brushed generator technology. It has to be mentioned that in the early days when electricity was introduced onboard, DC generators were used to supply power, a trend which regains attention nowadays.[38, 39]

The fuel consumption of the Generator driving engines is high; Modern state-of-the-art engines running at a -common- 900rpm speed, consume some 190 to 200 g/kWh of fuel oil[40], which yields to a daily consumption of 14,4 tons of fuel, solely for the electric power production on a vessel with a 3MW power grid. The burning of fuel increases the operational cost for the owner, burdens the engine crew with the maintenance of the generator sets and most importantly, it severely increases the environmental footprint of the vessel. Hence, both alternative power production and power consumption[41] rationalization become imperative[42, 43].

Towards the first, almost all of the conventional large cargo and oil carriers are equipped with “shaft generators”. Shaft generators onboard ships are driven by the main engine to supply power to the mains. The mains have to be supplied with constant voltage and frequency by the shaft generator whilst the speed of the main engine changes, i.e. when the vessel travels at different speeds or if the propeller speed strongly varies in heavy seas. On ships with fixed pitch propellers, the speed is set via the propeller speed. If using controllable pitch propellers, the shaft speed and the propeller pitch are adjusted simultaneously to achieve optimum propeller efficiency in this so-called combinator mode. Even with this type of propeller, it is thus economical to use shaft generator systems with frequency converters for variable speed in order to permit combinator mode from pier to pier[44]. To the best of the writer’s knowledge at the time

of writing this dissertation, no other type of effective, alternating type for producing energy onboard has been proposed or by any means suggested, internationally.

3.3 Waste heat recovery in modern vessels

During the operation of the marine power system, the greatest losses are in waste heat generated by the diesel main engine. Due to the implementation of combined heat and power economics and by seeking to meet increasingly rigorous requirements for environmental protection in terms of the emission of harmful exhaust gas components, waste heat recovery systems have been developed. Employing waste heat in the re-use process results in the reduction of fuel consumption by the ship's power system. As the effect of these systems, the following may be considered: a lower cost of purchased fuel, a lower amount of emitted exhaust gas components, and extended operational period of machines and devices on a ship. When deciding on employing the systems, one should know data regarding the amount of the waste heat contained in a particular medium and the methods of its application. The possible recovery systems' levels related to the degree of their development and use of the waste heat and generated steam are presented in Table 2.

The largest resources of waste heat in diesel engines are in exhaust gases, charge air, and engine cooling water. The heat in the exhaust gas is used to generate steam in exhaust gas boilers. The steam is a heat medium used for heating purposes and for driving the auxiliary steam turbine interfaced with power generators and pumps.

The heat in charge air is transferred in the multisector air cooler to heat the water feeding the boilers in order to reduce the amount of heat necessary to reach the saturation temperature for a particular steam working pressure. This should result in an

increased amount of steam generated in both the waste heat recovery boiler and the oil-fired boiler. In the following cooler sections, the water may be heated and then used in the ship's heating and sanitary systems, which should reduce the demand for heating steam generated by the ship's boilers. The waste heat in the water cooling the engine is used in evaporators to produce potable water, preheat the water, and heat sanitary water. The analysis regarding the amount of steam generated by the waste heat recovery boilers and used to meet the demand for heating and supplying power to turbogenerators showed that the demand for electricity and heating purposes will occur in marine power systems where the main power does not exceed 25 MW[45]. Such power of a propulsion system is applied on ships that have to develop high operational speeds (container ships, LNG tankers) and ships of high capacity, e.g., VLCC tankers.

Nowadays the main function of waste heat recovery systems employed in ship power systems is to generate saturated steam in the amount that is sufficient for heating purposes. This solution, applied since the mid-twentieth century, contributes to the reduction of fuel consumption in the marine power systems due to the option to resign from the oil-fired boilers. Such an approach to the function of the waste heat recovery boiler may mean that one has not used the available waste heat resources included in the exhaust gas generated by the main engine. Table 2 presents the waste heat resources generated in marine main engines and included in the particular medium. The data presented in the table refer to the technical data for engines manufactured by the market-dominant marine engine manufacturers such as MAN, Wartsila, Sulzer, Hyundai, Daewoo, etc.

Table 2: Exhaust Gas Temperatures of Marine Diesel Engines

Engine type	Waste heat medium							
	Exhaust gas			Charge air			Engine cooling water	
	Share in supplied heat	Temperature	Flow	Share in supplied heat	Temperature	Flow	Share in supplied heat	Temperature
	%	°C	kg/kWh	%	°C	kg/kWh	%	°C
Low-speed	26.0–31.5	240–300	8.0–9.3	11.2–14.5	160–190	7.8–9.1	6.3–7.9	80–115
Medium-speed	24.8–33.9	380–450	6.5–7.7	9.4–13.0	160–210	6.3–7.5	7.0–8.4	80–115

It is obvious that the proposed technique of turning waste heat directly into electricity skipping the use of steam or some other hot working means contributes severely to the overall safety of the vessel and on certain occasions will most probably be more efficient.

3.4 Ducting System considerations

A significant factor limiting the use of waste heat contained in exhaust gas is low-temperature corrosion. It is a result of the presence of sulphur oxides as oxidation products of sulphur contained in the fuel. Sulphur is oxidized to sulphur dioxide SO2 and, in the presence of catalysts, to sulphur trioxide SO3. Sulphur trioxide sequentially combines with water to form sulphuric acid H_2SO_4. Sulphuric acid is in a gas state at a high temperature and does not create a risk of corrosion of elements with which it has contact. The sulphuric acid condensation occurs when the temperature in the space filled with exhaust gas decreases below the dew point. Then, the acid condensates and reacts directly with metal elements. Figure 2 presents how the sulphur content in fuel affects the temperature of exhaust gas dew point[46]. The temperature values of the dew point are within the marked area in Figure 2 due to the variable composition of sulphur oxides, which is dependent on the conditions in the exhaust gas

pipe and local distribution of catalysts[47]. To prevent this phenomenon from occurring during the combustion process of fuel containing more than 1% of sulphur, the temperature of the exhaust gas down the waste heat recovery boiler should not be lower than 160°C.

The applicable requirements for environment protection state that sulphur oxides emission should be limited and reduced. In enclosed areas, such as alternative fuels, e.g., LNG, or it is permitted to install a device in exhaust gas pipes which would reduce sulphur oxides in the exhaust gas.

In our case, the formation of H_2SO_4 solution in liquid form is rather impossible due to two main reasons:

1. The fossil used as fuel in the main engine has a Sulphur content of 0,1%. The International Maritime Organization (IMO) regulations mandate that the sulfur content in fuels, which is carried by merchant vessels, has to be limited to 0.50% globally and 0.10 % m/m in ECAs (Emission Control Areas; The Baltic Sea Area, The North Sea area, The United States, Canada, and the United States Caribbean Sea area)[48].
2. The exhaust gas waste heat recovery will not drop the overall temperature of the gases in temperatures less than 200^o C, which is well beyond the dew point.

Nevertheless, provision should be taken during the duct system designing to include an arrangement for the occasional internal flushing of the duct system with a suitable scrubbing solution. These solutions are available on all modern vessels and are widely used in wet funnel scrubber systems. The scrubbing liquid used may be seawater or freshwater with chemical additives. The most commonly used additives used are caustic soda (NaOH) and Limestone solution (CaCO3). Scrubbing liquid is sprayed into the exhaust gas stream through nozzles to distribute it effectively.

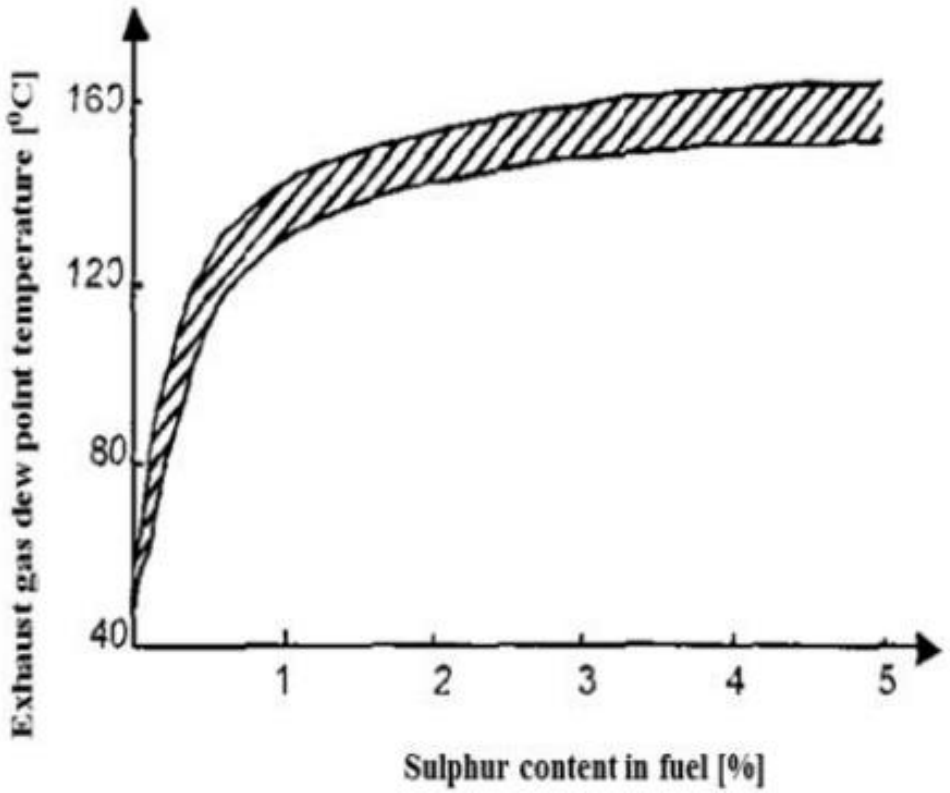

Figure 1 Impact of sulphur content in fuel on exhaust gas dew point temperature

3.5 Power producing using Seebeck element arrays.

Power producing onboard using Seebeck elements has not yet been thoroughly examined, let alone implemented mainly due to two reasons: the low efficiency of the first Seebeck modules commercially available, and the need for cooling which decreased the overall power factor of the installation so much, as to make the whole project unprofitable. As discussed earlier[49], the former is rapidly overcome. The latter is the basic issue to be solved in the solution which is proposed and examined by the Ph.D. research.

The supply of otherwise wasted heat in vessels, though complicated -especially when it comes to retrofitting a Seebeck Power Supply system on an existing vessel- is not an unsolvable problem. As the basic idea is not to bring the cooling media to the Seebeck array fitted on the heat source but rather bringing the heat source to the array fitted on the cooling surface, a significant part of the problem being the power needed for the pumping and circulation of seawater to the arrays is solved. In all modern vessels, there is an extended network of ducts and piping carrying the exhaust gases from the scavenge ports to the various ancillaries. “The exhaust gas piping system conveys the gas from the outlet of the turbocharger(s) to the atmosphere. For designing the exhaust piping system, the following important parameters are observed:

The exhaust gas flow rate

The maximum back force from exhaust piping on turbochargers

Exhaust gas temperature at turbocharger outlet

Maximum pressure drop within the exhaust gas system

Maximum noise level at the gas outlet to atmosphere

Sufficient axial and lateral elongation ability of expansion joints

Utilization of the heat energy of the exhaust gas.

The Exhaust gas from the cylinder unit is sent to the exhaust gas receiver where the fluctuating pressure generated from different cylinders is equalized. From here, the gases which are at constant pressure are sent to the turbocharger where waste heat is recovered to provide additional scavenging air to the engine. The most important thing to consider while designing the exhaust piping system is the back pressure on the turbocharger. The back pressure in the exhaust gas system at the specified Maximum Continuous Rating (MCR) of the engine depends on the gas velocity, and it is inversely proportional to the pipe diameter to the 4th power. It is general ship practice to avoid excessive pressure loss within the exhaust pipes, the exhaust gas velocity is maintained about 35m/sec to 50m/sec at specified MCR. The other factors which affect the gas pressure are the installation of EGB, Spark arrestor, etc. in the path of exhaust gas travel.

At the specified MCR of the engine, the total backpressure in the exhaust gas system after the turbocharger (as indicated by the static pressure measured in the piping after the turbocharger) must not exceed 350 mm WC (0.035 bar). In order to have a back pressure margin for the final system, it is recommended at the design stage to initially use a value of about 300 mm WC (0.030 bar)[50]". There are several points where the extraction of gases to the Seebeck array ducting is feasible. As the temperature of the gases should be within 400 and 280^{o} C an ideal position of the extraction port could be right after the Exhaust Gas Boiler and the Silencer[51] [52], and this is the position that will be considered in this Thesis models. Yet, as in strictly technical terms, this is a question to be answered individually for each different vessel, it goes beyond the scope of this research.

3.5.1 Exhaust Gas Production of a HYUNDAI-B&W 7G50ME-B9.3 (TIER II) marine engine.

3.5.1.1 Quantitive calculation of the Exhaust Gases

Quantitive and quality calculations of the expected exhaust gas data of the main propulsion system on the vessel equipped with Seebeck Power production arrays are of paramount importance as they affect the design, efficiency, and maintenance of the system. HYUNDAI-B&W 7G50ME-B9.3(TIER II) marine engine[53] project guide manual[54] provides both the calculation method and the results for the expected exhaust gas data at the ISO specified Maximum Continuous Rating (MCR). The exhaust gas temperature and mass data are as follows:

T_{L1} = 255 to 235 °C (T_{L1}: exhaust gas temperature after turbocharger in °C at nominal MCR)

T_{exh} = 203.5 °C ±5 °C (T_{exh}: exhaust gas temperature at the end of funnel)

$M_{exh,M}$ = 71,000 kg/h ±15% (Exhaust gas mass, at nominal MCR)

$T_{exh,M}$ = 231.1 °C ±5 °C (Exhaust gas temperature, after all utilization, at nominal MCR)

while the air consumption will be: 69,758 kg/h or, 19.4 kg/s.

3.5.1.2 Quality data of the Exhaust Gases - Eco footprint

During the last decades, emission control has become the measure for Thermal Engines' development even over shading the efficiency increase[55]. Soon of course was to

become clear that both issues were connected in many ways. Therefore the area of emission control had to be the area of research where the main development effort should be allocated. The emissions proven to be more responsible for the ecological footprint of modern Thermal engines are CO_x, SO_x, particulates, HCs, and NO_x, the former reflecting the engine efficiency, the latter two being of the most contemned greenhouse gases. Though the rate of CO2 emissions per unit load by transport load for ships is only 1 to 4 Relative Units RU per weight x distance units (compared to 6, 50, and 400 for rail, truck, and air transportation respectively)[56], increasing the efficiency using waste heat recovery and achieving a total efficiency of the fuel energy used of up to 60%. This will definitely reduce the CO_2, NO_x, SO_x, and HC emissions. However, things are more difficult when it comes to low speed, two-stroke engines being the main propulsion systems of large contemporary vessels. CO_2 emissions, in particular, are directly an index of high thermal efficiency[57] . Hence, the investigated method of using Seebeck arrays for waste Heat recovery shows to be not only capable of improving the overall efficiency of the vessel thermal engines system but contributing to less fuel consumption turning it into a win-win case, when combined with existing and new emerging technologies such as IAM (intake air humidification), EGR (exhaust gas recirculation), Extended combustion configuration, Scrubber system installation, the extension of LNG use as the main propulsion fuel, to name but a few.

Engine exhaust gases are discharged into the environment through the exhaust. The exhaust includes several specialized components, ranging from mufflers to emission after-treatment devices. The designer of the exhaust and/or exhaust components must bear in mind a vast variety of exhaust gas properties.

Compared to the composition of air, the marine diesel exhaust gas contains increased concentrations of water vapor (H_2O) and CO_2 (CO_2)—the main combustion products. The concentrations of both H_2O and CO_2 can vary from a couple of percent units, up to about 12% in HFO exhaust. These combustion products displace oxygen, the concentration of which may vary from a couple of percents, up to about 17% (compared

to 21% in ambient air). The main component of diesel exhaust, even as is that the case with ambient air, is nitrogen (N_2). By comparison, the concentrations of almost all diesel exhaust pollutants are very small—for the aim of calculating the physical properties of diesel exhaust gas, they will be neglected.
As an approximation, the properties of air are often used for diesel exhaust gas calculations, Table 1 [Perry 1984]. The error related to neglecting the combustion products is typically not more than 2%. In a more rigorous approach, corrections must be taken to account for the particular exhaust gas composition (increased H_2O and CO_2, decreased O_2). An additional difficulty with this approach is that the necessity to account for the variable exhaust gas composition, which changes with the engine ratio and therefore the air-to-fuel ratio. Physical properties of mixtures of gases, and methods to calculate them from the properties of components are quite often found within today's literature[58].

Table 3: Physical properties of hot air/exhaust gases

Physical properties of exhaust gases/air (p = 101.13 kPa)
T temperature, K; **ρ** density, kg/m^3; **h** specific enthalpy, kJ/kg; **s** specific entropy, kJ/(kg·K); **C_p** specific heat at constant pressure, kJ/(kg·K); **μ** viscosity, 10^{-4} Pa·s; **k** thermal conductivity, W/(m·K)

T	**ρ**	**h**	**s**	**C_p**	**μ**	**k**
260	1.340	260.0	6.727	1.006	0.165	0.0231
280	1.245	280.2	6.802	1.006	0.175	0.0247
300	1.161	300.3	6.871	1.007	0.185	0.0263
350	0.995	350.7	7.026	1.009	0.208	0.0301
400	0.871	401.2	7.161	1.014	0.230	0.0336
450	0.774	452.1	7.282	1.021	0.251	0.0371
500	0.696	503.4	7.389	1.030	0.270	0.0404
600	0.580	607.5	7.579	1.051	0.306	0.0466
800	0.435	822.5	7.888	1.099	0.370	0.0577
1000	0.348	1046.8	8.138	1.141	0.424	0.0681
1200	0.290	1278	8.349	1.175	0.473	0.0783
1400	0.249	1515	8.531	1.207	0.527	0.0927

(NOTE: Temperatures in the a.m. table are given in degrees of the Kelvin scale)

A Typical composition of Exhaust Gases at MCR of the main Engine is as follows[59]:

Table 4: Typical Composition of Control Gases at Maximum Continuous Rating

Component	N_2	O_2	CO_2	H_2O	NOx	SOx	CO	HC	Dust
%	77.50	13.75	6.25	0.025	0.212	0.17	0.005	0.005	0.0075

Whereas the term "Dust" refers to all particulates and combustion solid remains.

3.5.1.3 Exhaust Gas duct network and gas extraction

As already discussed in 3.3 above exhaust gases after the exit from cylinders are driven into the secondary heat recovery units in order to use most of the enthalpy still available. In general, the total enthalpy available enthalpy is defined as the sum of the internal energy and the product of the pressure of the given thermodynamic system. In this case, it represents the energy state of the gas system and is calculated by the following formula:

$$Enthalpy(Q_P) = \Delta E + P \Delta V \qquad (8)$$

To calculate the Enthalpy of the gas system the following data should be known:

Internal energy of Products (in Joules)

Internal energy of Reactants (in Joules)

Pressure of system (in Pascals)

Volume of Products (in m^3)

Volume of Reactants (in m^3)

Given the exhaust gas quantitive data for the specific IC Engine, it is possible to calculate the enthalpy of the exhaust gas at any point of the duct network provided the pressure and temperature can be monitored. Typical temperatures marked are as follows:

Table 5: Typical Heat Source temperatures of the specific Engine when ship at sea

Type of sources	**Temperature °C**
Steam boiler exhaust	230–480
Gas turbine exhaust	370–540
Engine exhaust	315–600
Engine exhausts with turbocharging	230–370

Though the ideal point of exhaust gas extraction appears to be the turbocharger exit, due to insurance policy restrictions the most suitable point should be the duct leg after the steam boiler exhaust and before the entrance to the lub and fuel oil preheating network.

Separate inlets can be driven from auxiliary heat sources (e.g. Incinerator, Generator Diesels, etc). At this point, several considerations should be taken into account, e.g. the minimum temperature needed for the preheating of fuel and lub oil, the ambient temperature, the vessel's itinerary, etc. By own means, these issues are to be dealt with independently and according to each vessel's demand and design particularities. For the case study of this Dissertation, the extraction point will be discussed in Chapter 3.3.2.

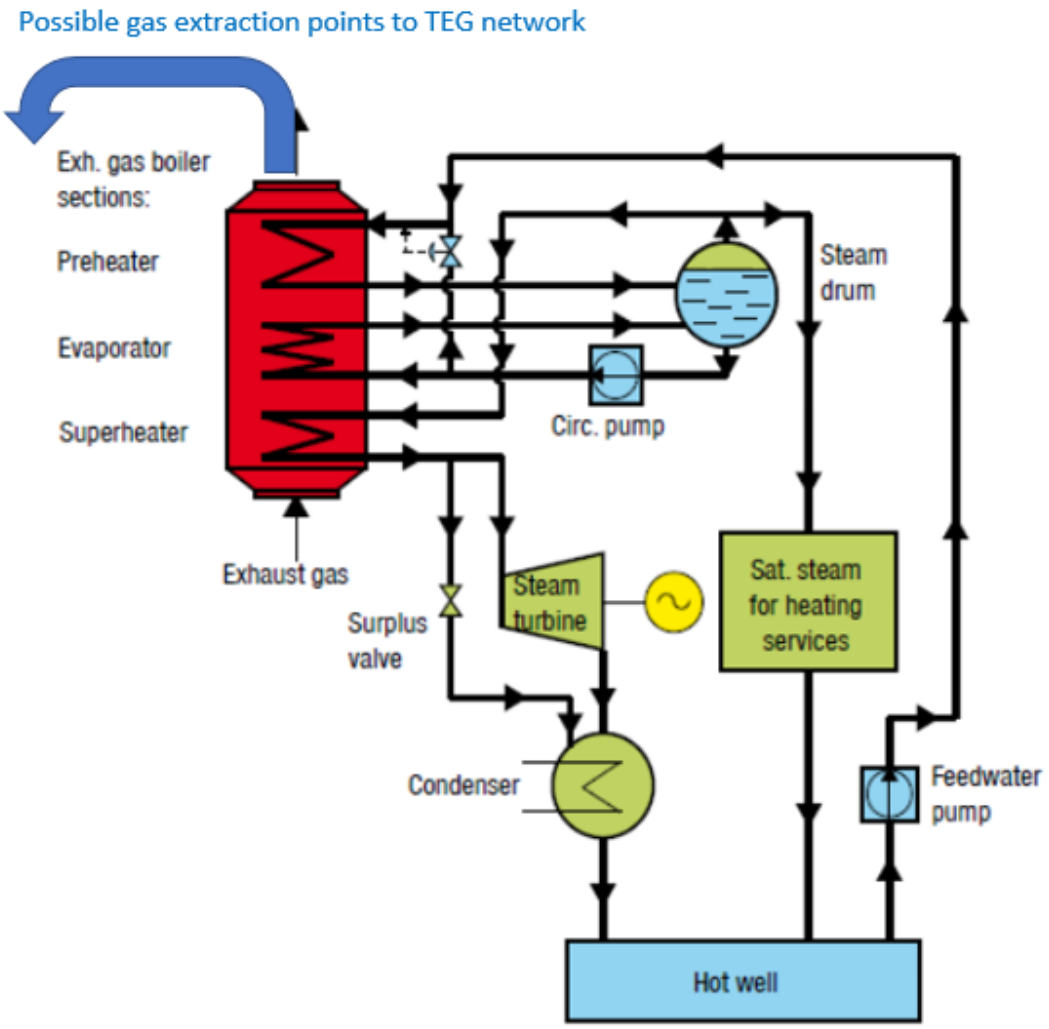

Figure 2: Design of a Typical exhaust gas boiler-steam turbine system (Courtesy: Wartsila) [60]

3.5.2 Exhaust Gas duct network parts and design

The most commonly used fluids especially gases are transferred in round cross-sectional hoses because they can withstand high pressure differences between their walls without significant deformation. Non-circular ducts are mainly used in

applications where the pressure difference is small, the available installation budget, and space is limited i.e. building heating and ventilation networks. For a standard given cross-sectional area the round duct (tube) offers the maximum possible heat transfer for minimum pressure loss. However, in the TEG arrays network design, tube ducting cannot be used but in parts of the network which guide the exhaust gases to the TEG arrays, and the parts leading them from the arrays to the funnel or scrubbing system. In all other parts, orthogonal ducts will have to be used. This is dictated by the form of the TEG elements and the necessity of close contact of the elements to the duct from one side and the wet plate on the other.

Although the theory of fluid flow is reasonably well known, theoretical solutions are obtained only for a few simple cases such as fully developed laminar flow in a circular pipe. Therefore, we must rely on experimental results and empirical relations for most fluid flow problems rather than closed-form analytical solutions. Noting that the experimental results are obtained under carefully controlled laboratory conditions and that no two systems are exactly alike, we must not view the results obtained as "exact." An error of some 10% in friction factors calculated using the relations in this chapter is to be characterized as "normal"[61].

The fluid velocity in a pipe or duct changes from zero at the surface because of the no-slip condition to a maximum at the geometrical center of the duct or pipe. In fluid flow,

it is convenient to work with an average velocity V_{avg}, which remains constant in incompressible flow when the cross-sectional area of the pipe is constant (Fig. 3).

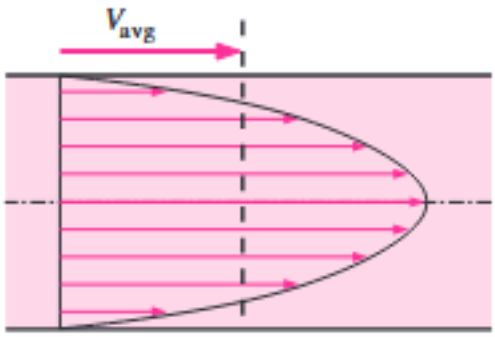

Figure 3: Average velocity Vavg is defined as the average speed through a cross-section. For fully developed laminar pipe flow, Vavg is half of the maximum velocity.

As the full design of a System for a specific vessel is a task for the Engineering design team of the vessel rather than the scope of this study, only partial-modular computations can be considered here. To these computations, the velocity of the gases within the duct system will be considered initially as standard (average).

The average velocity in heating and cooling applications may change somewhat because of changes in density with temperature. But, in practice, we evaluate the fluid properties at some average temperature and treat them as constants. The convenience of working with constant properties usually more than justifies the slight loss in accuracy. Also, the friction between the fluid particles in a pipe does cause a slight rise in fluid temperature as a result of the mechanical energy being converted to sensible thermal energy. But this temperature rise due to frictional heating is in our case too small in comparison with the temperature of the fluid itself, to warrant any consideration in calculations and thus is disregarded.

The ducts and parts consisting the Exhaust Gas operating Seebeck arrays network are of paramount importance as they have to be designed in such a way as to -among others:

1. Minimize the exhaust gas pressure loss and backpressure built, hence not adding more exhaust work to the engine providing the gases[62] [63],
2. Provide sufficient thermal insulation against the inner space of the vessel,
3. Facilitate easy replacement in case of damage or excessive wear, having a modular structure,
4. Allow the neutralization of the condensates or acid deposits on their inner walls due to the dew point phenomenon, by flushing the interior with Sodium Bicarbonate solution.
5. Accommodate suitable inspection and/or extraction ports,
6. Fulfill all the relevant standards and existing legislation and meet the safety requirements set by the Shipping Registers and insurance underwriters.

Approaching the solution to No1 above, which obviously is the greatest challenge of all involves two separate considerations:

a. To draw the components of the network keeping the pressure loss as low as possible, and,
b. To design the network with a topology such as to keep the back pressure built to a possible minimum.

Assuming a steady flow of gases[64] we need to calculate each of the items required to determine the friction loss in the network.

- Duct Friction Loss Calculations
- Gas Density
- Gas Viscosity
- Duct internal Roughness
- Reynold's Number - Laminar (rarely) Flow, Transient or (mainly) Turbulent Flow
- Friction Factors - Moody Chart and Colebrook-White Equation
- Friction Loss in the duct - Darcy-Weisbach Method

The fact that the network to be designed for each vessel will be a complex set made of pipes and ducts, correlations for pipe flow may be used for computations involving non -circular ducts provided that their cross-sections are not very large. This correlation for turbulent pipe flow can be extended to noncircular geometries by introducing the "hydraulic diameter" defined as

$$D_h = \frac{4A}{P} \quad (9)$$

where A is the cross-section and P is the wet perimeter. For rectangular ducts, intended for use in the Seebeck arrays network, assuming a width b and height h we have:

$$D_h \equiv \frac{4A}{P} = \frac{4bh}{2(b+h)} = \frac{2h}{1+ar} \qquad ar = h/b$$

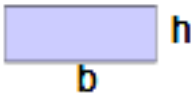

(10)

The hydraulic diameter concept can be applied in the approximate range ¼<ar<4, hence flow give acceptably accurate results acceptably accurate results for rectangular ducts[65]. The pressure at the end of the pipe under consideration is therefore given by the following relation (where all items are specified in m Head of Fluid):

$P_{[end]} = P_{[start]}$ - Friction Loss - Fittings Loss - Component Loss + $Elevation_{[start-end]}$ + Pump Head

Where:

$P_{[end]}$ = Pressure at end of duct

$P_{[start]}$ = Pressure at start of duct

$Elevation_{[start-end]}$ = (Elevation at start of pipe) - (Elevation at end of pipe)

Pump Head = 0 if no pump present (which is exactly the case when it comes to exhaust gases).

The pressure drop or rather pressure difference ΔP between the start and the end of a pipe is therefore given by this relation:

$$\Delta P = \text{Friction Loss} + \text{Fittings Loss} + \text{Component Loss} - \text{Elevation}_{[start\text{-}end]} - \text{Pump Head}$$

Note dP is generally specified as a positive value relating to the drop in pressure.

Regarding the topology of the ducting architecture and the feeding and circulation of the exhaust gases inside the ducts, there are two approaches one could choose: In series and parallel gas circulation, as shown in the following pictures.

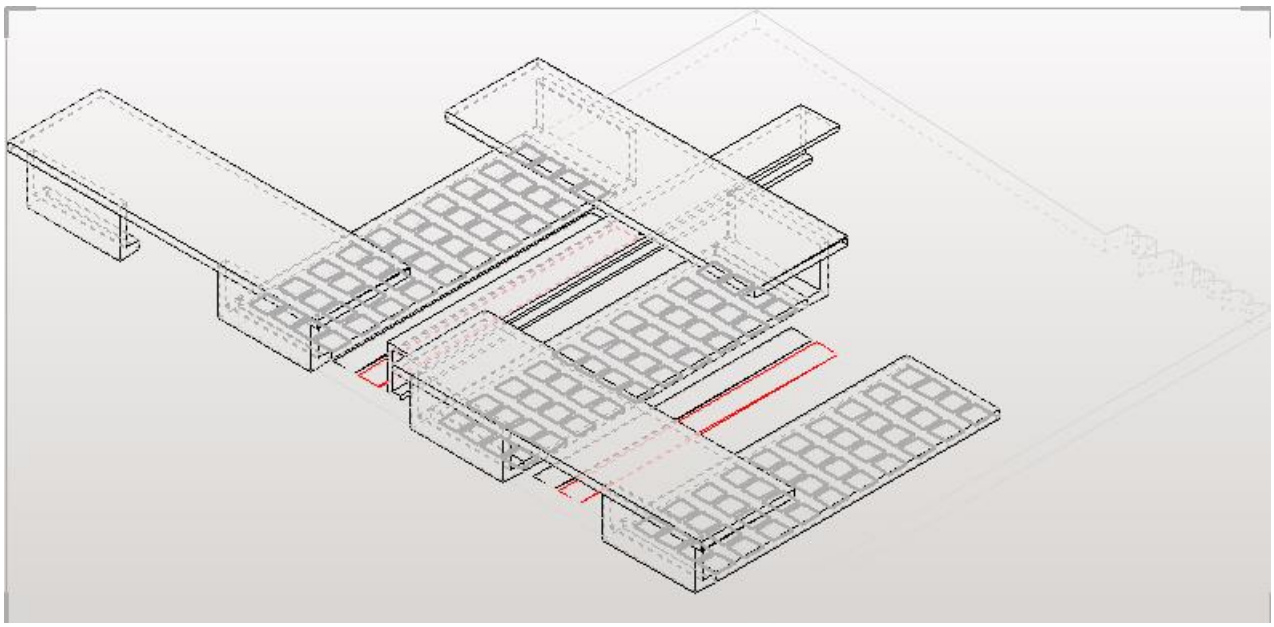

Figure 4:Schematic of a series duct config. on wet sheet

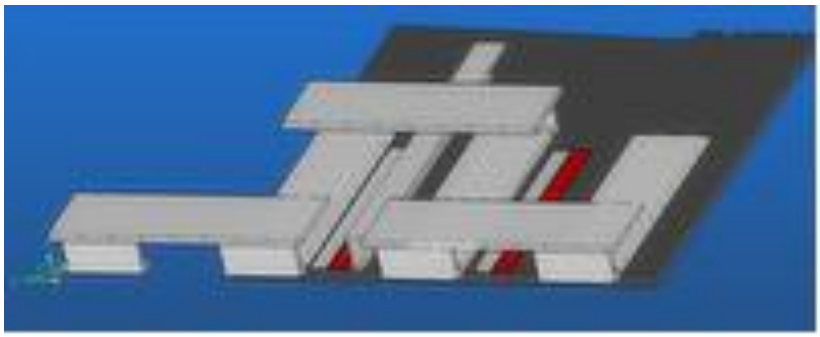

Figure 5: Series duct configuration

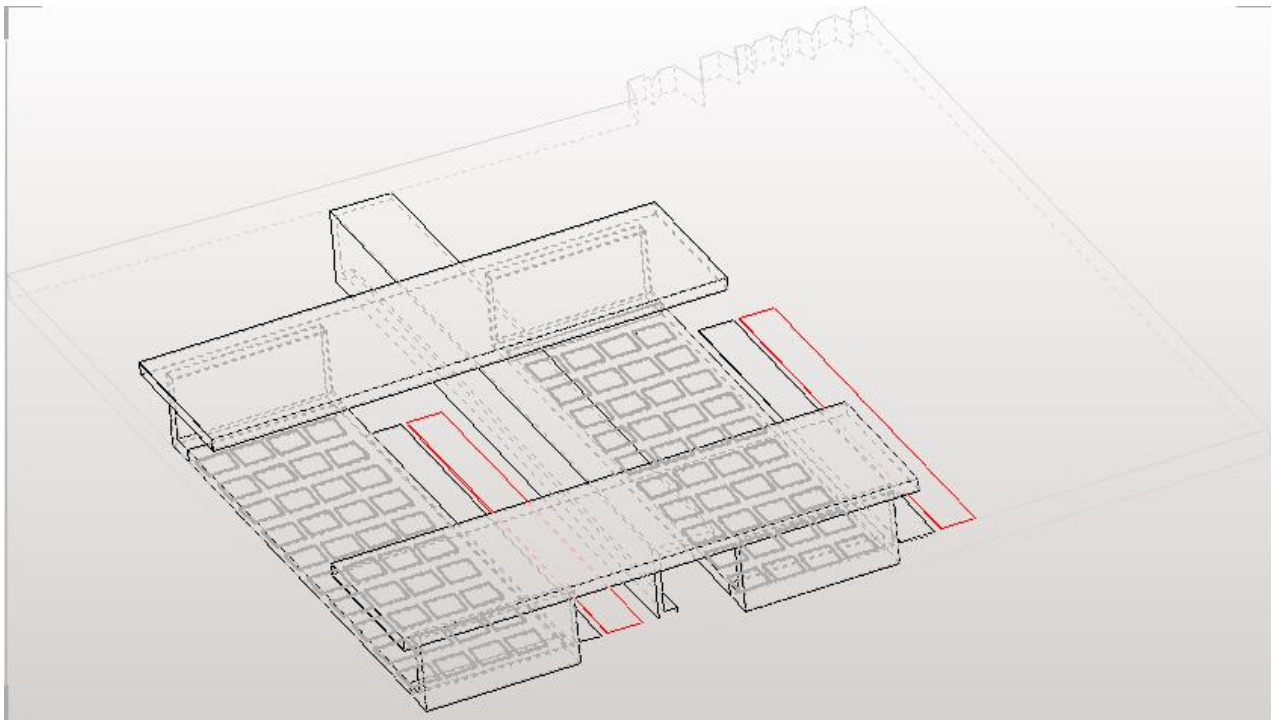

Figure 6: Schematic of a parallel duct configuration on a wet sheet

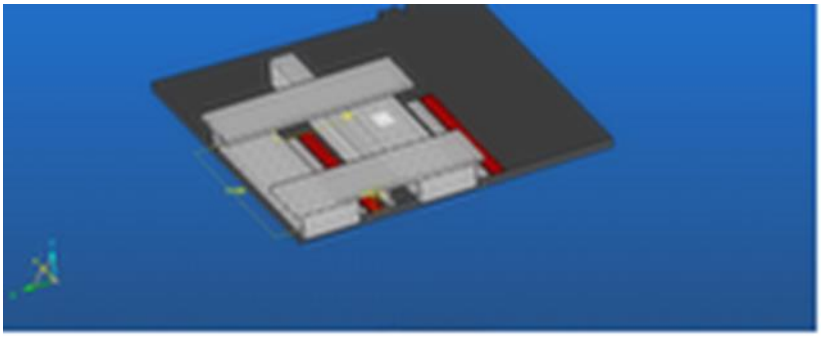

Figure 7: Parallel duct configuration

Having in mind the data given by the main engine manufacturer datasheet and the contents of table 1, we can assume always a turbulent flow, which is confirmed by the calculation of the Raynolds Number for several velocities and geometries of the ducts.

For two basic elements of the network, the main extractor tube, and the main duct TEG plate we could propose two drafting approaches:

1. A tube of an internal diameter (D) of 400 mm as the main extractor tube, and

2. A square duct of 200 x 50 mm, as the main duct TEG plate. This, using the equations (9) and (10) will produce a Hydraulic Diameter (D) of 160mm or 16 cm.

In a first theoretical approach, assuming that the main gas extraction point will be the outlet of the main steam boiler, having a temperature of 500º to 800º K, then the density (ρ) of the gases will be 0,696 Kg/m^3 and 0,435 Kg/m^3 respectively.
The relevant viscosities (μ) will be 0,270*10^{-4} Pa.s and 0,370*10^{-4} Pa.s respectively. For this first approach, the basic average velocity (V) of the gases will be considered to be 1 m/s. The application of the Reynolds equation then yields:

$$R = \frac{\rho V D}{\mu} \qquad (11)$$

It is generally accepted that for flow in a pipe of diameter *D*, for "fully developed" flow, the laminar flow form occurs when $Re_D < 2300$, and turbulent flow occurs when $Re_D > 2900$. At the lower end of this range, a continuous turbulent flow will form, but only at a very long distance from the inlet of the pipe. The flow in between will begin to transition from laminar to turbulent and then back to laminar at irregular intervals, called intermittent flow. This is due to the different speeds and conditions of the fluid in different areas of the pipe's cross-section, depending on other factors such as pipe roughness and flow uniformity. Laminar flow tends to dominate in the fast-moving center of the pipe while slower-moving turbulent flow dominates near the wall. As the Reynolds number increases, the continuous turbulent flow moves closer to the inlet and the intermittency in between increases, until the flow becomes fully turbulent at $Re_D > 2900$. This result is generalized to non-circular channels using the hydraulic diameter, allowing a transition Reynolds number to be calculated for other shapes of a channel.[66]

Using the above equation the following table and the relevant graphs showing the exhaust gases Reynolds number behavior, are prepared:

Table 6: Exhaust gases Reynolds number behavior for certain duct geometries and basic velocity of 1m/s

EXHAUST GASES REYNOLDS NUMBER BEHAVIOR						
Network	**Density (kg/m^3)**	**Viscosity (Pa.s)**	**Temperature (^oK)**	**Hydraulic Diameter (m)**	**Average Fluid Velocity (m/s)**	**Reynolds number**
Duct 400x100	0,696	2,70E-05	500	0,16	1	**4,12E+03**
Duct 400x100	0,435	3,70E-05	800	0,16	1	**1,88E+03**
Steel Tube ø200	0,696	2,70E-05	500	0,2	1	**5,16E+03**
Steel Tube ø200	0,435	3,70E-05	800	0,2	1	**2,35E+03**

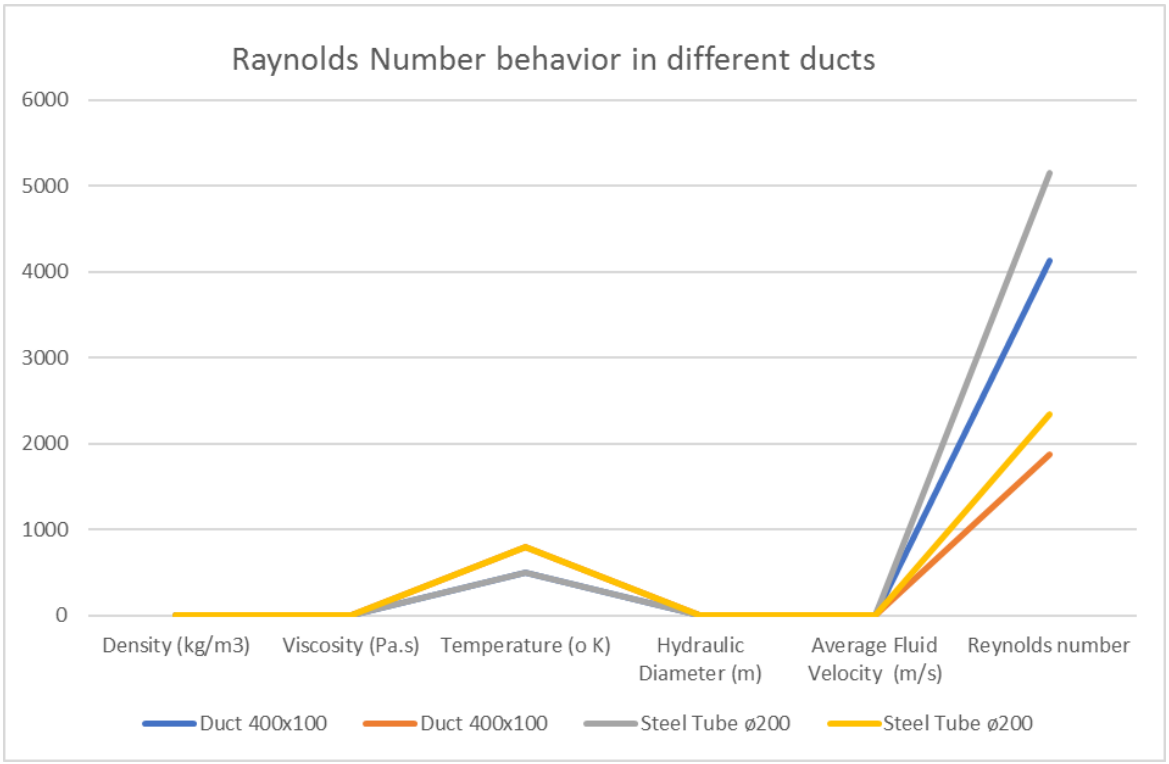

Figure 8: Raynolds Number for certain ducting geometries for the basic velocity of 1 m/s

From the graph and the table above it becomes clear that:

1. For the chosen part geometries the flow lies in the upper boundaries of the laminar form as the temperature rises.
2. The flow becomes turbulent as the temperature of the gases gets higher.

Yet, in the data given by the main engine manufacturer suggest gas velocities varying from 35m/s to 50 m/s, in accordance with the following table[67]:

Table 7: Main Engine's Gas mass flow and gas velocities

Gas velocity				Exhaust gas pipe diameters			
35 m/s	40 m/s	45 m/s	50 m/s	D0			D4
Gas mass flow				1 T/C	2 T/C	3 T/C	
kg/s	kg/s	kg/s	kg/s	[DN]	[DN]	[DN]	[DN]
15.0	17.2	19.3	21.5	900	650	500	900
16.7	19.1	21.5	23.9	950	650	550	950
18.6	21.2	23.9	26.5	1,000	700	600	1,000
20.5	23.4	26.3	29.2	1,050	750	600	1,050
22.4	25.7	28.9	32.1	1,100	800	650	1,100
24.5	28.0	31.5	35.1	1,150	800	650	1,150
26.7	30.5	34.3	38.2	1,200	850	700	1,200
31.4	35.8	40.3	44.8	1,300	900	750	1,300
36.4	41.6	46.8	51.9	1,400	1,000	800	1,400
41.7	47.7	53.7	59.6	1,500	1,050	850	1,500
47.5	54.3	61.1	67.8	1,600	1,150	900	1,600

Since the Raynolds equation (Eq.11) is linear, the variations of the Raynolds number differ only in magnitude and not in waveform from the ones produced in Table 3 and figure 7. Therefore, having in mind the data of Table 5, the following table and graph are produced:

Table 8: Exhaust gases Reynolds number behavior involving realistic velocities

EXHAUST GASES REYNOLDS NUMBER BEHAVIOR						
(involving realistic velocities)						
Network	Density (kg/m^3)	Viscosity (Pa.s)	Temperature (^oK)	Hydraulic Diameter (m)	Average Fluid Velocity (m/s)	Reynolds number
Duct 400x100	0,696	2,70E-05	500	0,16	35	**1,44E+05**
Duct 400x100	0,435	3,70E-05	800	0,16	50	**9,41E+04**
Steel Tube ø200	0,696	2,70E-05	500	0,4	35	**3,61E+05**
Steel Tube ø200	0,435	3,70E-05	800	0,4	50	**2,35E+05**

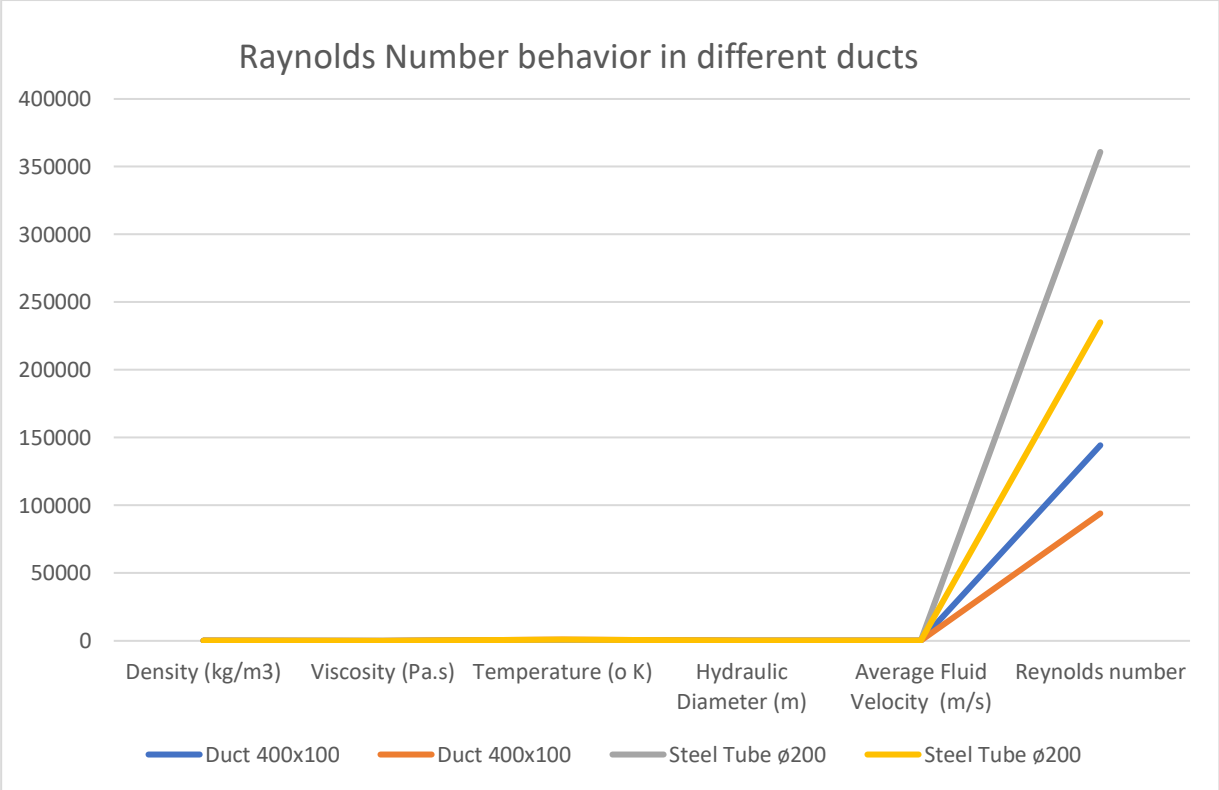

Figure 9: Raynolds number Behavior in different ducts involving realistic velocities

From the above table (4) and the graph of figure 8, it becomes clear that the flow within the ducts has a turbulent form at all times. This is a very positive development as turbulent flow is related to a much higher rate of heat transfer than laminar flow[68]. Although we have assumed that the velocity of the gases remains constant during the theoretical calculations, it is reasonable to suppose that in the real-world application this will not be the case, as the fluid media is a mixture of gases, and we have to consider not a part but the whole of the ducting network. Hence, as the temperature, velocity and pressure of the gases fall, all physical properties like density and viscosity of the gases

will also change, reflecting their change to the Reynolds Number and therefore to the form of flow.

As discussed above, in this particular case study, the most prominent point to extract gases is right after the boiler or between the boiler and the spark arrester and silencer (if present). The boiler fitted is A SAACKE CMB-VS® combined vertical exhaust gas and oil-fired boiler, able to burn liquid and gaseous fuels. The boiler has a Steam capacity of 1,5 t/h using the fired section, or 1 to 6 t/h (depending on the main engine type and layout), by using the exhaust gas section.

As the use of the burner in oil-fired mode is irrelevant to this thesis, the data of the flue gas will be taken from the documentation of the main engine.

The basic rate equation for convective energy exchange is

$$q = h\,A\,\Delta T \quad (12)$$

where q is the rate of the heat transfer between the surface and fluid, A is the area of contact, ΔT is the temperature difference between the surface and the bulk of the fluid and h is the convective heat transfer coefficient. In this particular case, it is clear that we deal with a classic case of forced convection, as the fluid flows due to the influence of the mechanical work given by the engine's pistons which in this case act as a pump[69].

It is up to the design Marine engineers to choose the topology of the network to be followed in each case, yet the experiments and the FEA done so far have shown that a parallel configuration shows lower pressure drop and backpressure built compared with the in series configuration which however could be dictated by the vessels internal structure. In general, the more vertical beams per length of the ship’s hull unit are present the more effective is the parallel configuration.

Having in mind the above, it becomes clear that the design of the optimal network for any vessel is a task quite complicated. Furthermore, it is actually a job that is to be carried out during the initial design of the vessel. When retrofitting the System to an existing marine construction, things can be even more complicated due to limitations

dictated by the existing internal architecture of the vessel and the alterations which have to be done. In any case, the design of a duct network fulfilling all the above requirements is a subject of a thorough study and on that, it depends greatly the decision for the feasibility and financial viability of the investment.

The process of building such a network prerequisites a thorough knowledge of fluid mechanics, and full access to the manufacturing data and plans of the vessel in question. Computer-Aided Design skills are also self-evidently required knowledge.

3.3.3 TEG array circuitry parts and design

In the Case Study being carried out in this Ph.D. research, several software tools are used in order to realize a typical module structured duct branch. The first approach is to use 2D (AutoCAD®) and 3D CAD (TopSolid®) software to form a number of basic network elements. These elements are then put together to form a typical duct network branch.

The methods of attaching the Seebeck Elements on the ducts are also examined, with the mechanical retention to excel in relation to chemical methods, for reliability reasons.

Getting into the drawing details of a first duct network design approach several designing considerations should be taken into account:

1. The duct network should consist of identical or at least similar duct modules which should be interchangeable to the maximum possible degree. The modules should be designed in such a way, to provide exhaust gas sealing, rapid change, and quick connection to the electrical network The modules should be designed in such a way as to make it possible for the Crew to repair on-site, replace, or electrically bypass or disconnect them when the vessel is at sea. The exhaust gas sealing ability of the modules is paramount, as it eliminates the risk of gas leakage which could result to fire, poisoning of the crew, and contamination of goods. It will also prevent leakage of the gas treatment solution (alkalis, mainly Sodium or Magnesium Hydroxide solution), which is needed for the neutralization of SOx contained in the exhaust gases and obtain particle removal[70].
2. The sizing of the ducts is critical, hence the following parameters should be taken into account during the design of the system:

a. The Exhaust gas volumetric speed or flow rate at specified MCR
b. The temperature of the gases at the extraction point (turbocharger, EGB, or silencer-if present- outlet),
c. The allowable maximum pressure drop within the duct system,
d. Maximum allowable back pressure to the exhaust piping, set by the engine manufacturer.

The cross-section of the duct network is to be determined considering all of the above-mentioned factors. In the following figures, the possible extraction points (D0 and D4) related to the temperature of the gases, are shown.

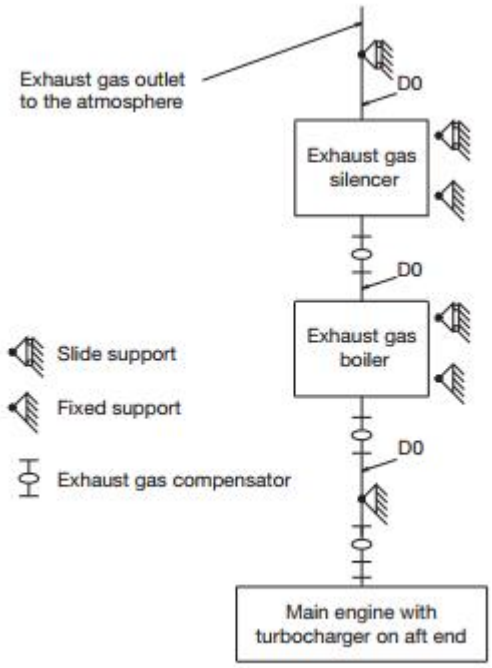

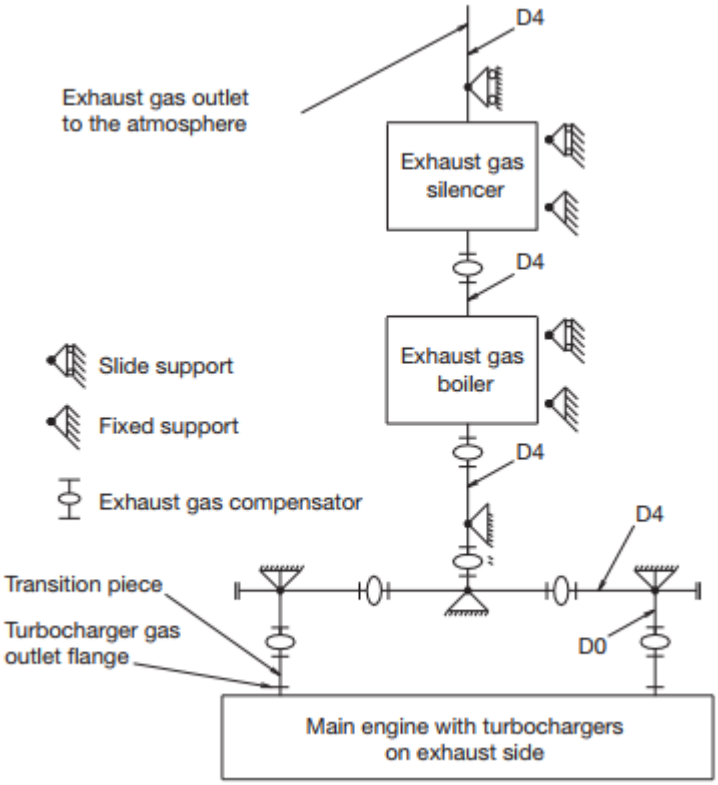

Figure 10: Possible Rxhaust gas extraction points (Courtesy MAN)

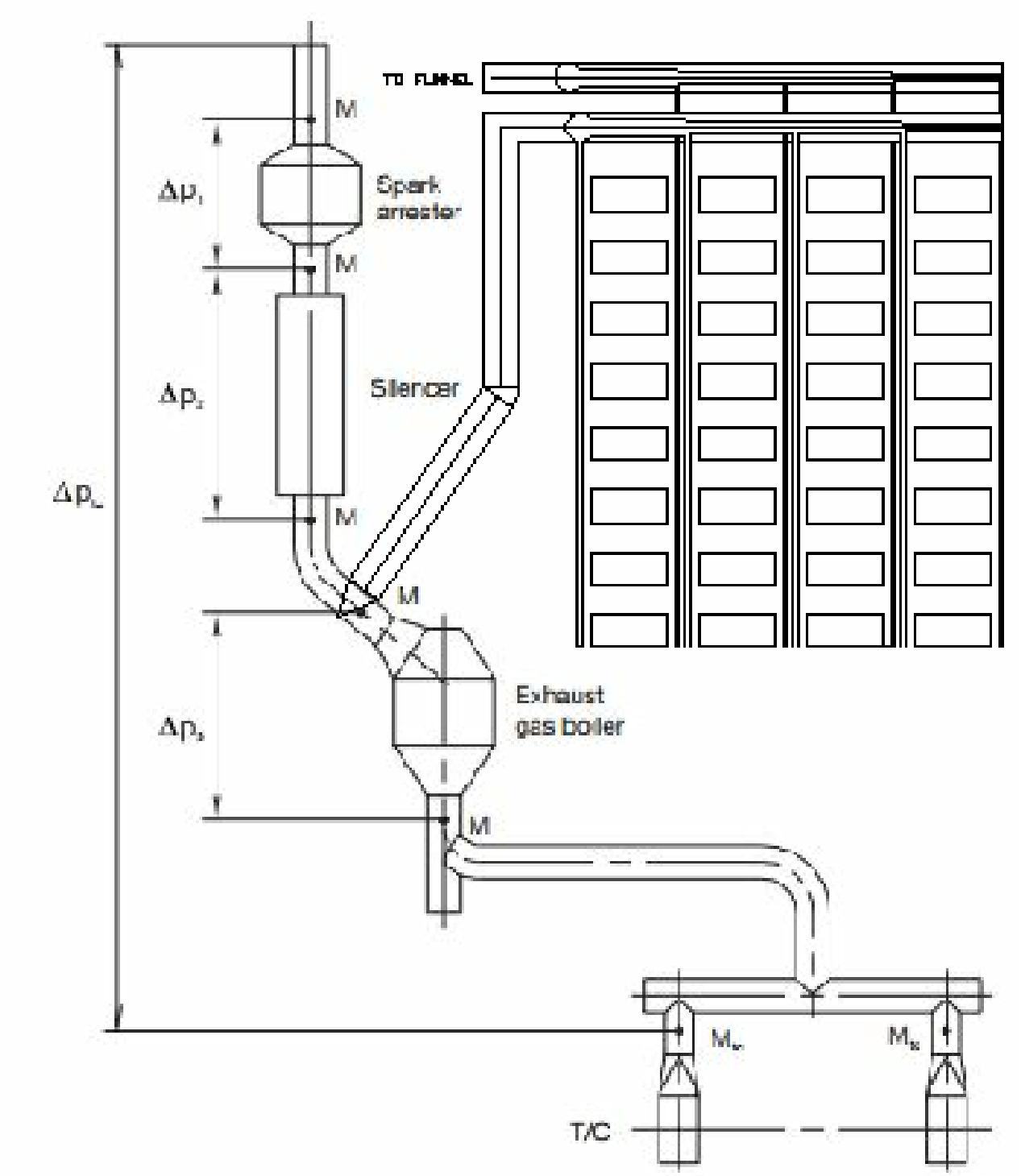

Figure 11 Possible extraction point configuration

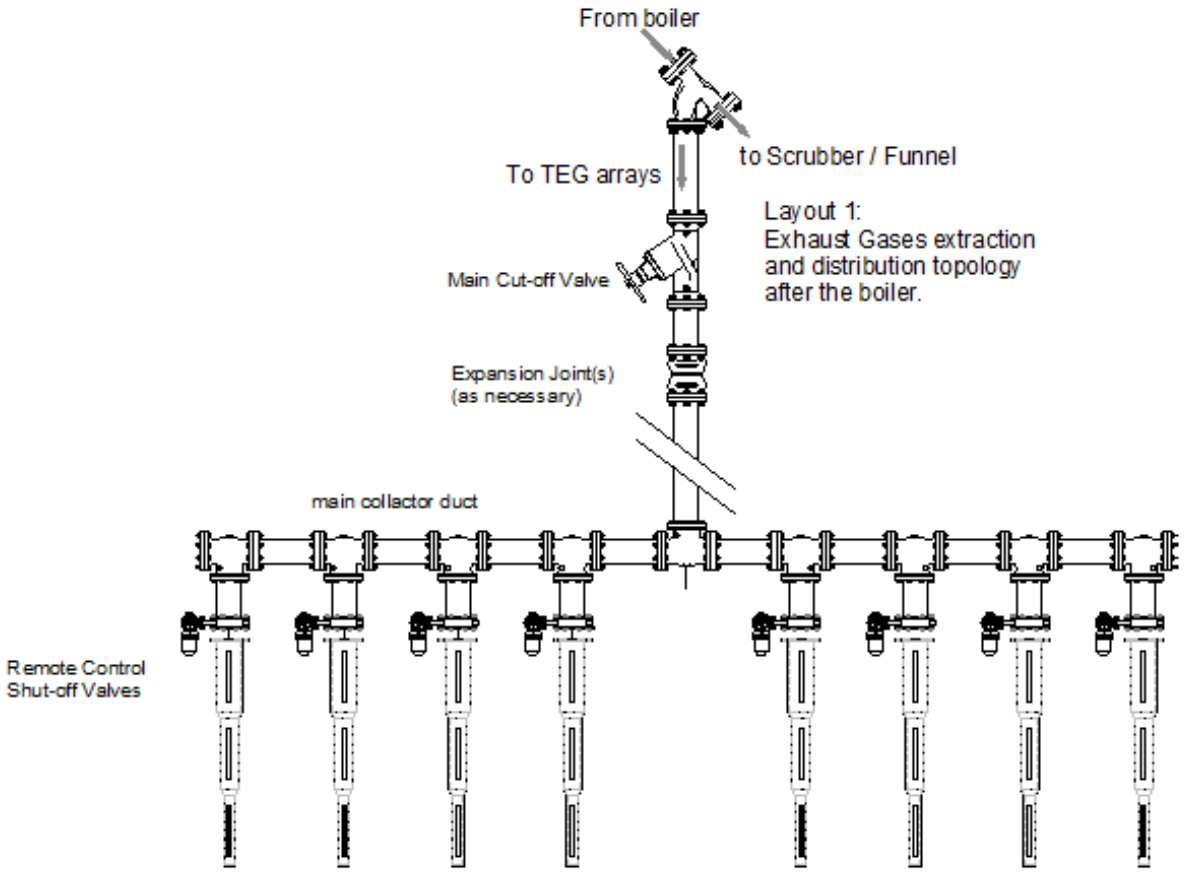

Figure 12: Possible distribution duct circuit layout

3. The ducting system should be well protected from mechanical, thermal, and chemical hazards. Hence a form of mechanical protection guarding rail could be fitted in areas involving high mechanical risk due to moving loads or cargo areas. The need for thermal insulation of the outer three sides of the ducts is obvious for several reasons having to do both with safety and efficiency of the system: Minimizing the risk of severe burning or fire due to unwanted contact with the ducts external surfaces and sealing off the heat loss due to radiation to the much colder vessel environment. Insulating methods and materials like stone wool with a specific thermal capacity from 0,9 to 1,5 kJ/(kg*K) iaw ISO 10456, currently in use with onboard steam, exhaust, or flue gas networks are quite satisfactory[71]. This methodology was applied in the FEA simulation of the system, presented in Chapter XXXX.
4. Another issue examined is the topology of the DC conductor circuitry:

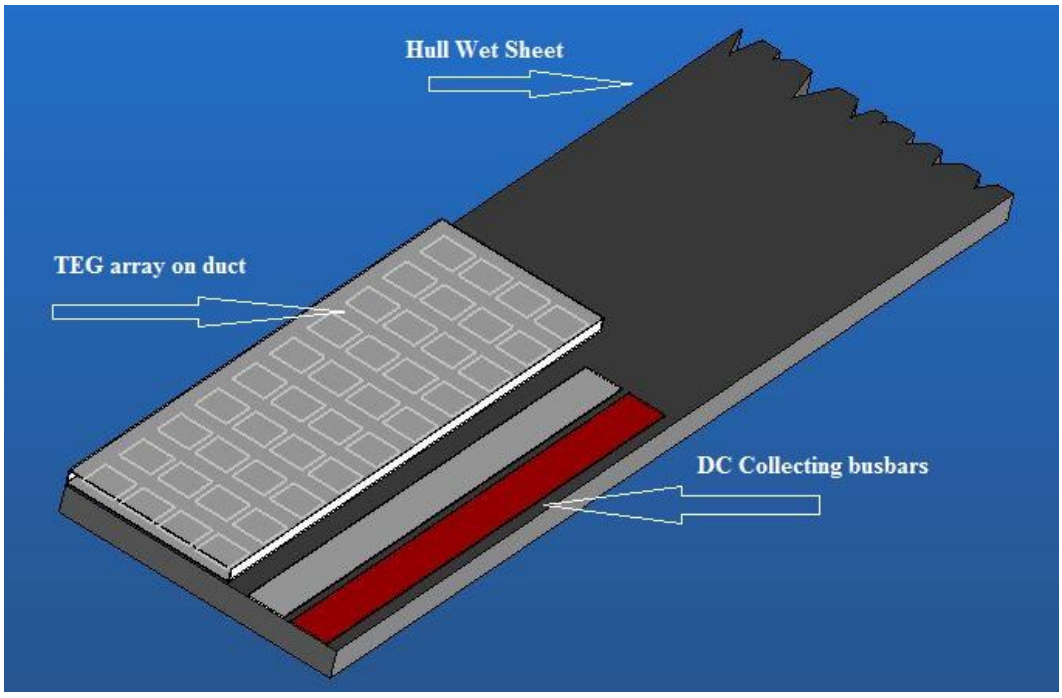

Figure 13:TEG Array on duct attached to wet sheet

The collection of the energy produced in the form of DC and its distribution is a subject strongly dependent on several factors such as:

a. The vessel's main electrical network demands and particularities
b. The type of vessel in question (Bulk carrier, tanker, cruise ship, etc)

c. The vessel's annual utilization (i.e. days at sea p.a.)

Since the early stages of this study, it was clear that the need for the full and thorough monitoring of the whole power production process. Towards this, a full-scale monitoring and switching program based on the Siemens Soft Comfort® software has been developed and is thoroughly discussed in Chapter XXXXXX.

After the general form of the duct network has been decided, the design of individual branches can commence. In the present case study, a branch of parallel topology duct branch has been designed and set up.

The brunch is then introduced to FEA (ANSYS FluidSim®) software and fed with exhaust gases. Gases varied both in their chemical syntheses as well as in their physical state of energy (pressure, temperature), in all cases within the limits given by the specific vessel's main Engine manufacturer[72]. The thermal energy transferred to the Seebeck elements, as well as the pressure and temperature drop and backpressure formed is calculated. The results, together with other parameters (i.e. seawater temperature e.t.c.) are fed to a model developed by MATLAB® Simulink® for the evaluation of the benefits resulted from the use of Seebeck arrays in terms of fuel economy and reducing the eco-footprint of the vessel's operation.

3.6 Estimation of the recovered Energy -Theoretical and Simulating approach

3.6.1 Energy transfer in turbulent flow

Turbulent flow is encountered more frequently than laminar flow, yet it is not nearly as amenable to analytical treatment. The fluid and flow variables in turbulent flow vary with time for flow in a tube (or duct with roughly the same cross-section area) is shown in fig. 14.

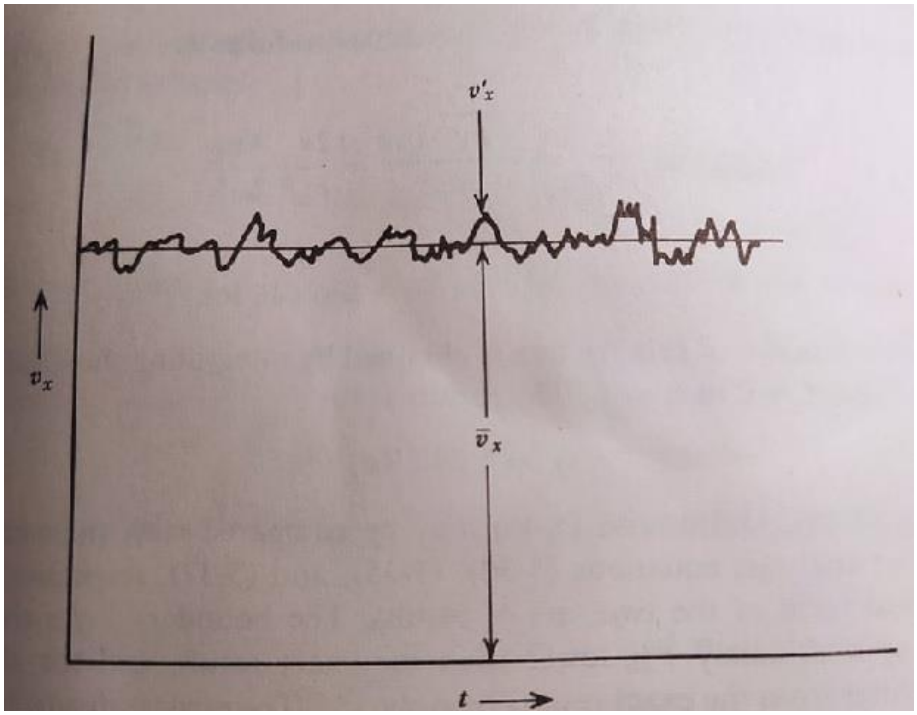

Figure 14 Average fluid velocity in turbulent flow

The mean value of velocity v_m is constant indicating steady flow in the mean; however, at any instant in time the actual velocity differs from the mean value by the relatively small amount v_x'. The mean or time-average velocity over the time interval $t_1 \leq t \leq t_2$ is represented by:

$$\bar{v}_x = \frac{1}{t_2 - t_1} \int_{t_1}^{t_2} v(x, y, z) dt$$

In terms of $\bar{v}_x$ then, the axial velocity at any time may be written as :

$$v_x(x, y, z, t) = v_x\,(x, y, z) + v_x'(x, y, z, t)$$

The time-dependent quantity on the right-hand side of the above equation is called the fluctuating velocity and is due to the local randomness and the chaotic nature of turbulent flow. These fluctuations characterize the effect on axial velocity of eddies or

"packets" of fluid particles moving in a direction normal to that of bulk flow. The period of any velocity fluctuation is quite short. Intuitively, one should expect the time average of v_x', over any reasonable time interval to be zero[73]. An integration of the above equation in time will yield the result:

$$\bar{v}_x^{'} = \frac{1}{t_2 - t_1}\int_{t_1}^{t_2} v_x^{'} dt = 0$$

This result, $\bar{v}_x^{'} = 0$, is quite reasonable since, over a long period of time the fluctuating velocity $\bar{v}_x^{'} = v_x - \bar{v}_x$ will be positive and negative in equal amounts.

No simple analytical solution exists for the case of heat transfer in turbulent pipe/duct flow[74]. However empirical expressions based on numerous experiment results correlations are widely used nowadays, especially in Finite Elements Analysis software solutions. An often used correlation for turbulent pipe flow is the Dittus-Boelter[75] equation involving the Prandtl and Nusselt numbers.

The Prandtl number (Pr) is a dimensionless number, defined as the ratio of momentum diffusivity to thermal diffusivity. The Prandtl number is given as:

$$\mathrm{Pr} = \frac{\nu}{\alpha} = \frac{\text{momentum diffusivity}}{\text{thermal diffusivity}} = \frac{\mu/\rho}{k/(c_p\rho)} = \frac{c_p\mu}{k}$$

where:

- : momentum diffusivity (kinematic viscosity), (SI units: m^2/s)
- : thermal diffusivity, (SI units: m^2/s)
- : dynamic viscosity, (SI units: Pa s = N s/m^2)
- : thermal conductivity, (SI units: W/(m·K))
- : specific heat, (SI units: J/(kg·K))
- : density, (SI units: kg/m^3).

Small values of the Prandtl number, Pr ≪ 1, means the thermal diffusivity dominates. Whereas with large values, Pr ≫ 1, the momentum diffusivity dominates the behavior. The Prandtl numbers of gases are about 1, which indicates that both momentum and heat dissipate through the fluid at about the same rate. In heat transfer problems, the Prandtl number controls the relative thickness of the momentum and thermal boundary layers. When Pr is small, it means that the heat diffuses quickly compared to the velocity[76].

The Nusselt number (**Nu**) is the ratio of convective to conductive heat transfer at a boundary in a fluid. Convection includes both advection (fluid motion) and diffusion (conduction). The conductive component is measured under the same conditions as the convective but for a hypothetically motionless fluid. It is a dimensionless number, closely related to the fluid's Rayleigh number. A Nusselt number of value one represents heat transfer by pure conduction. A value between one and 10 is characteristic of slug flow or laminar flow. A larger Nusselt number corresponds to more active convection, with turbulent flow typically in the 100–1000 range.

Nusselt number is an important parameter that can contribute to a better rate of heat exchange. It is basically a function of Reynolds and Prandtl numbers. The correlation is provided in the Dittus-Boelter equation:

$$Nu_D = 0.023 \mathrm{Re}_d^{0.8} \mathrm{Pr}^n$$

Where *Nu* = Nusselt number; *Re* = Reynolds number; *Pr* = Prandtl number;

n=0.3 if the fluid is being cooled (our case).

n=0.4 if the fluid is being heated

$Re_d > 10^4$

L/D>60 (length to hydraulic diameter ratio)

Note that several researchers have concluded lately, that the standard term of 0,023 may vary up to 0,027, as their experimental results correlations have proven the

amended equation less faulty[77]. Therefore in our calculations, the constant term will be 0,027.

If the Nusselt number is about 1, it represents that the heat transfer is conduction only, but if the value is between 1 and 10, then it shows laminar or slug flow. If the range is more, it is active convection with turbulence in the 100–10000 range. Nusselt number is a non-dimensional heat transfer coefficient.

Having all the above and using the data given in table 1 we could proceed to a theoretical estimation of the power transfer that will theoretically take place in the basic ducting elements described above.

For the case of a main extraction conductor steel tube of 0.4 m in diameter, gas fluid velocity of 35m/s, and temperature 500 ºK (227 ºC) the calculation will be as follows:

$$\mathrm{Re} = \frac{Vdr}{\mu} = \frac{35*0,4*0,696}{2,7E^{-5}} = 360888.88$$

$$\mathrm{Pr} = \frac{C_p * \mu}{\lambda} = \frac{1,009*2,7\mathrm{E}^{-5}}{0,0404} = 6,74\mathrm{E}^{-4}$$

$$Nu = 0,027*\mathrm{Re}^{0.8}*\mathrm{Pr}^{0,33} = 0,027*360888.88^{0,8}*6,74E^{0,33} = 67,72$$

Hence, the theoretical heat transfer per area and degree C will be:

$$P = \frac{Nu*\lambda}{D} = \frac{67,72*0,0404}{0,4} = 6,84\frac{W}{m^2\,{}^oC}$$

And for the minimum temperature of 227 ºC, (well above the dew point), the heat transfer will be:

$$H_{(227)} = P*T = 6,84*227 = 1552,68\frac{W}{m^2}$$

Following the above algorithm for various temperatures and the proposed Hydraulic diameters, the following table will be produced:

Table 9: Total Power transferred per m^2 for the specific geometry of ducts, Vs the flue gas temperature

(V) Velocity (m/s)	(μ) Viscosity (Pa.s)	(Cp) Specific Heat (KJ)	(D) Diameter / Hydraulic Dia (m)	(p) Density (Kg/m^3)	(λ or K) Thermal Conductivity of Fluid (W/mK)	Fluid temp. °C	Power transferred (W/m^2* °C)	Total power transferred in KW per m^2
35	0,000027	1,03	0,400	0,696	0,0404	227	6,13	1,39
35	0,000037	1,099	0,400	0,435	0,0577	527	5,29	2,79

A thorough practical case study estimation of the recovered energy for a specific vessel and a specific trip is presented in the following Chapter.[78]

3.6.2 Mathematical modeling of the application

Thermo-electrical Phenomena modeling

As already mentioned in Chapter 1, five energy phenomena take place in the TEM chips: (1) Joule heating, (2) Thermal conduction, (3) Peltier heating/cooling, (4) Seebeck effect, and (5) Thompson effect. The last effect is small enough to be neglected in the next derivations.

A. Seebeck effect modeling[79]*:* As explained in Chapter 1, Seebeck effect is the generation of a difference of the potential between two dissimilar materials when imposed to a temperature gradient. The TEM Seebeck voltage also called EMF and open-circuit voltage is the multiplication of the Seebeck coefficient, α (V / K), with the temperature gradient applied on a pn chip, and is expressed by:

$$V_{OC} = \alpha \, \Delta T$$

where $\alpha = \alpha_p - \alpha_n$ and $\Delta T = T_{hot} - T_{cold}$

For a TEM composed of N p-n chip pairs, the EMF of the TEM becomes:

$$V_{TEM} = \alpha_{total} * \Delta T$$

where $\alpha_{total} = N * \alpha$

B. Peltier heating/cooling effect

This phenomenon results in heat absorption/dissipation due to the flow of current through a junction of two dissimilar materials. TEM Peltier effect can be modelled as:

$$Q_{a/d} = a_{total} * T_{hot/cold} * I$$

where, $Thot{=}cold(K)$ is the hot and cold temperatures, and $I(A)$ is the current passing through the material.

C. Joule heating effect

Joule heating is the phenomenon that appears when current flows through a resistive (semiconductor) element. The heat dissipated from this effect is described as:

$$Q_{joule} = I^2 * R_E * t$$

where R_E is the electrical resistance of the semiconductor, and t the time the phenomenon occurs.

D. Thermal conduction effect

Also known as the Fourier process, this phenomenon describes the thermal conductivity or resistivity through a material. The heat transfer of thermal conduction in a TEM is presented as:

$$Q_{p,n}(x) = -\frac{A_{p,n}}{\rho_{T,p,n}} \frac{dT_{p,n}(x)}{dx}$$
$$\simeq -\left(\frac{A_p}{\rho_{T,p} L_p} + \frac{A_n}{\rho_{T,n} L_n}\right)\Delta T = -\frac{\Delta T}{R_T}$$

where,

• $A_p(m^2)$ and $A_n(m^2)$ are the cross-sectional areas of p and n-type pellets,

• $L_p(m)$ and $L_n(m)$ are the lengths of p- and n-type pellets,

• $\rho_{T,p}\,(mK/W)$ and $\rho_{T,n}(mK/W)$ are the thermal resistivities of the p- and n-type respectively.

Teg modeling

As mentioned in Chapter1, TEGs consist of several arrays of n-p semiconductors connected electrically in series and thermally in parallel.

The electrical resistance, *RE*(Ω), and the thermal resistance, *RT* (*K*=*W*), of a p- and n-type pellets are given by[80] :

In series: $$R_E = R_{E,p} + R_{E,n} = \rho_{E,p}\frac{L_p}{A_p} + \rho_{E,n}\frac{L_n}{A_n}$$ (electrical)

Parallel $$R_T = R_{T,p} \| R_{T,n} = \frac{\rho_{T,p}L_p\rho_{T,n}L_n}{\rho_{T,p}L_pA_n + \rho_{T,n}L_nA_p}$$ (thermal)

Where,

• $R_{E;p}$ and $R_{E,n}$ are the electrical resistance values of the p- and n-type pellets

• $\rho_{E,p}$(Ωm) and $\rho_{E,n}$(Ωm) are the electrical resistivity values of the p- and n-type respectively.

A. TEG thermal modeling

Along the length, *L*, of a pellet pair, the variation of heat flow is given by the conduction at a distance *dx* from the initial position *x*, where its differential equation can be derived as:

$$dQ_{p,n}(x) = Q_{p,n}(x+dx) - Q_{p,n}(x) = I_{TEM}^2 dR_{E_{p,n}}(x)$$

where

$Q_{p,n}$ is the conduction heat flow and $I_{TEM}{}^2 * RE_{p,n}$ represents the joule heating generated by the flow of current, I_{TEM}, in the partial resistance of length *x* of the p- and n-type, given by

$$dR_{E_{p,n}}(x) = \rho_{p,n}\frac{dx_{p,n}}{A_{p,n}}$$

According to Equation 7 and Fourier heat given in Equation 5 and by using the temperature boundary condition $T_{p,n}(0) = T_{hot}$ and $T_{p,n}(L) = T_{cold}$, the heat conduction rate at the hot and the cold junctions of the n-type and p-type pellets are described as:

$$Q_p(0) = \frac{T_{hot} - T_{cold}}{R_{T,p}} - \frac{I_{TEM}^2 R_{E,p}}{2}$$
$$Q_p(L) = \frac{T_{hot} - T_{cold}}{R_{T,p}} + \frac{I_{TEM}^2 R_{E,p}}{2}$$

$$Q_n(0) = \frac{T_{hot} - T_{cold}}{R_{T,n}} - \frac{I_{TEM}^2 R_{E,n}}{2}$$
$$Q_n(L) = \frac{T_{hot} - T_{cold}}{R_{T,n}} + \frac{I_{TEM}^2 R_{E,n}}{2}$$

Introducing the Peltier terms $\alpha I_{TEM} T_{hot}$ and $\alpha I_{TEM} T_{cold}$ at the two boundary points, the rate of heat transfer from the heat source to the single-couple TEG and from the device to the heat sink can be derived as:

$$Q_{hot} = Q_p(0) + Q_n(0) + \alpha I_{TEM} T_{hot}$$
$$Q_{cold} = Q_p(L) + Q_n(L) + \alpha I_{TEM} T_{cold}$$

Substituting the Quantities $Q_p(0)$, $Q_n(0)$, $Q_p(L)$ and $Q_n(L)$ we have:

$$Q_{hot} = \frac{T_{hot} - T_{cold}}{R_T} - \frac{I_{TEM}^2 R_E}{2} + \alpha I_{TEM} T_{hot}$$
$$Q_{cold} = \frac{T_{hot} - T_{cold}}{R_T} + \frac{I_{TEM}^2 R_E}{2} + \alpha I_{TEM} T_{cold}$$

The above equations describe the heat transfer of one pair of TEM. For N pairs the equations become:

$$Q_{hot} = \frac{T_{hot} - T_{cold}}{R_{TEM,T}} - \frac{I_{TEM}^2 R_{TEM,E}}{2} + \alpha_{total} I_{TEM} T_{hot}$$

$$Q_{cold} = \frac{T_{hot} - T_{cold}}{R_{TEM,T}} + \frac{I_{TEM}^2 R_{TEM,E}}{2} + \alpha_{total} I_{TEM} T_{cold}$$

Where:

$R_{TEM,T}$ = *RT* tal electrical resistance.

B. TEM electrical modeling

A TEG connected to an external load could be presented by the following schematic:

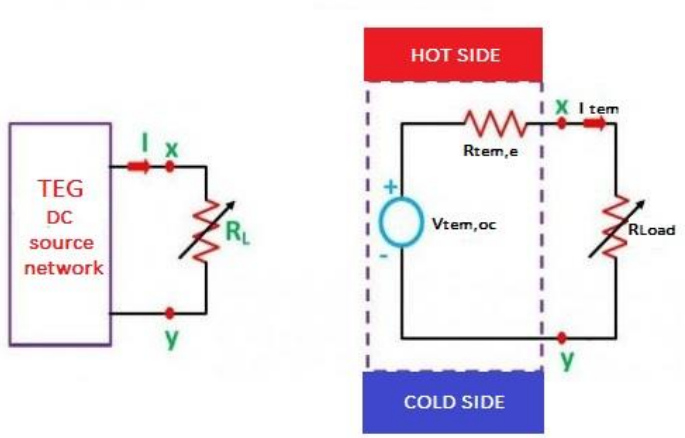

Figure 15: TEG Connected to load (schematic)

The electrical power generated by the TEG is proportional to the difference in the hot- and cold-side temperature (ΔT) and can be initially expressed as:

$$P = f(\Delta T)$$

In Electrical terms, a TEG element connected to a load R_{load} and supplying DC on it can be presented as a real-world battery, having an EMF ($V_{TEM, OC}$) and an internal

Resistance $R_{TEM,E}$, both connected in series with the load and through all of them passing the same current, causing a voltage drop on the load (V_{tem}). Then, according to Ohm's Law in the closed-circuit we have:

$$V_{TEM} = V_{TEM,OC} - I_{TEM} R_{TEM,E}$$

If we multiply by I_{TEM} both sides of the above equation we end up with the equation of DC Power in the full circuit:

$$V_{TEM} I_{TEM} = V_{TEM,OC} I_{TEM} - I_{TEM}^2 R_{TEM,E}$$

which gives us the "useful" power, dissipated on the load.

This last equation of power is a parabolic function of the form $Y = aX\text{-}bX^2$, which is physically reasonable only if $a > bX$ or when $\alpha_{total}\Delta T > I_{TEM} R_{TEM,E}$.
In physical terms that means that we cannot have any useful power (as a product of Voltage and Current) if the voltage produced by the Seebeck element as a*ΔT is lower than the one being consumed in its internal resistance.
Mathematically, it can be easily derived from the previous equation that the power on the Load is zero on two points:

1. When I_{TEM}= 0, (the obvious case of open-circuit) or,
2. When $I_{TEM} = V_{TEM,OC} / R_{TEM,E}$ (which obviously again is the case of short circuit).

Although in the real-world application this is practically never the case, it might be useful to derive the maximum power point which can be achieved by the application of the Rolle theorem[81] i.e. by setting the 1st derivative of the Power vs Current to zero.

$$I_{TEM} = I_{TEM}^{op,P}\Big|_{\frac{dP_{TEM}}{dI_{TEM}}=0} = \frac{V_{TEM,OC}}{2R_{TEM,E}}$$

where $\frac{dP_{TEM}}{dI_{TEM}} = V_{TEM,OC} - 2I_{TEM}*R_{TEM,E}$ and $I_{TEM}^{op,P}$ is the optimum current leading to the maximum power which can be calculated by replacing $I_{TEM}^{op,P}$ to the previous Eq.

$$P_{max}\Big|_{I_{TEM}=I_{TEM}^{op,P}} = \frac{V_{TEM,OC}^2}{4R_{TEM,E}}$$

This practically means that the maximum power transfer we can have is when we have a total Resistance in the closed-circuit equal to 2 times the Internal Resistance of the TEG ($R_{TEM,E}$). This leads to the conclusion that we have maximum power transfer when the Load matches the internal resistance of the TEG, or in practical cases of the whole TEG array, which obviously is not the case in practical applications where the load changes all the time. This is the application of the well-known "maximum power transfer theorem"[82]. We would have come to the same conclusion by replacing I_{TEM} by $(V_{TEM,OC} - V_{TEM})/R_{TEM,E}$ and deriving (and setting the derivative equal to zero) the Power equation which would occur:

$$P_{TEM} = \frac{V_{TEM,OC}V_{TEM} - V_{TEM}^2}{R_{TEM,E}}$$

Which, following the same algorithm as with current, will end up to the conclusion that the maximum power will be transferred to the load when R_L equals the internal R of the TEG or TEG array.

3.6.3 Modelling of the application by means of MATLAB® Simulink®.

The magnitude and the cost of a true scale or even near true scale simulation of a TEG network on a real vessel is such, as to make the extended use of simulation and mathematical modeling a necessity. At the earliest stage of this research, it became clear that the most suitable modeling method for the simulation and the evaluation of the efficiency of the system is the MATLAB® Simulink®. Upon the conclusion of this research, several models of the system have been developed and studied. The most important part of the modeling procedure is the forming and development of a large number of subsystems.

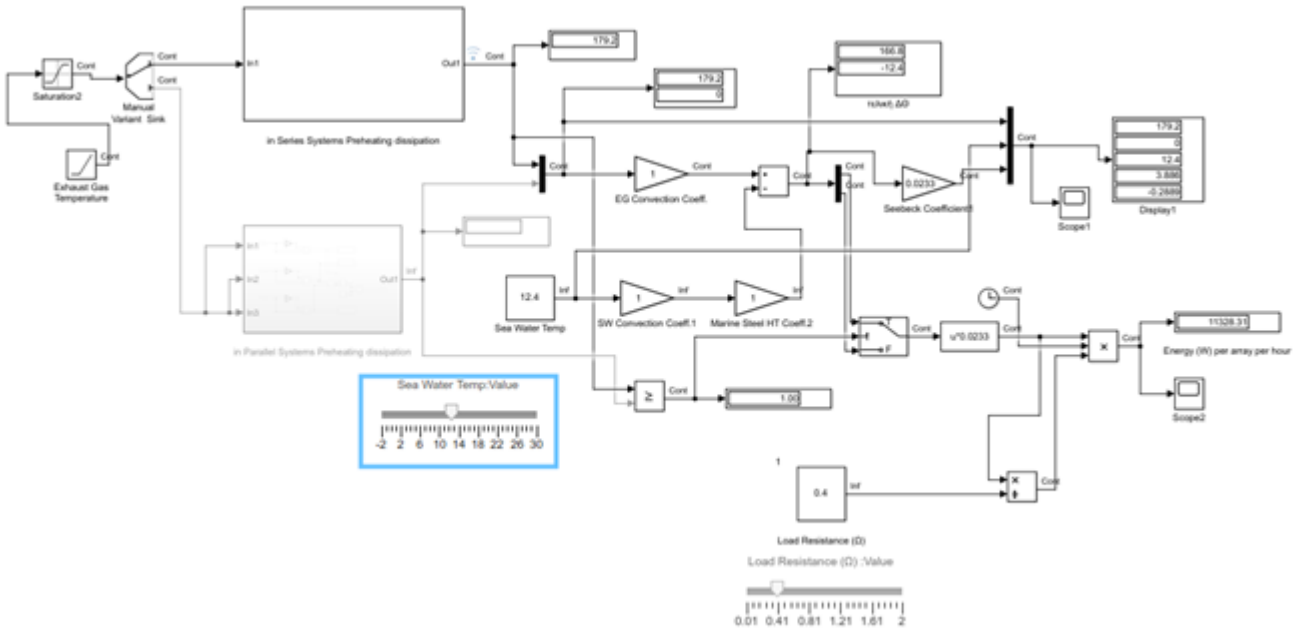

Figure 16:Vessel's TEG array network modeling: Part A' Core model routine (partial)

The model finally created and was thoroughly tested is being described in the Appendix. The model gives the operator the ability to change all critical parameters as follows:

The Sea Water Temperature

The Exhaust Gas Temperature

The Seebeck Coefficient of the TEG Chip in use

The Internal Resistance of the TEG Chip in use

The Resistance of the load attached to the array

The model then returns answers regarding:

The Power applied to the Load

The total Energy dissipated on the load over time

The maximum voltage produced by the array

The maximum voltage produced by each element

The full code of the Model is given in the Appendix of this Thesis in order to enable the reader to reproduce and run it. All parameters and crucial factors are editable providing the programmer with the ability to examine multiple waste heat recovery le scenarios.

CHAPTER 4: Thermal and Fluid Dynamics simulation

4.1. Simulating the arrays

The following two figures show the Ship's general arrangement, in the bow section, and a typical web cross-sectional cut, being quite typical for contemporary ships of this kind. Based on that, there are two basic geometries the duct system could follow the topologies proposed: parallel and series, depicting the routing of the gases inside the ducting system. It has to be mentioned again, that an exact design of a "real world" duct system is beyond the scope of this dissertation, as this is a matter highly dependable on several design parameters, distinctive for each vessel, and sometimes –inevitably- for different parts of the same vessel.

A thorough CFD study analysis for each duct arrangement took place during the design stage of a real case application scenario, incorporating both FEA and modelling techniques. A series of thermal conduction simulations were run in order to estimate the efficiency of the cooling by their attachment to the inner side of the hull plates, when ship was sailing at its rated speed when fully loaded.

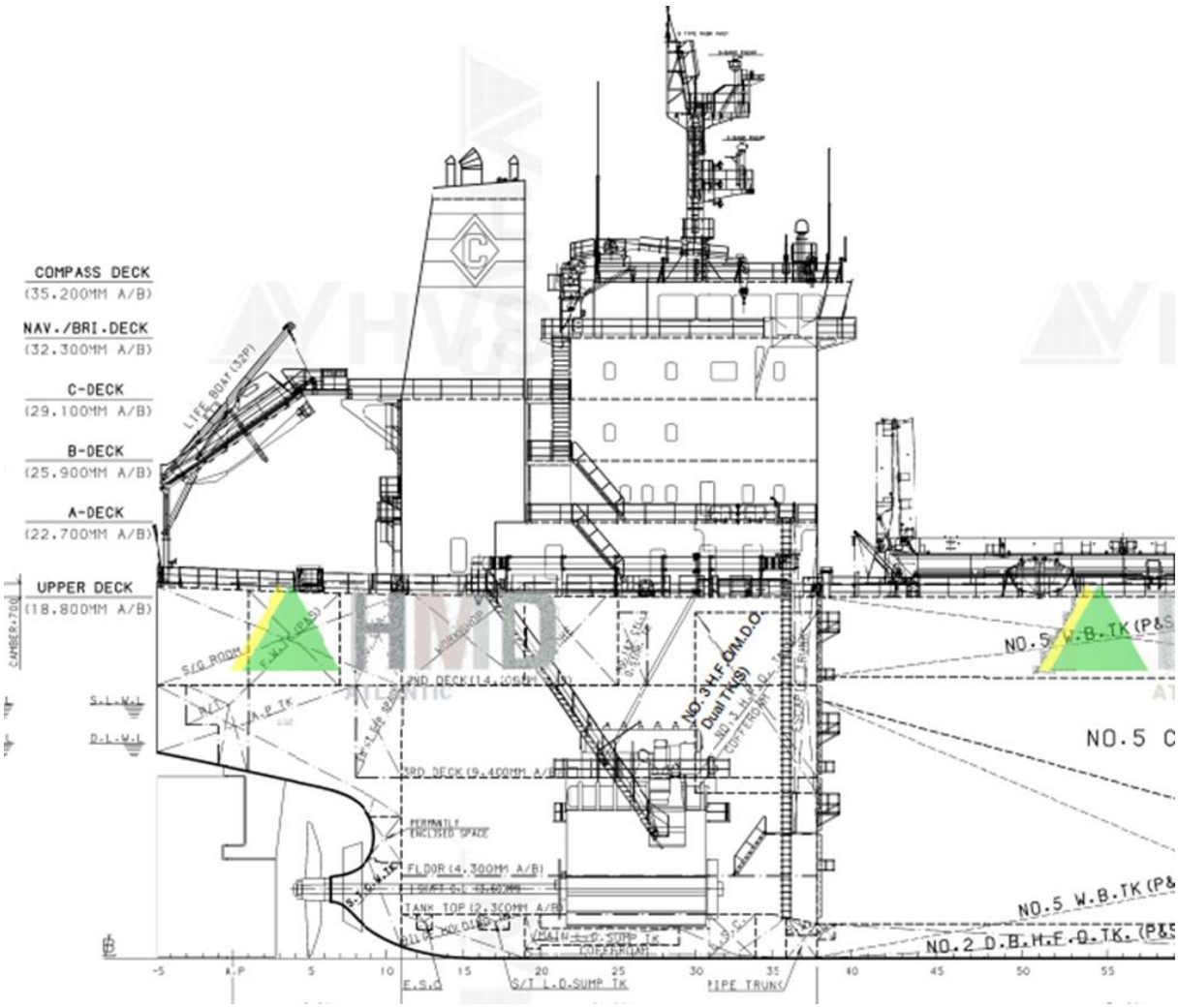

Figure 17: Desert Challenger General Arrangement Plan, Bow Section. Courtesy Atlantic Bulk Carriers Shipping

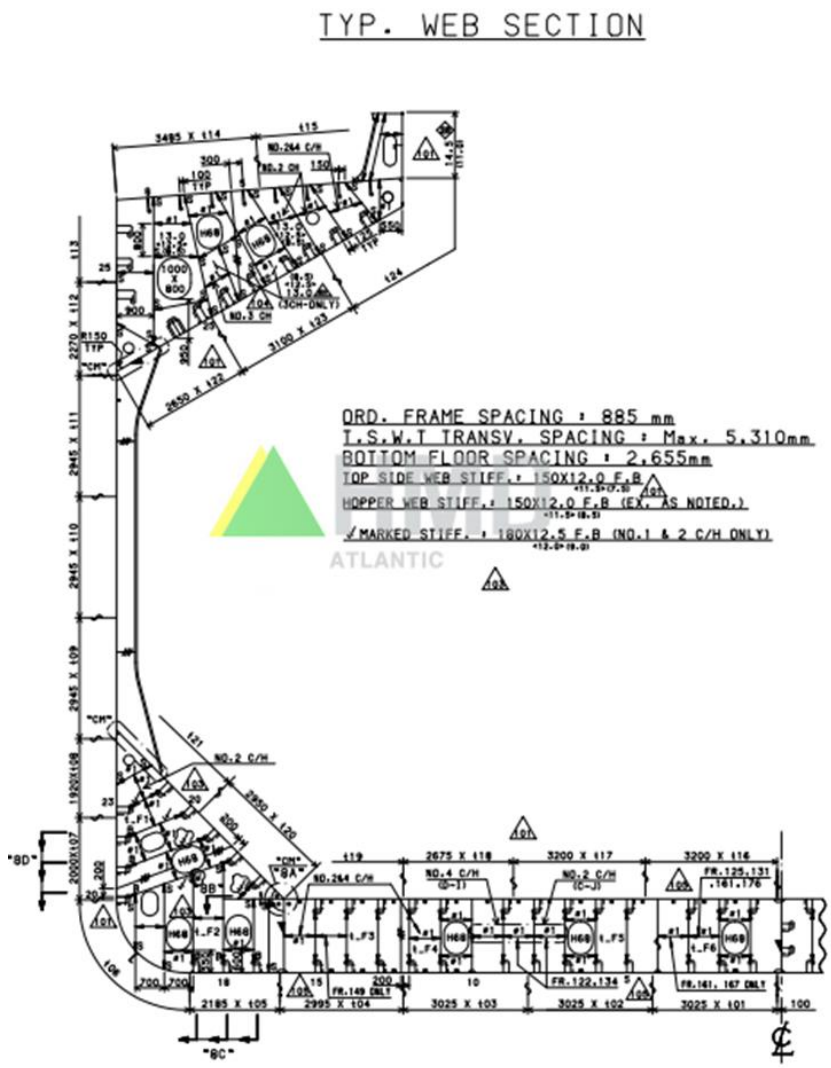

Figure 18: Desert Challenger. Typical Web Section Plan. Courtesy Atlantic Bulk Carriers

A CFD analysis of both, parallel and series configurations was run using ANSYS® CFD software, during this research and the results have shown that effective ducting design is both feasible and necessary to maintain backpressure values within the acceptable limits. The CFD and thermal behavior of the Flue gases is given in the following pages:

4.1.1 Flue Gas CFD simulation

In line configuration

Mesh

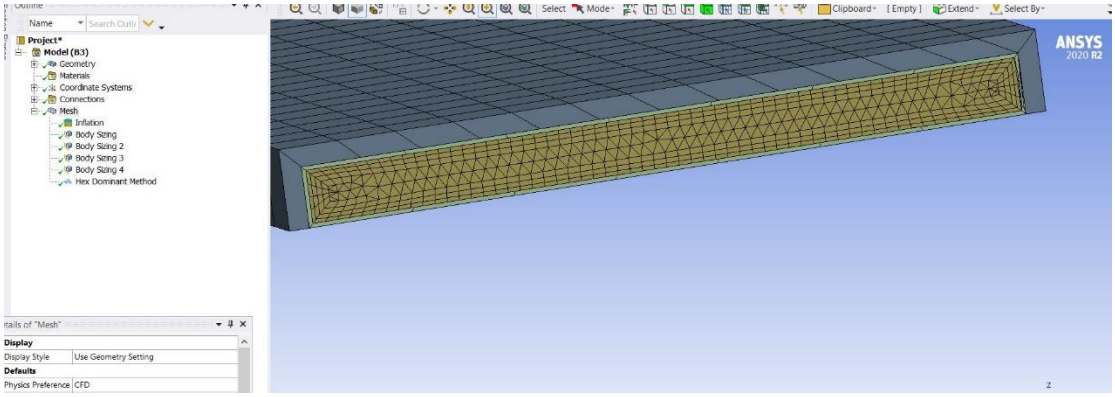

Figure 19: Main duct meshing detail

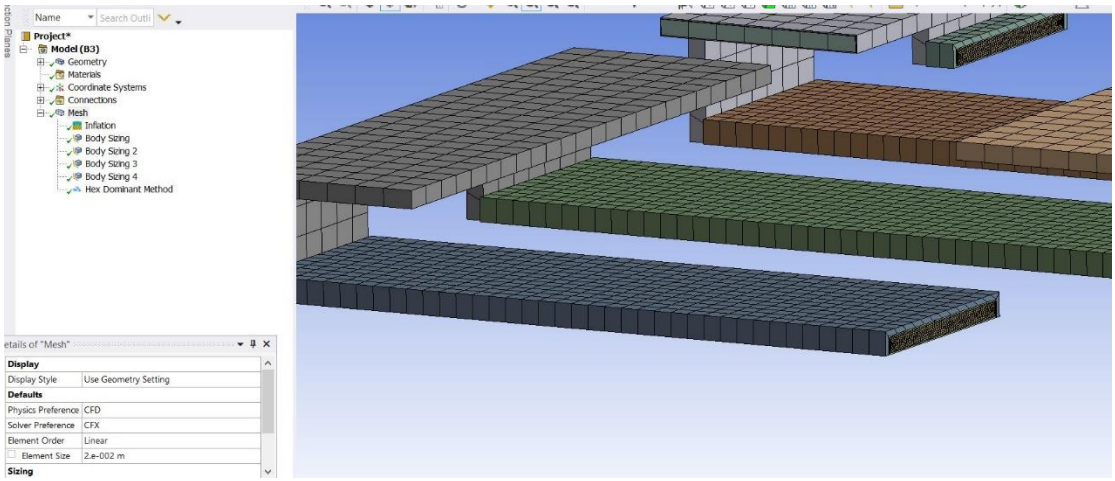

Figure 20: Meshing view of the parallel configuration assembly

Meshing details are as follows:

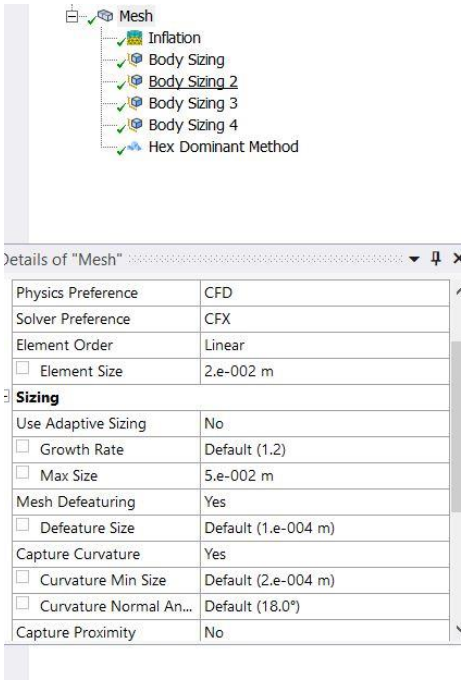

As the turbulence phenomena are denser near the duct walls, meshing should be denser there. This is done using the “inflation” command.

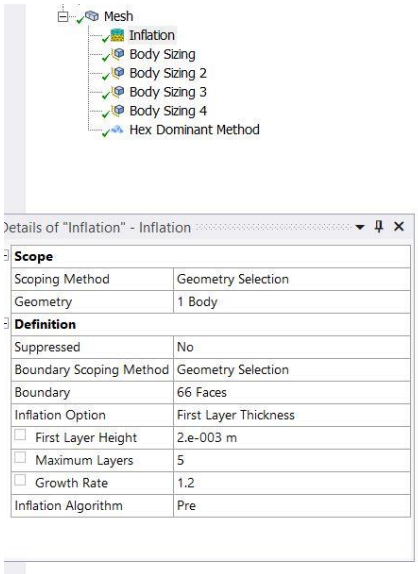

The body sizing below refers to the environment mesh. In general, since it is actually, a solid domain, it does not need to be that dense in order to enable a faster program elaboration time. If it was denser, the difference would be negligible, since it mainly affects the temperature. In contrast, the fluid domain is dense as it should be.

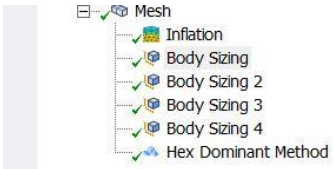

Details of "Body Sizing" - Sizing

Scope	
Scoping Method	Geometry Selection
Geometry	1 Body
Definition	
Suppressed	No
Type	Element Size
Element Size	6.e-002 m
Advanced	
Defeature Size	Default (1.e-004 m)
Behavior	Soft
Growth Rate	Default (1.2)
Capture Curvature	No
Capture Proximity	No

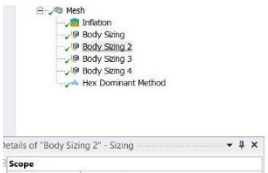

Details of "Body Sizing 2" - Sizing

Scope	
Scoping Method	Geometry Selection
Geometry	9 Bodies
Definition	
Suppressed	No
Type	Element Size
Element Size	5.e-002 m
Advanced	
Defeature Size	Default (1.e-004 m)
Behavior	Soft
Growth Rate	Default (1.2)
Capture Curvature	No
Capture Proximity	No

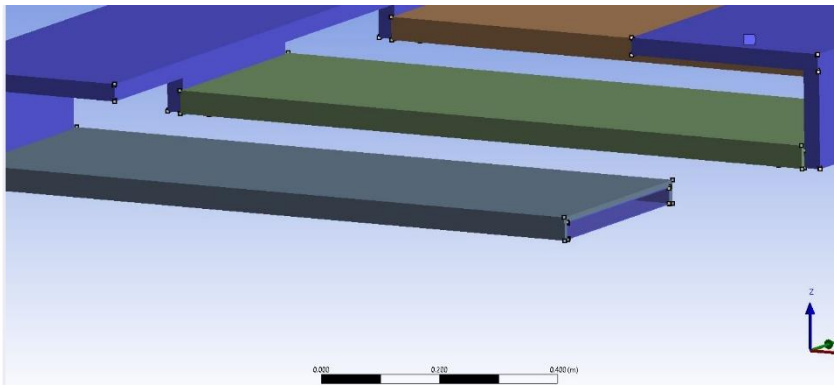

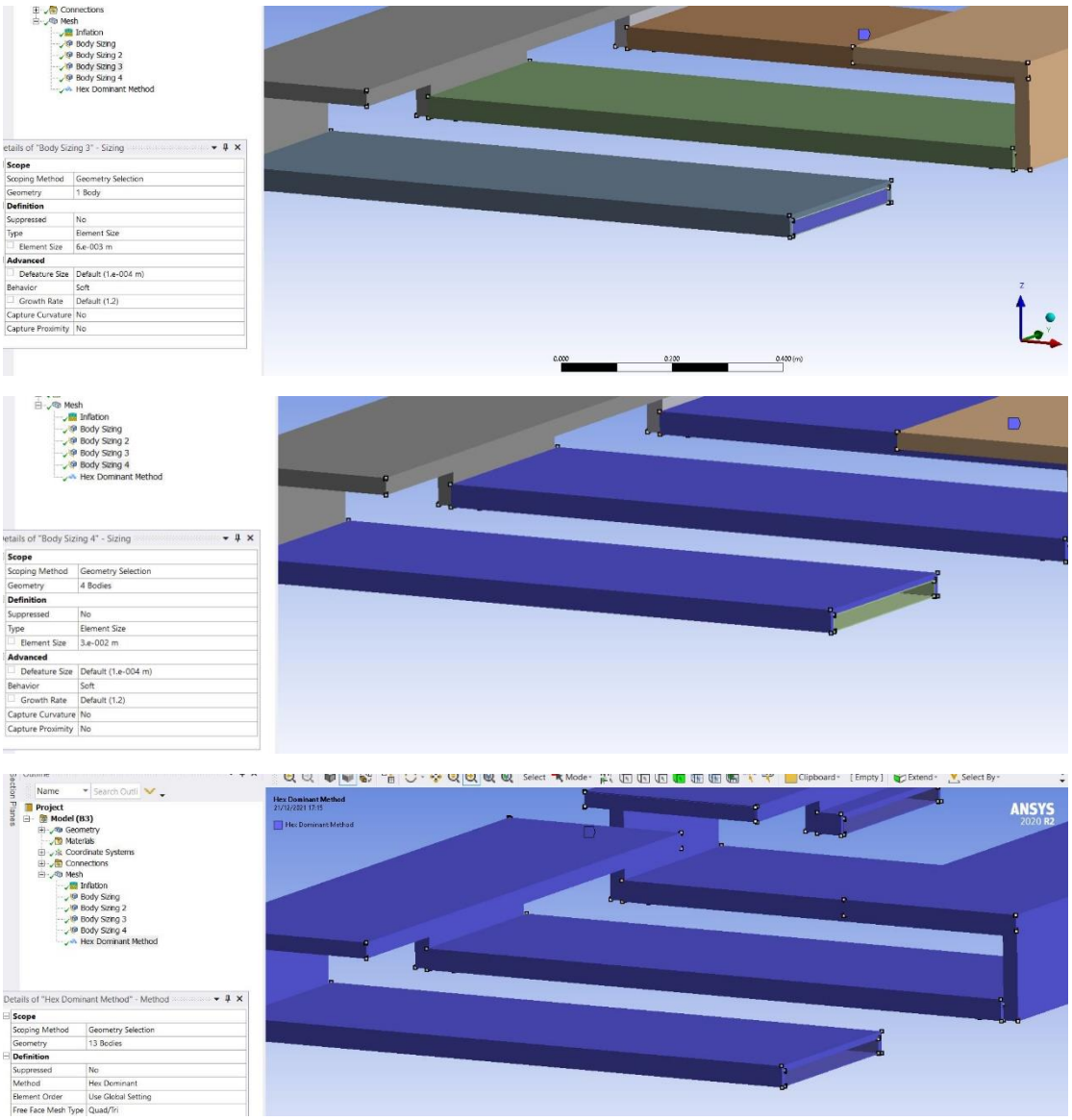

Figure 21: Body sizing of the environmental conditions (Group Figures, Engine room)

Setup

Where the inlet boundary condition is shown in the figure, is set to a speed of 0.1 km/h, (i.e. apnea[83]) was simply entered for CFD running purposes. The blue arrows are opening conditions and the environment has a temperature of 35 degrees C and 1 bar pressure[84].

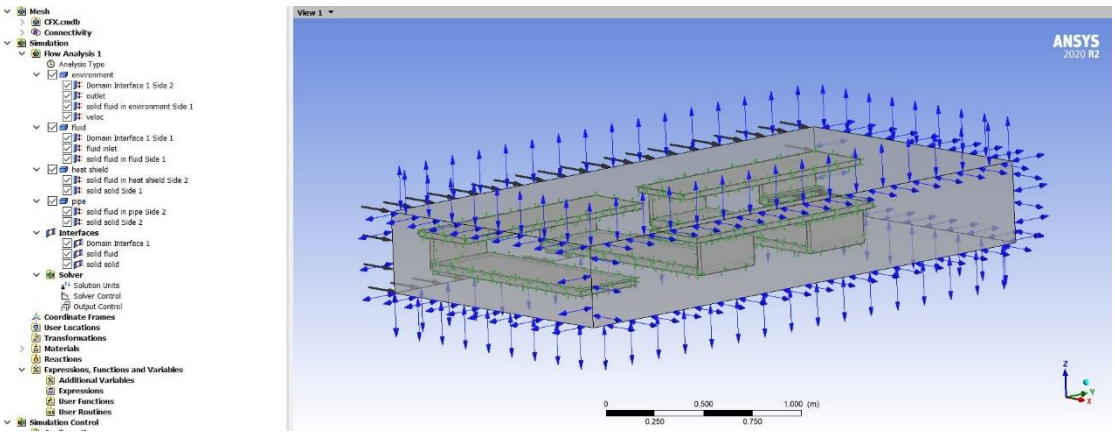

Figure 22: Environmental Conditions Setup (Vessel's Inner)

<u>Input gas velocity set at 35 m/s</u>

Total wall clock time: 1.488E+04 seconds

or: (0: 4: 7: 57.670)

(Days: Hours: Minutes: Seconds)

With the following command set, the total pressure at the outlet and inlet respectively is obtained:

=massFlowAve(Total Pressure)@(output) = 1.007e+5 [Pa]

= massFlowAve(Total Pressure)@(input) = 1.079e+5 [Pa]

Drop: 0.072e+5 [Pa]

With the following command set, the total temperature at the outlet and inlet respectively is obtained:

=massFlowAve(Total Temperature)@(output) = 4.268e+2 [K]

= massFlowAve(Total Temperature)@(input) = 5.080e+2 [K]

Drop: 0.812e+2 [K]

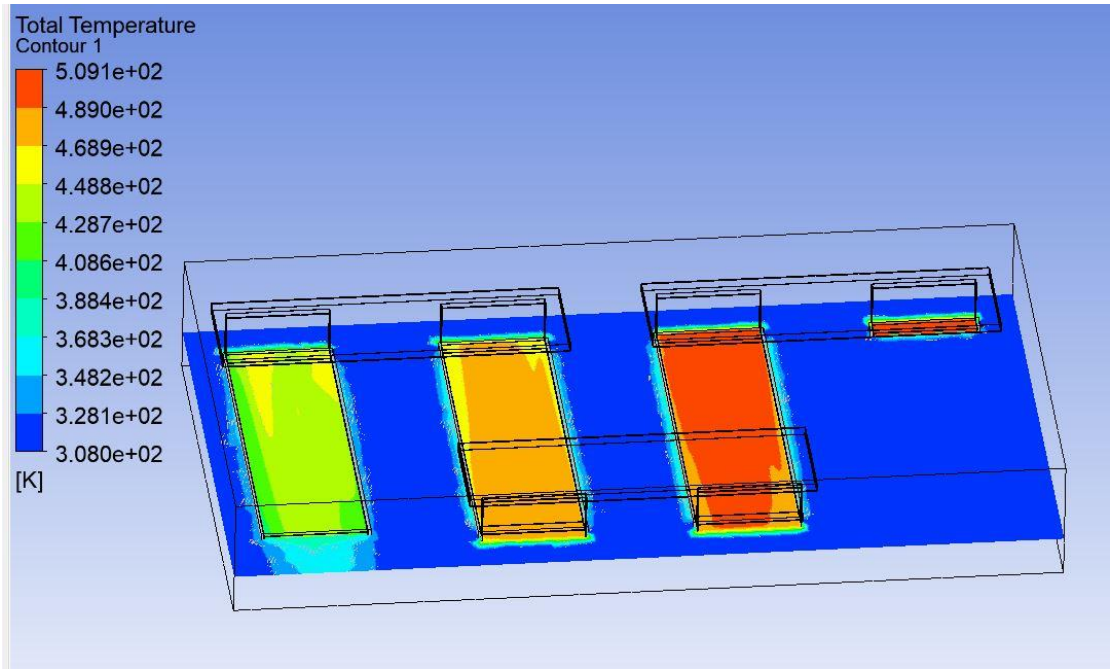

Figure 23: In series Arrangement: Total Temperature Contour

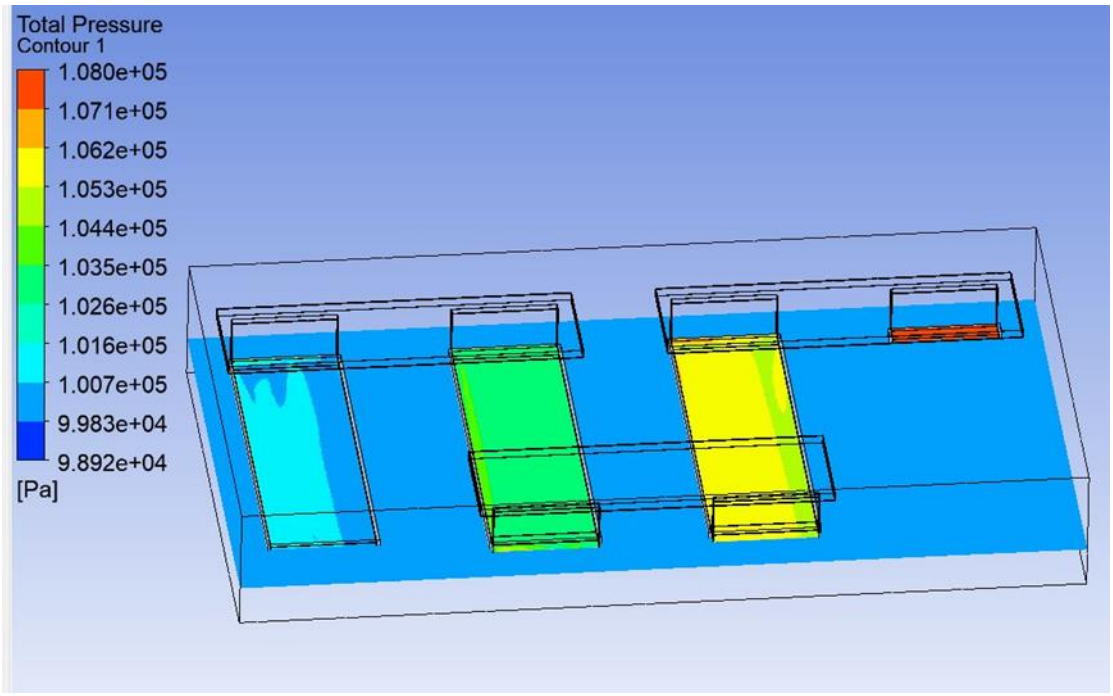

Figure 23: In Series Arrangement: Total Pressure Contour

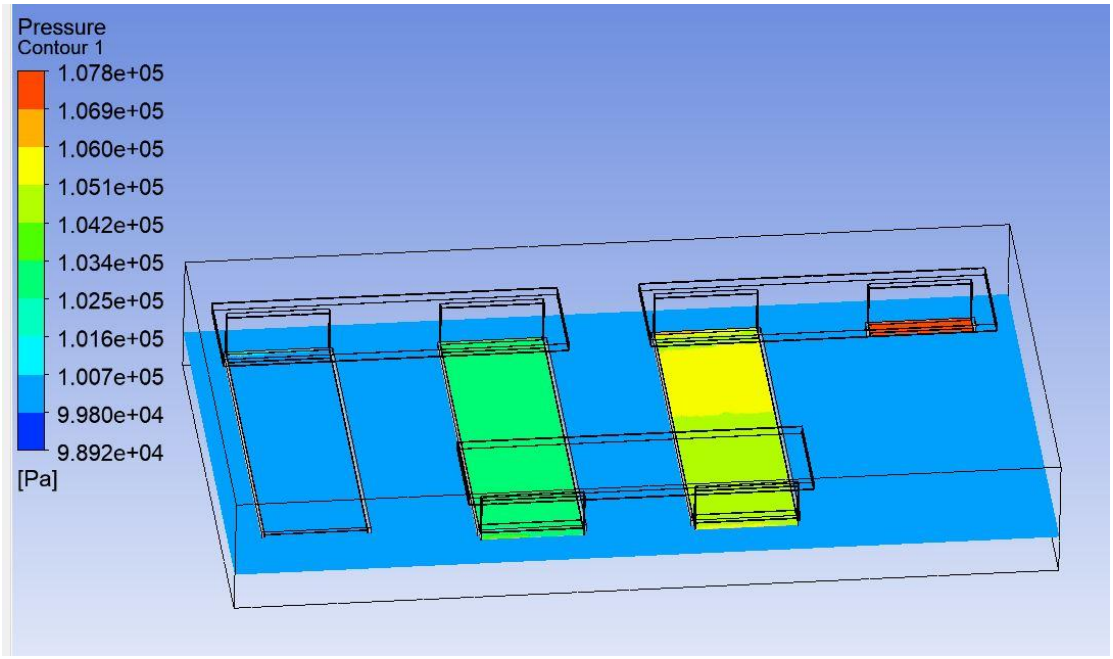

Figure 24: In Series Arrangement: Pressure Contour

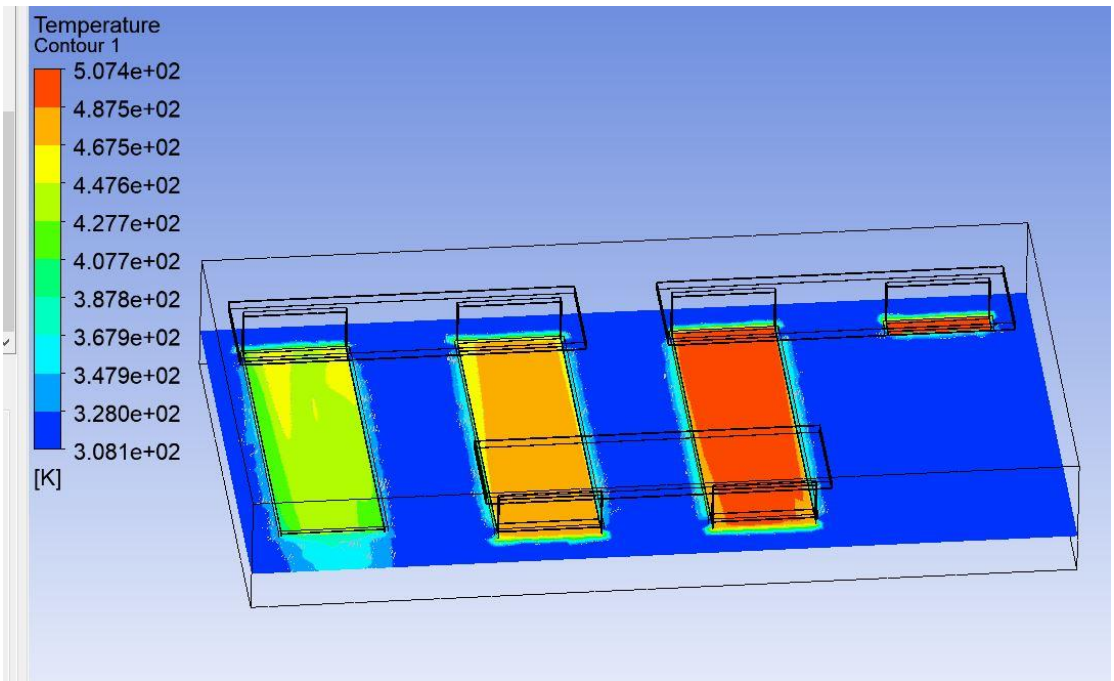

Figure 24: Arrangement: Temperature Contour

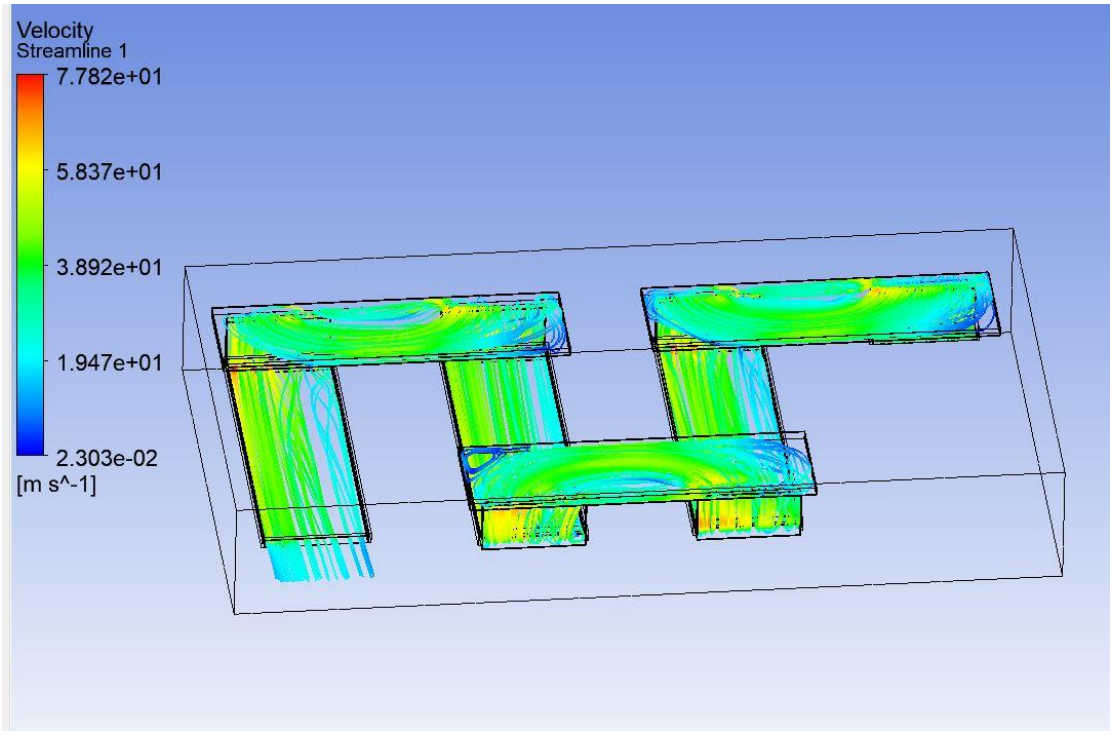

Figure 25:In Series Arrangement Gas Velocity Streamline (View1)

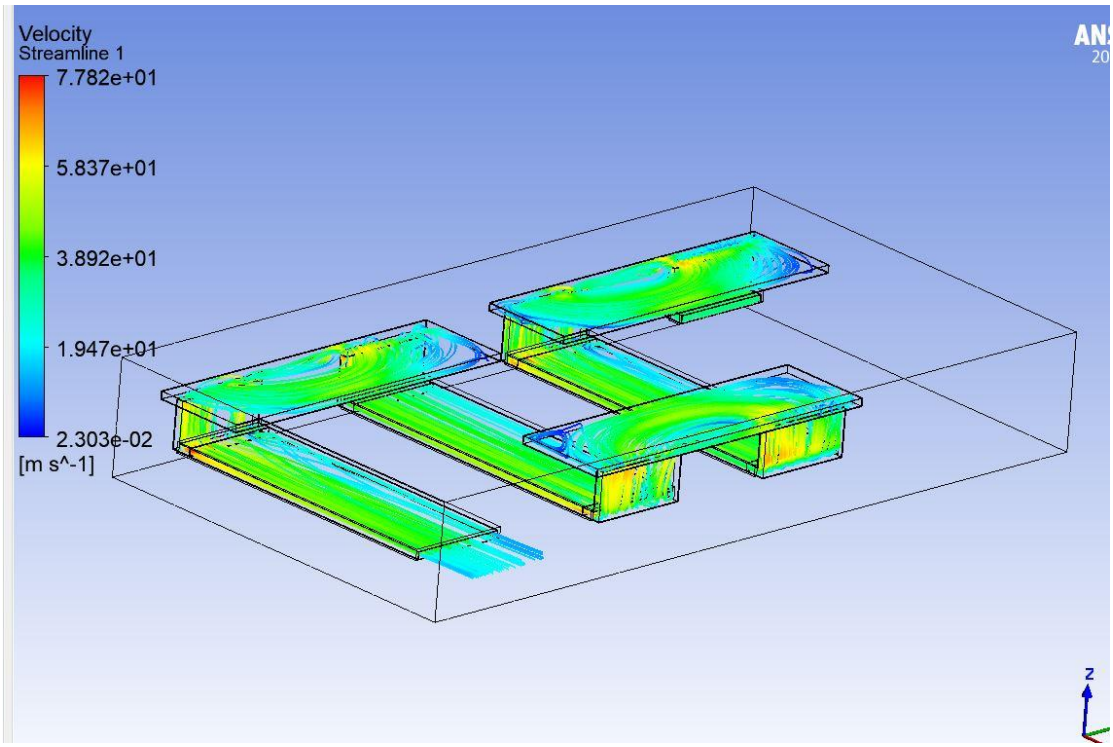

Figure 26; In Series Arrangement Gas Velocity Streamline (View2)

Inlet Condition: Total pressure set at 2.5 bar

Total wall clock time: 5.778E+04 seconds

or: (0: 16: 3: 4.586)

(Days: Hours: Minutes: Seconds)

With the following command set, the total pressure at the outlet and inlet respectively is obtained:

=massFlowAve(Total Pressure)@(output) = 1.145e+5 [Pa]

= massFlowAve(Total Pressure)@(Input) = 2.500e+5 [Pa]

Difference: 1.355e+5 [Pa]

With the following command set, the total temperature at the outlet and inlet respectively is obtained:

=massFlowAve(Total Temperature)@(outlet) = 5.054e+2 [K]

= massFlowAve(Total Temperature)@(inlet) = 5.080e+2 [K]

Drop: 0.026e+2 [K]

The gas velocity at the outlet is obtained:

=massFlowAve(Velocity)@(outlet)= 1.620e+2 [m s^-1]

The following images give a visual depiction of the Pressure and Temperature contours in the series configuration.

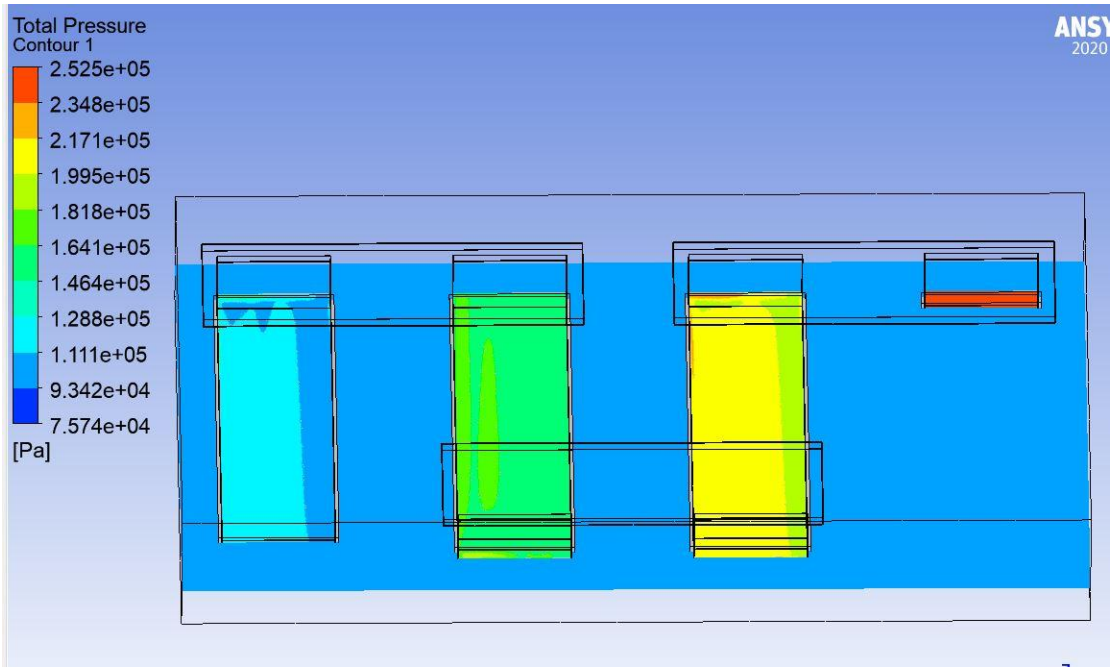

Figure 27: In series arrangement Total Pressure Contour -Initial pressure set to 2.5 bar

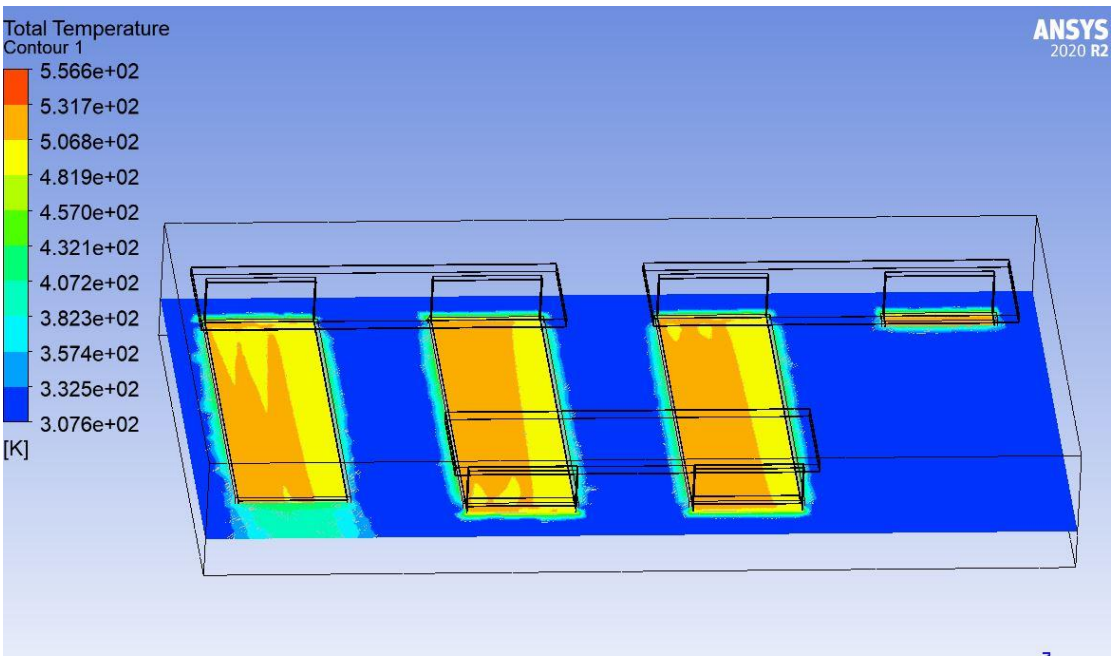

Figure 28: In series arrangement Total Temperature Contour -Initial pressure set to 2.5 bar

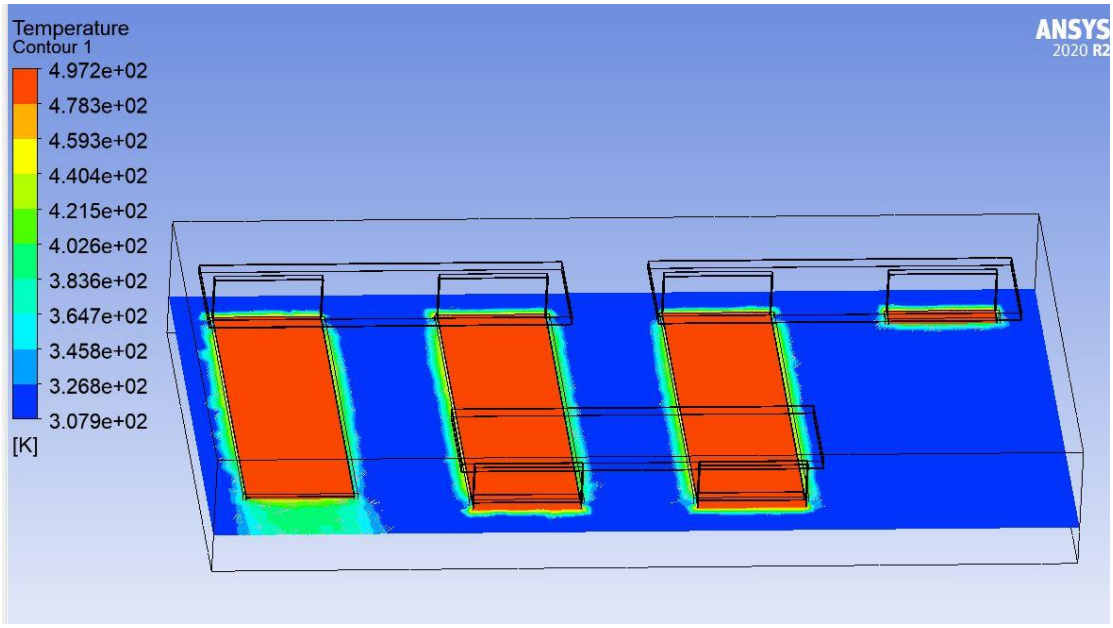

Figure 29: In series arrangement Settle downTemperature Contour -Initial pressure set to 2.5 bar

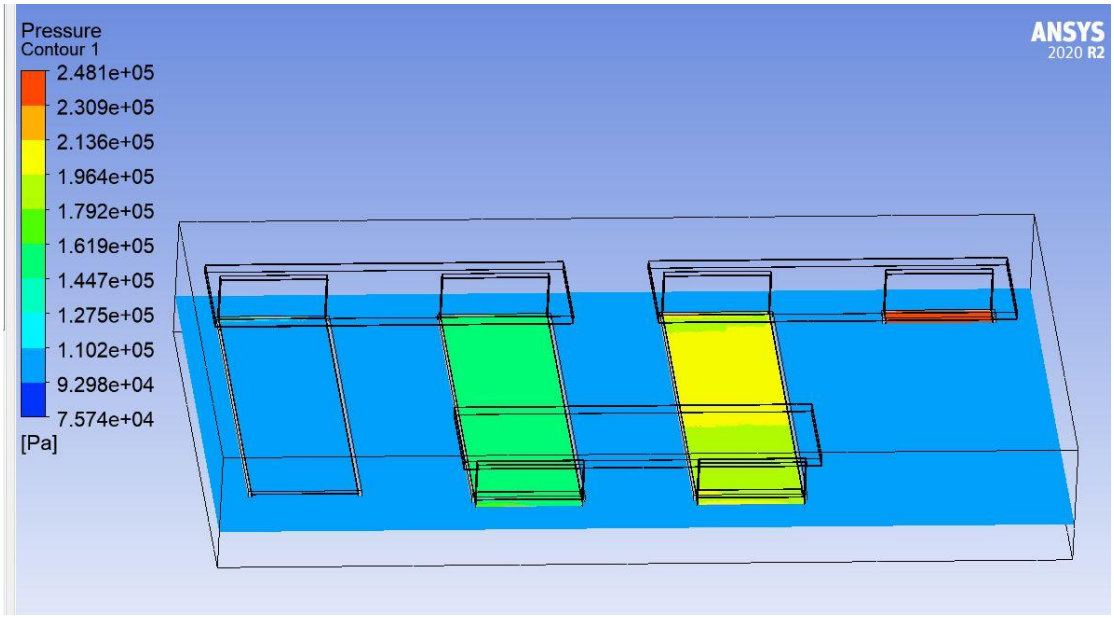

Figure 30: In series arrangement settle down Pressure Contour -Initial pressure set to 2.5 bar

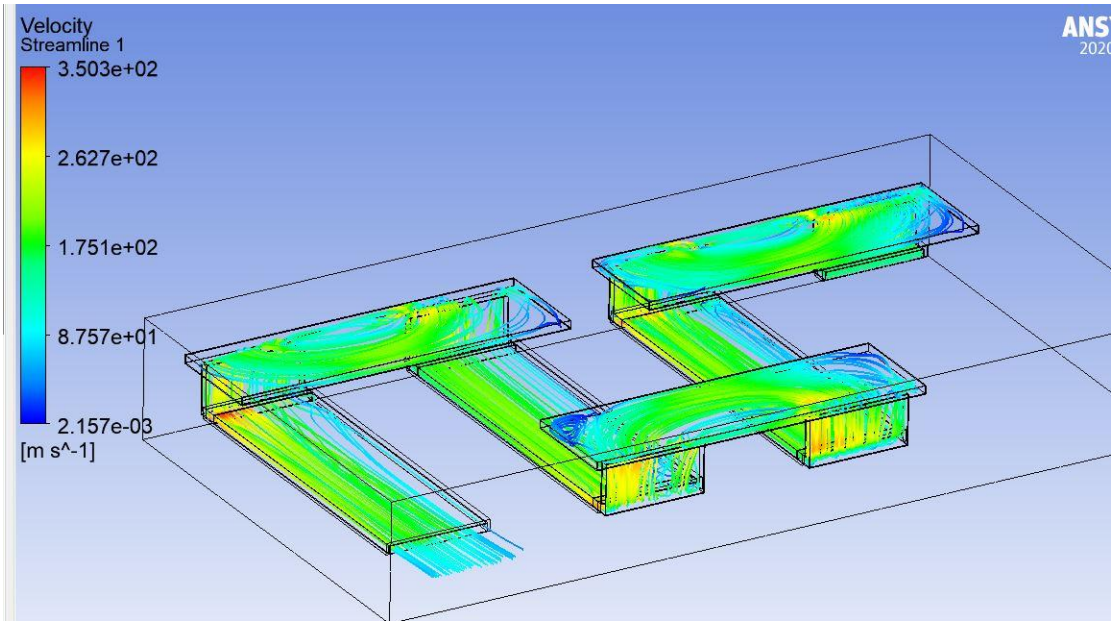

Figure 31: Velocity streaming. Compare with Fig 25 & Fig. 26 and notice the lower Velocity drop.

Parallel configuration

Mesh

The same mesh approach was applied as per in the series configuration

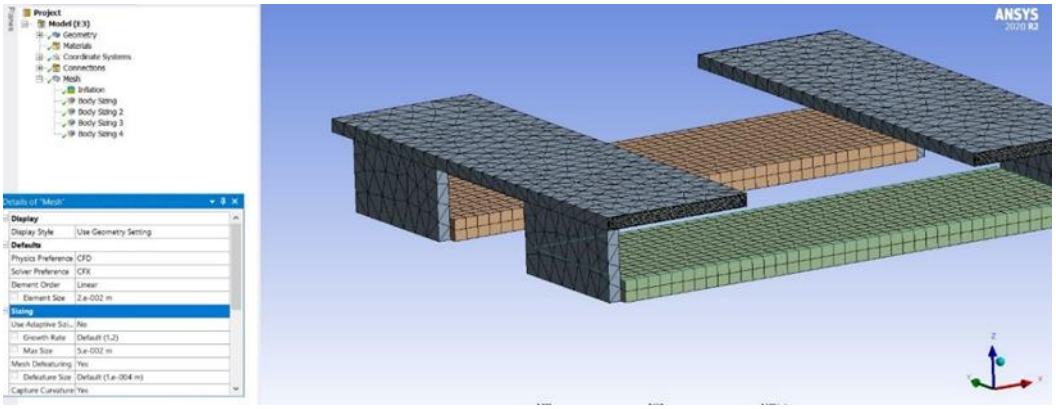

Figure 32: Parallel Configuration. Meshing view 1

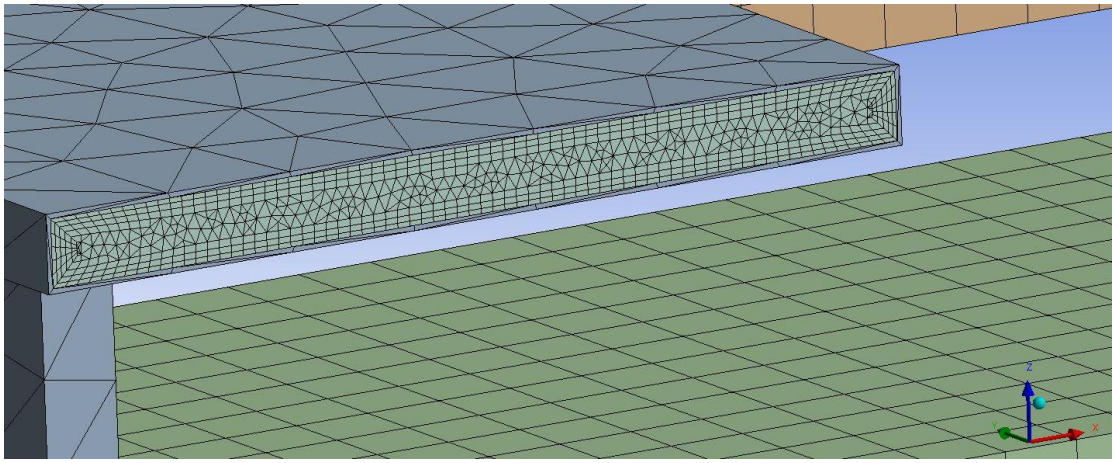

Figure 33: Parallel Configuration. Meshing view 2

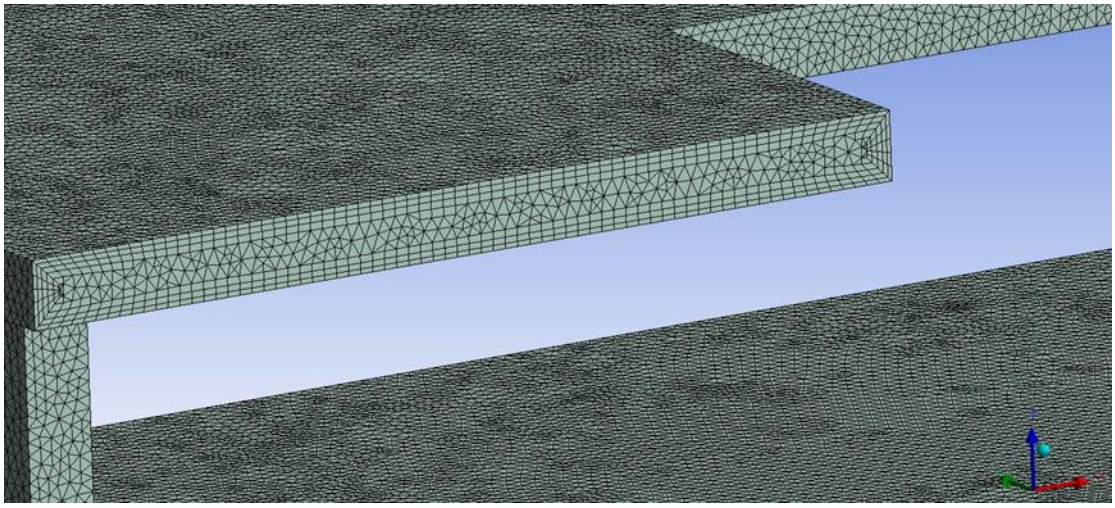

Figure 34: Parallel Configuration. Meshing view (3 detail)

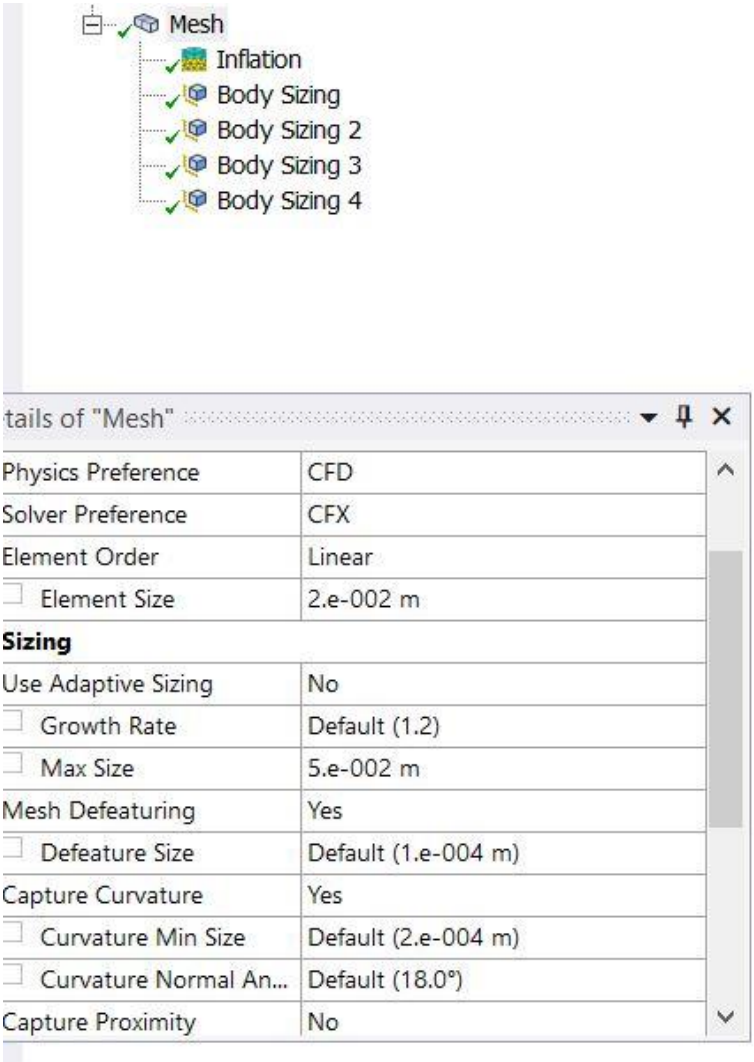

Figure 35: Parallel configuration: Main meshing setup

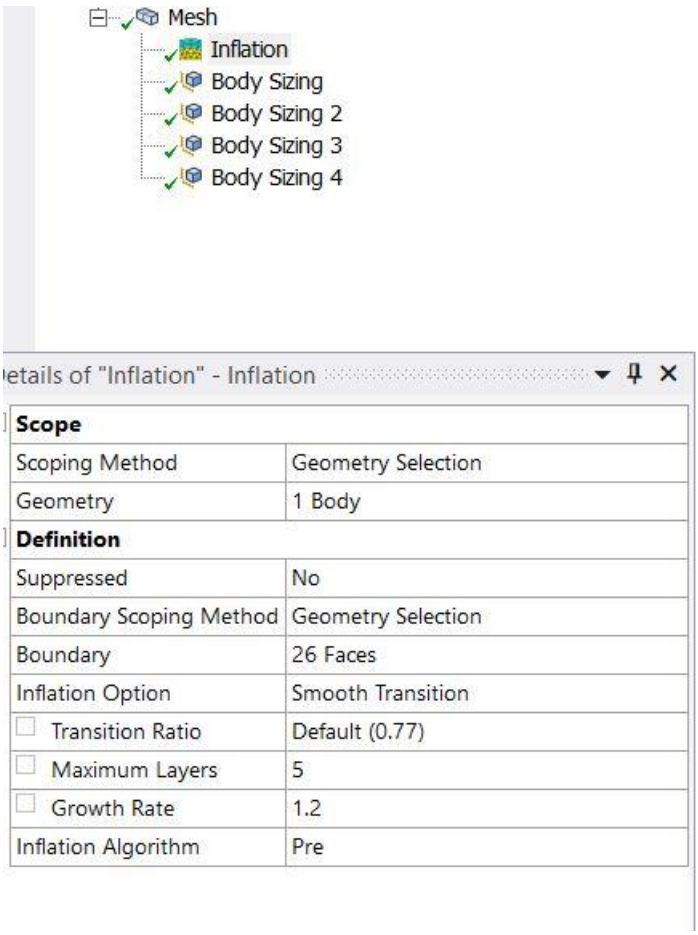

Scope	
Scoping Method	Geometry Selection
Geometry	1 Body
Definition	
Suppressed	No
Boundary Scoping Method	Geometry Selection
Boundary	26 Faces
Inflation Option	Smooth Transition
Transition Ratio	Default (0.77)
Maximum Layers	5
Growth Rate	1.2
Inflation Algorithm	Pre

Figure 36: Parallel configuration: Main meshing setup (Cont.)

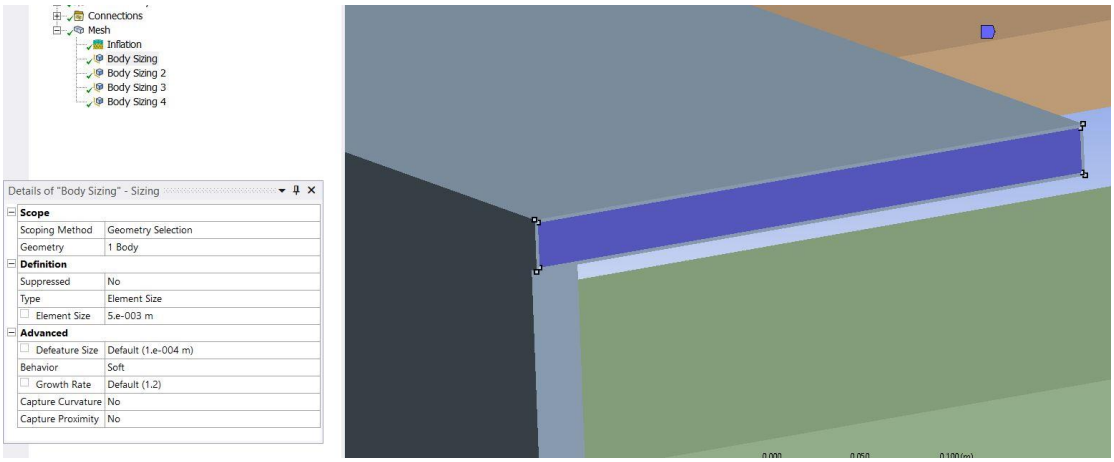

Figure 37: Parallel configuration Flow Duct Detail

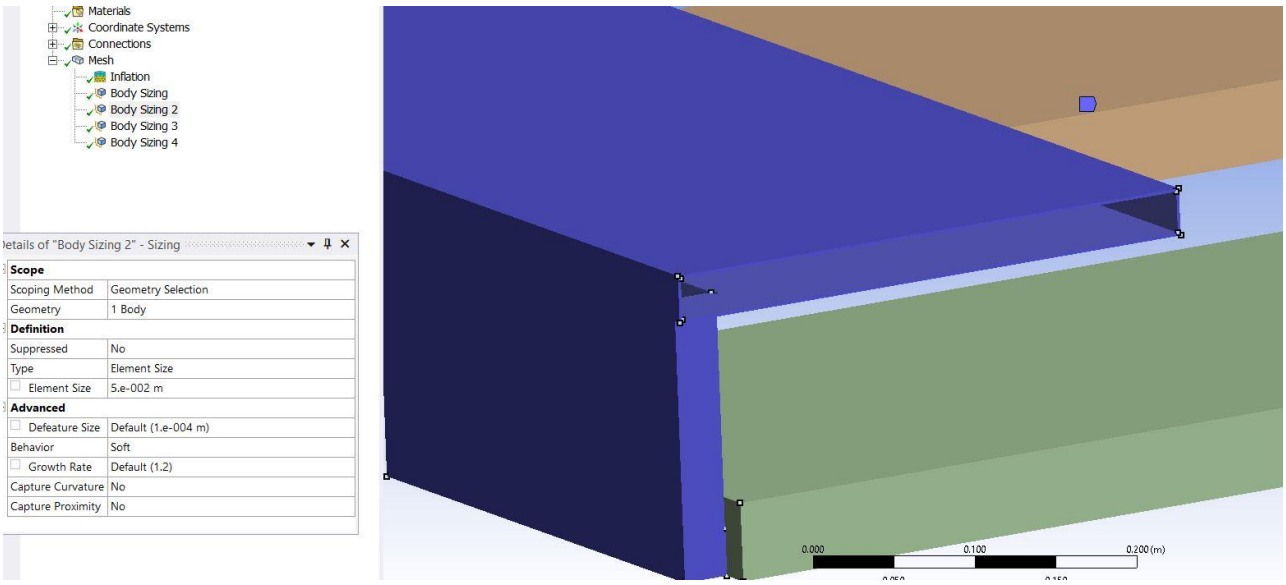

Figure 38: Parallel configuration Flow Duct Detail: Upper part.

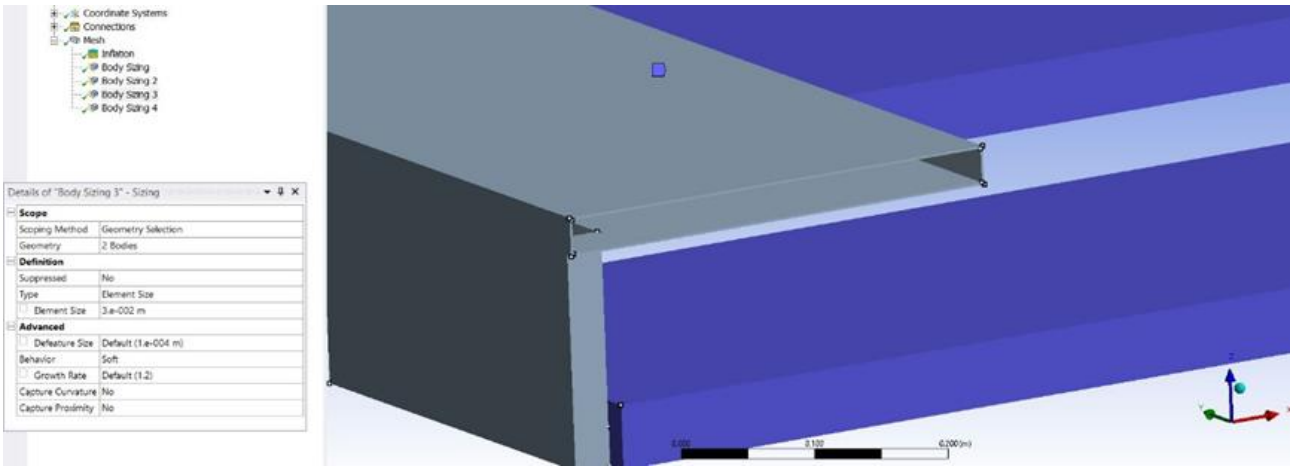

Figure 39: Parallel configuration Flow Duct Detail: Lower Horizontal part.

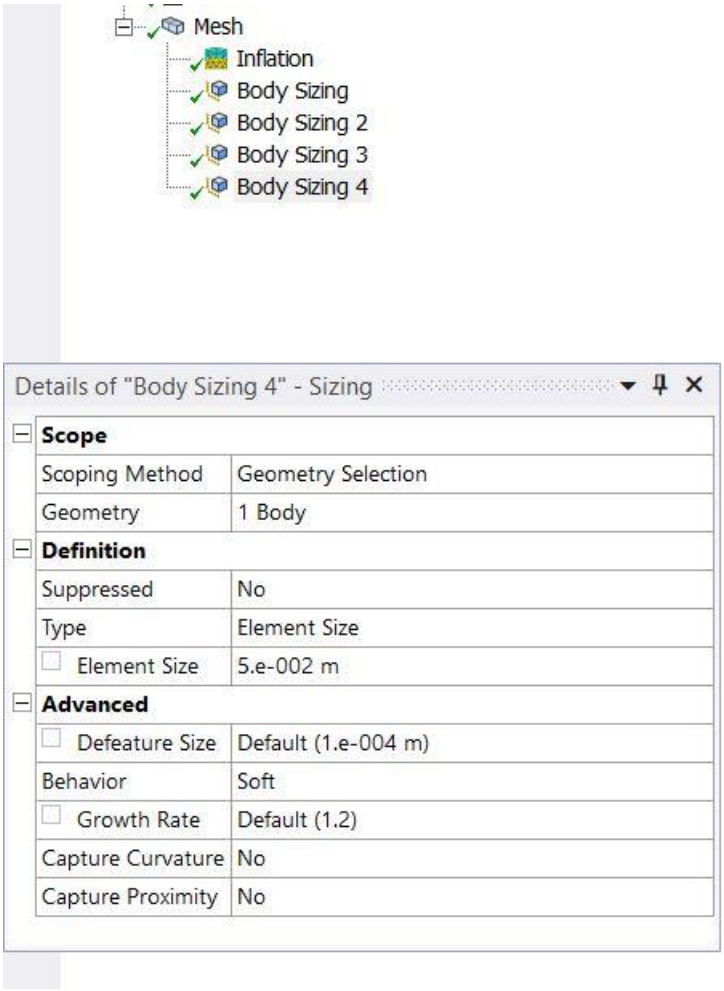

Figure 40: Body sizing of the geometry. Notice the Defeature size set to 0.1mm.

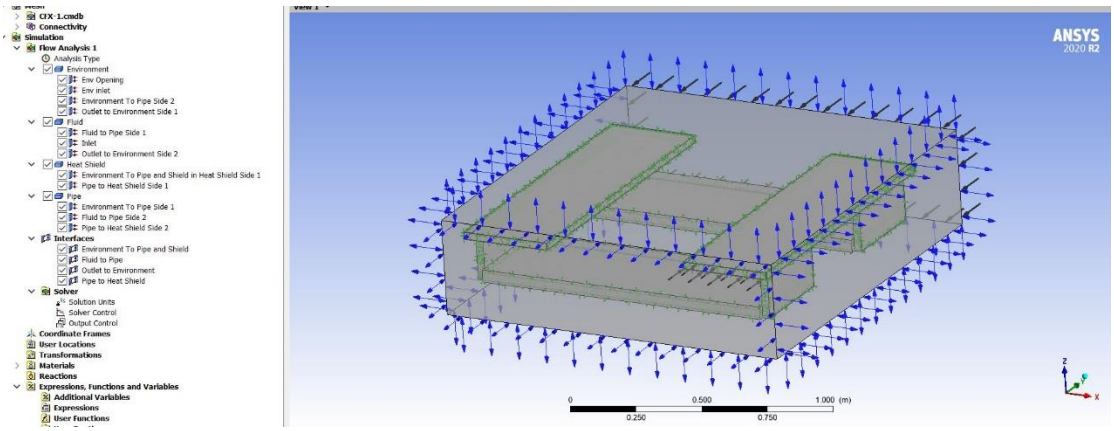

Figure 41: Parallel configuration. Environmental Conditions Setup (Vessel's Inner)

Inlet condition: 35 m/s

Total wall clock time: 1.995E+04 seconds

or: (0: 5: 32: 32.490)

(Days: Hours: Minutes: Seconds)

With the following command set, the total pressure at the outlet and inlet respectively is obtained:

=massFlowAve(Total Pressure)@(έξοδο) = 1.008e+5 [Pa]

= massFlowAve(Total Pressure)@(είσοδος) = 1.016e+5 [Pa]

Drop: 0.008+5 [Pa]

With the following command set, the total temperature at the outlet and inlet respectively is obtained:

=massFlowAve(Total Temperature)@(έξοδο) = 4.979e+2 [K]

= massFlowAve(Total Temperature)@(είσοδος) = 5.080e+2 [K]

Drop: 0.101e+2 [K]

The following images give a visual depiction of the Pressure and Temperature contours in the parallel configuration.

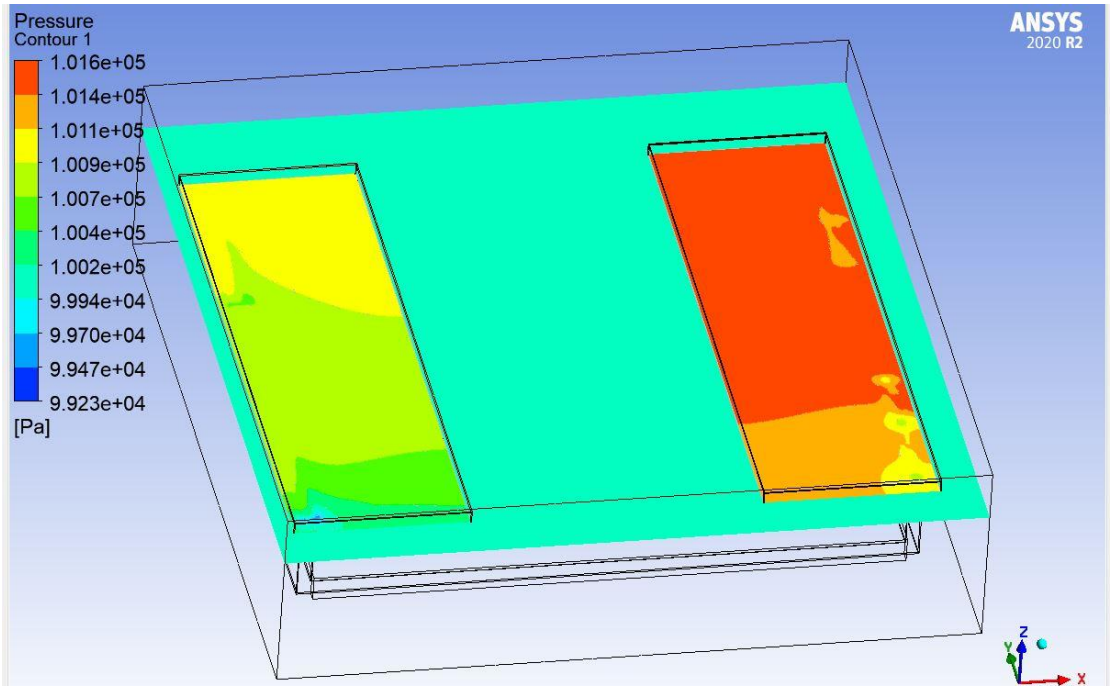

Figure 42: Parallel settle down Configuration Pressure Contour

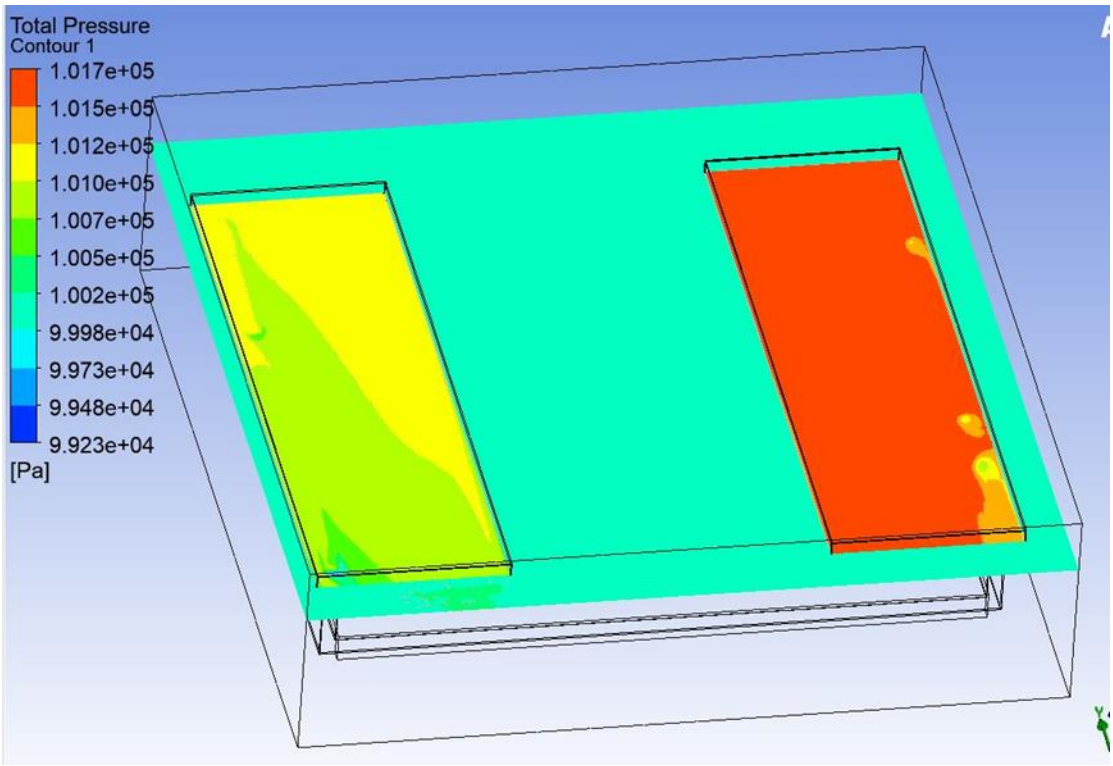

Figure 43: Parallel Configuration Total Pressure Contour

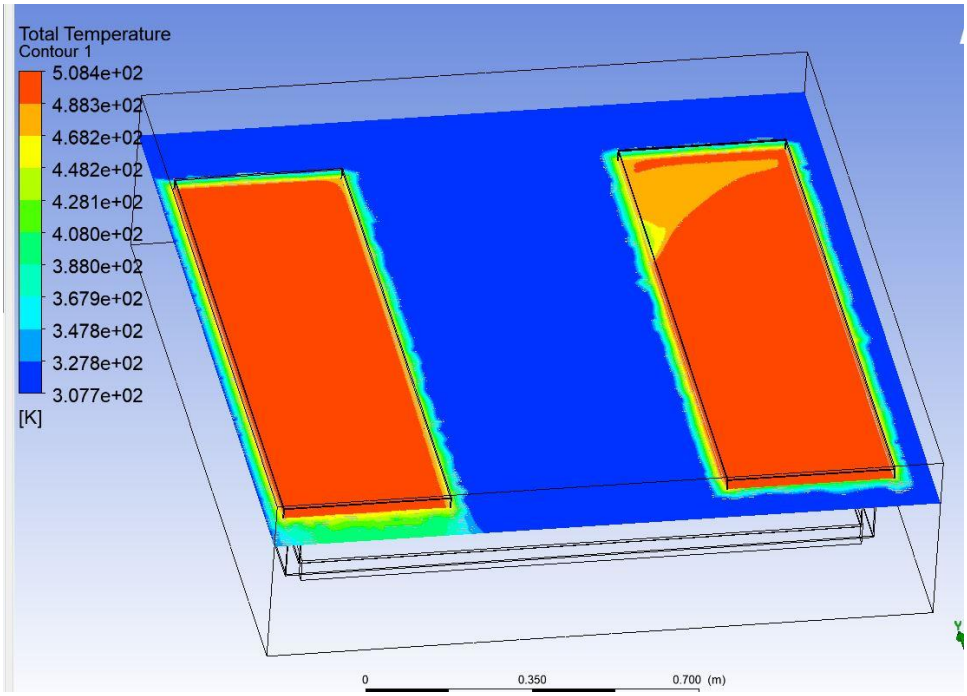

Figure 44: Parallel configuration Total Temperature Contour

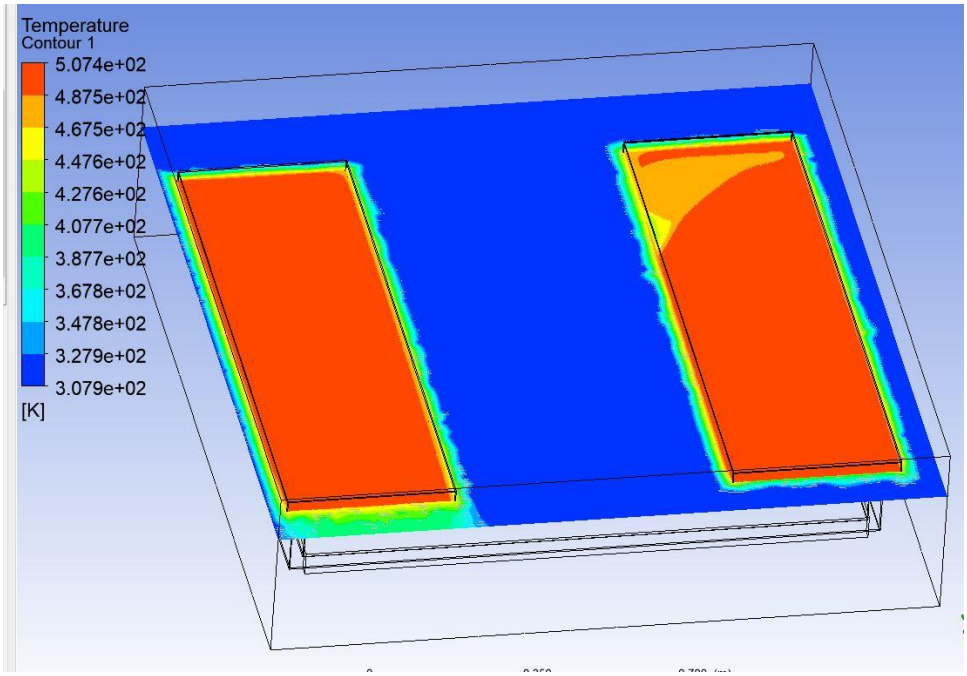

Figure 45: Parallel Settle down configuration Temperature Contour

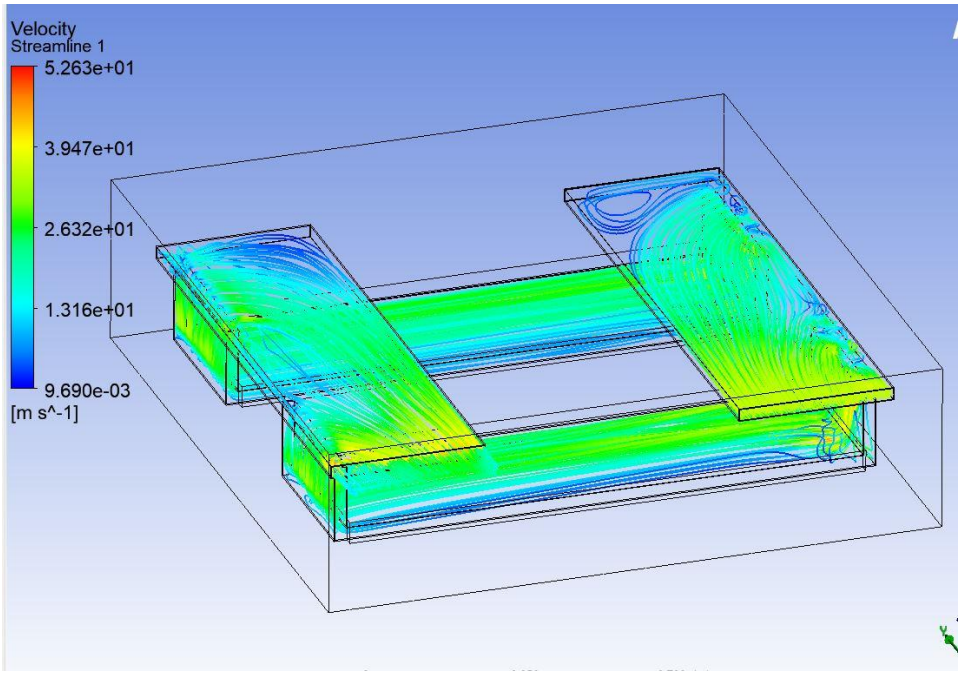

Figure 46:Parallel Configuration: Velocity Streamline (view1)

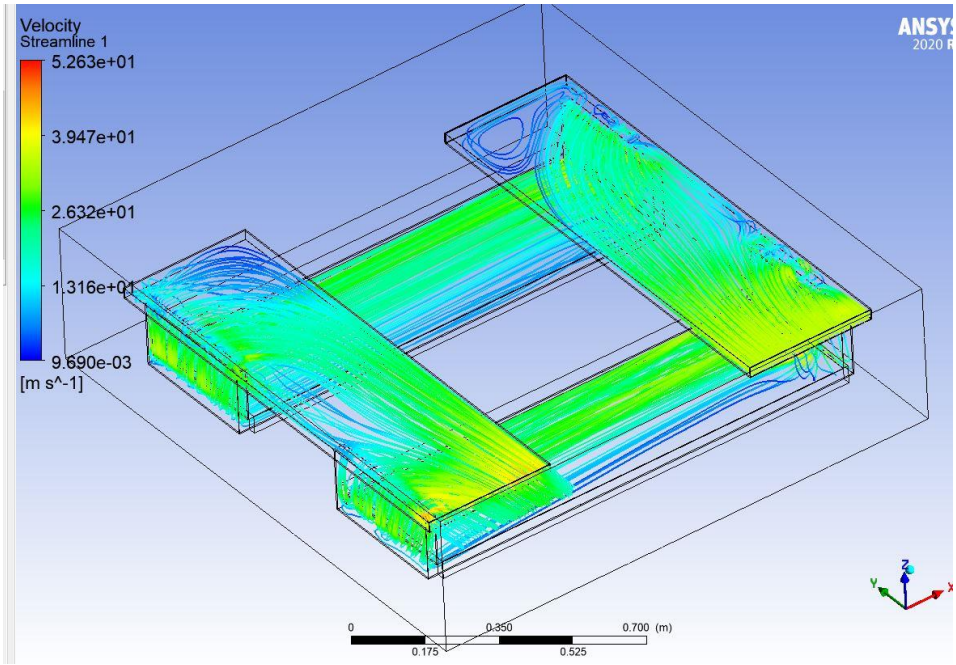

Figure 47:Parallel Configuration: Velocity Settle down Streamline (view2)

Inlet Condition: 2.5 bar total pressure

Total wall clock time: 7.456E+04 seconds

or: (0: 20: 42: 39.312)

(Days: Hours: Minutes: Seconds)

With the following command set, the total pressure at the outlet and inlet respectively is obtained:

=massFlowAve(Total Pressure)@(έξοδο) = 1.741e+5 [Pa]

= massFlowAve(Total Pressure)@(εἰσοδος) = 2.500e+5 [Pa]

Drop: 0.759+5 [Pa]

The Total Temperature drop is practically negligible, near 0^{o} K.

Important Notice

By comparing the pressure and temperature drop between the two configurations we see as expected, that in parallel configuration the pressure drop is lower, while the temperature loss is greater. In the contrary, in series configuration the pressure drop is higher whereas the temperature loss is lower.

The following images give a visual depiction of the Pressure and Temperature contours in the parallel configuration based on the 2.5 bar total Inlet pressure condition.

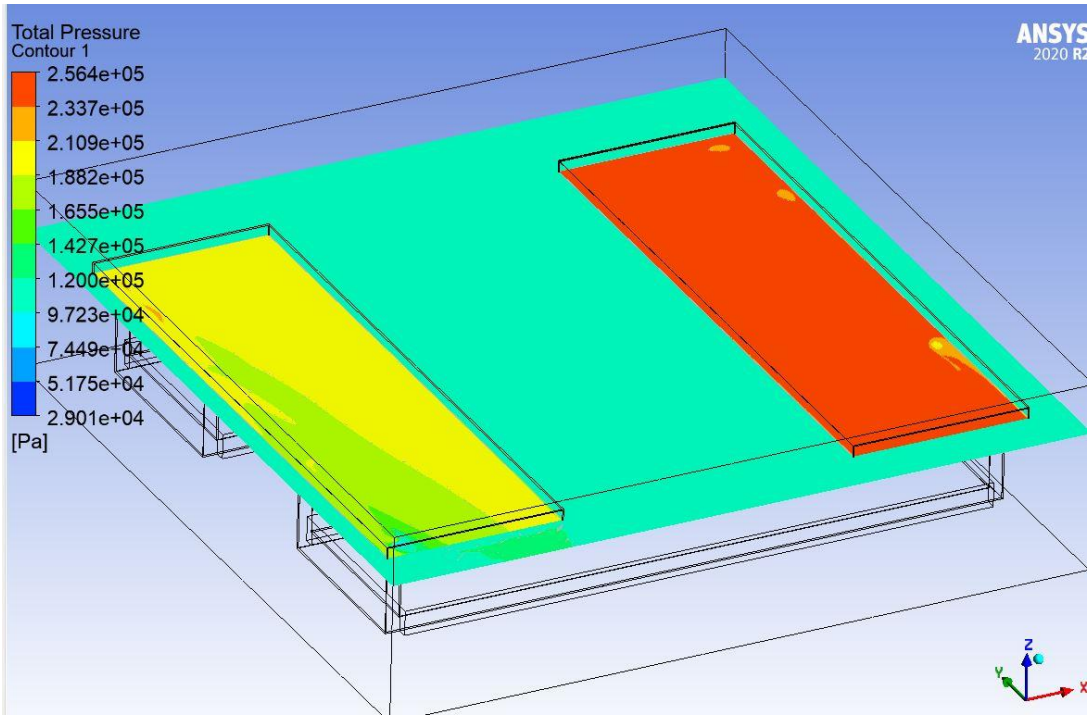

Figure 48: Total Pressure Contour in Parallel Configuration (2.5 Bar Inlet)

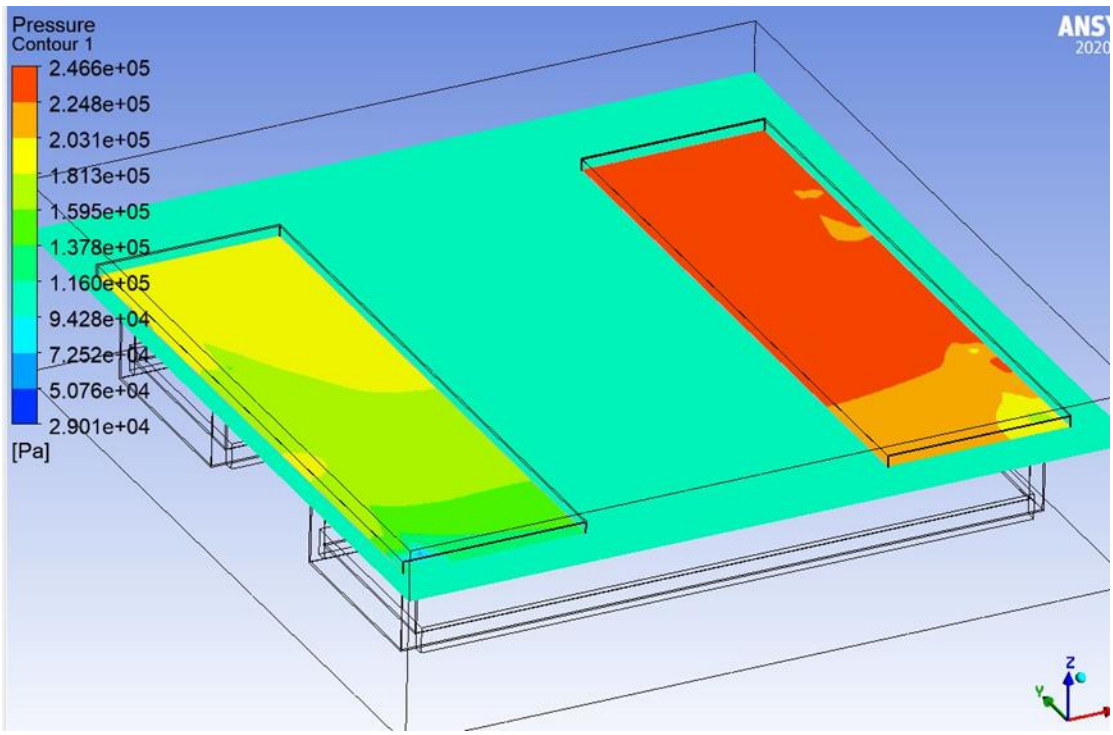

Figure 49: Pressure Settle down Contour in Parallel Configuration (2.5 Bar Inlet)

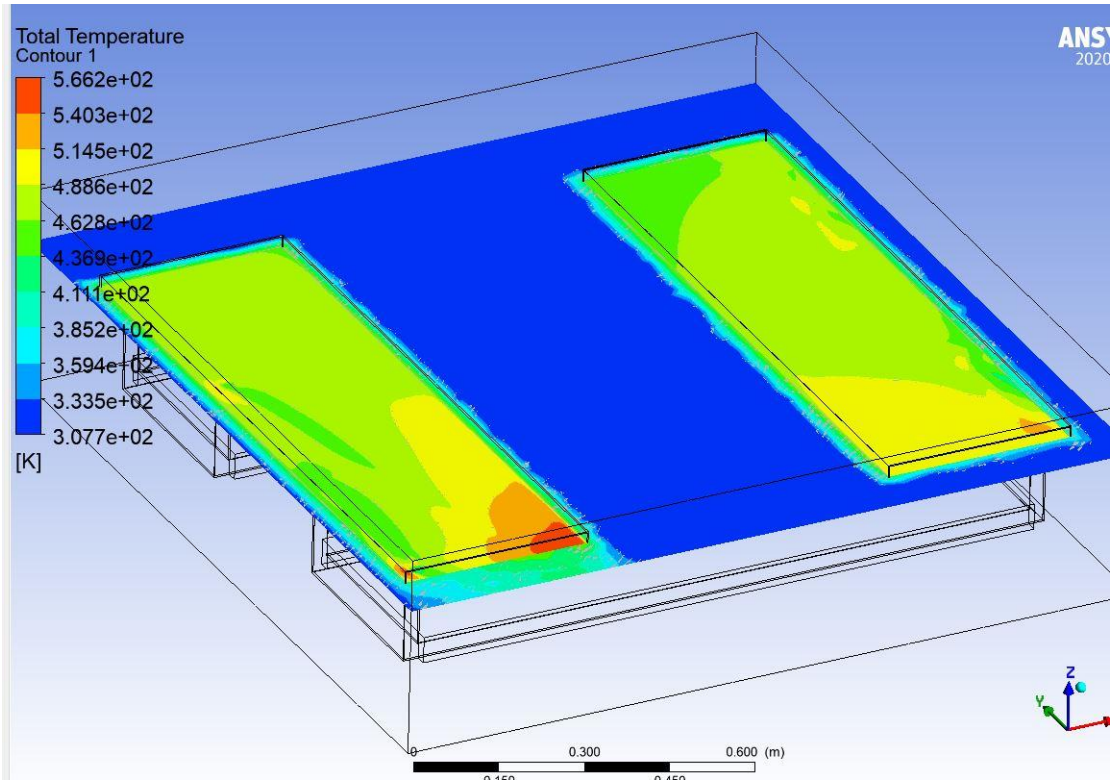

Figure 50: Total Temperature Contour in Parallel Configuration (2.5 Bar Inlet)

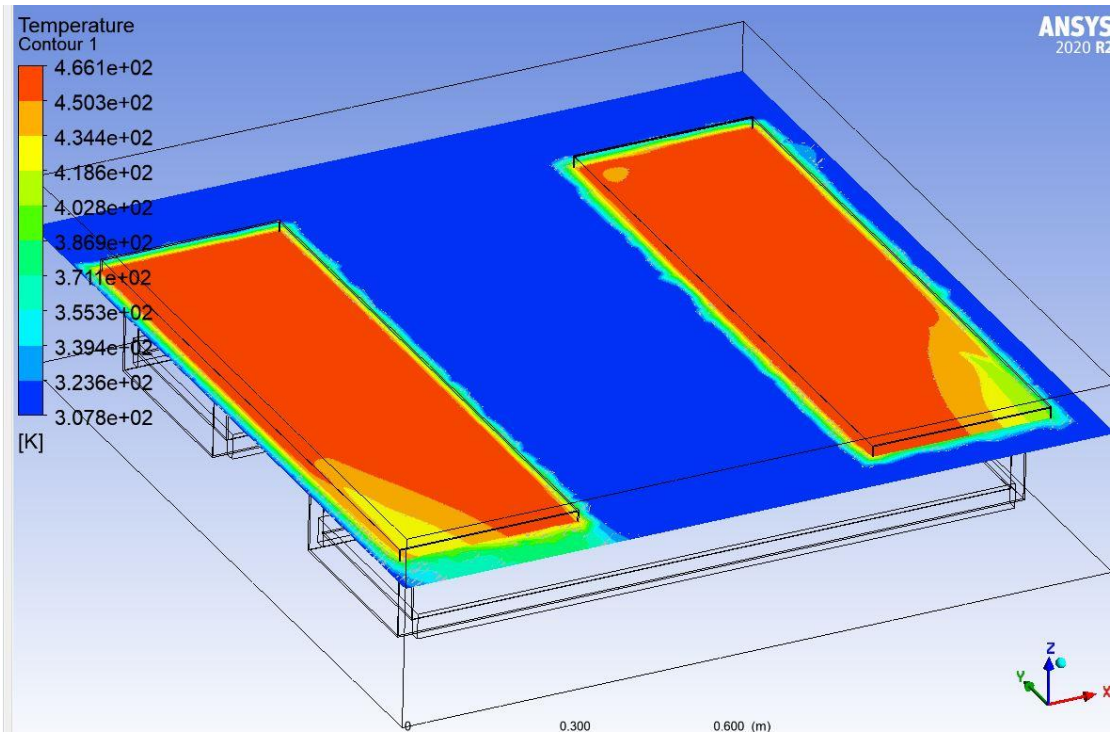

Figure 51: Temperature Settle down Contour in Parallel Configuration (2.5 Bar Inlet)

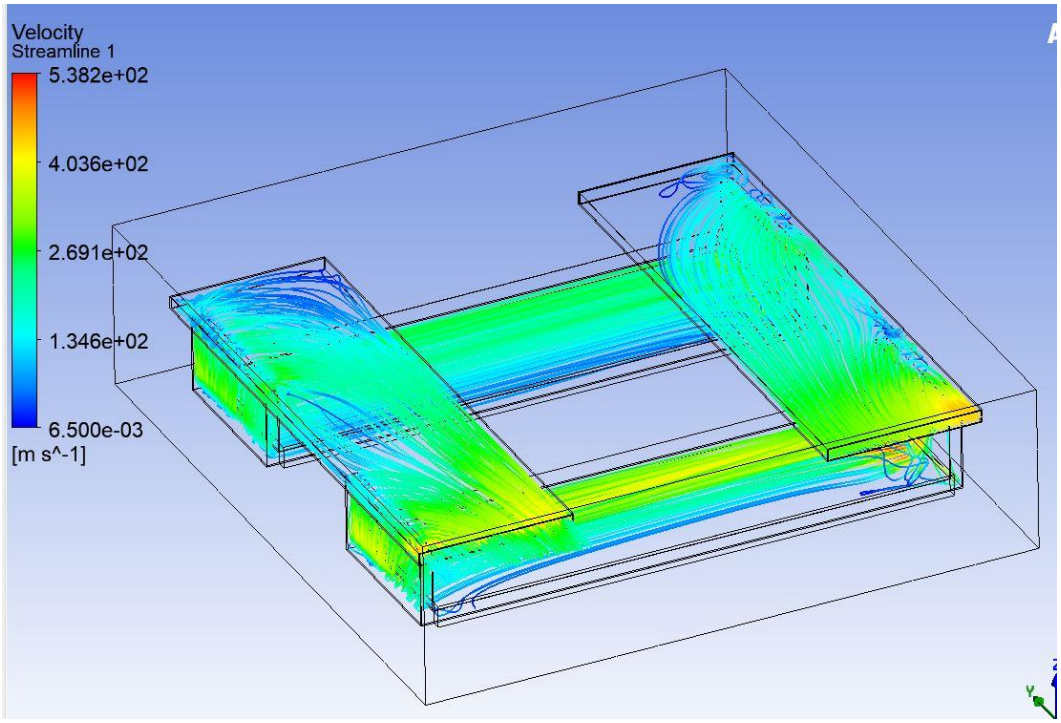

Figure 52: Velocity Contour in Parallel Configuration (2.5 Bar Inlet) View 1

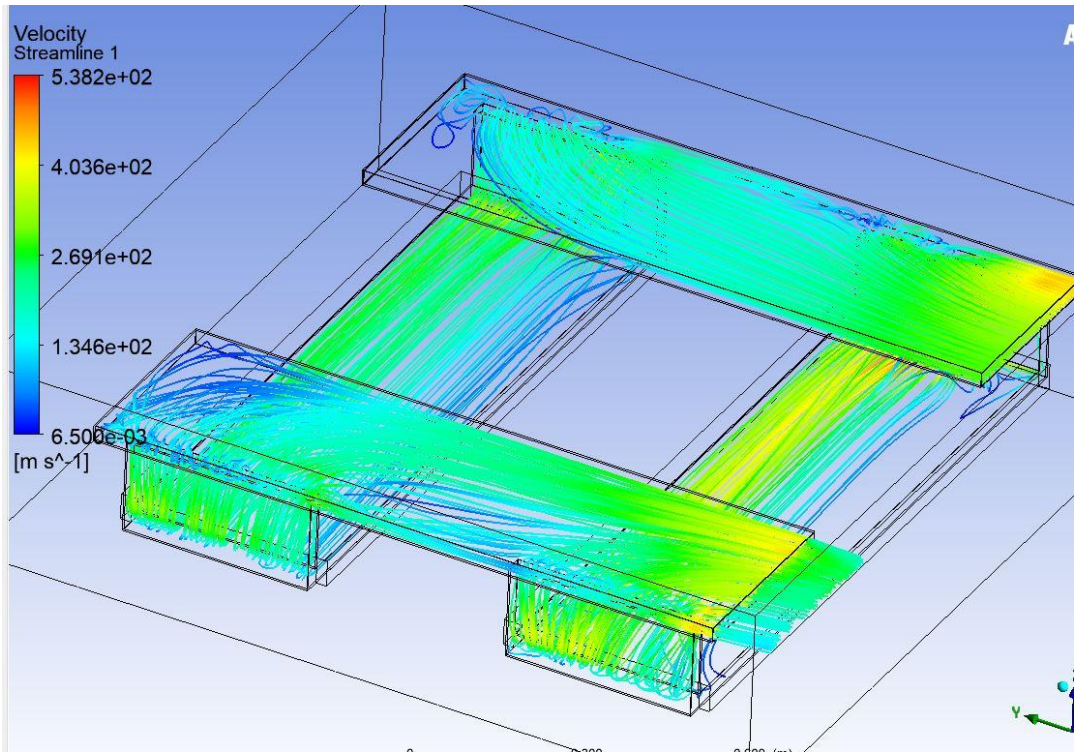

Figure 53: Velocity Contour in Parallel Configuration (2.5 Bar Inlet) View 2

4.1.2 Heat dissipation elaboration:

The heat dissipation simulation was performed by use of the Simscale® software. The simulation boundaries included among others, the average high sea temperature as described in the statistical section (20^{o} C), the average sea water speed when the vessel maintained the average trip speed (10,9 Kt, 5,6 m/s) and the navigation steel heat dissipation factor (45W/m·K). The aim of the simulations run was to determine the maximum temperature of the inner surface of the wet steel plate, at the contact point with the TEG elements. This, in conjunction with the monitored gas temperature, made the calculation of the $\Delta\theta$ possible, hence the estimation of the total power recovery.

The maximum outer surface temperature of the wet plate was found to be 31.09^{o} C, while the maximum inner surface temperature was estimated to 38.31^{o} C.

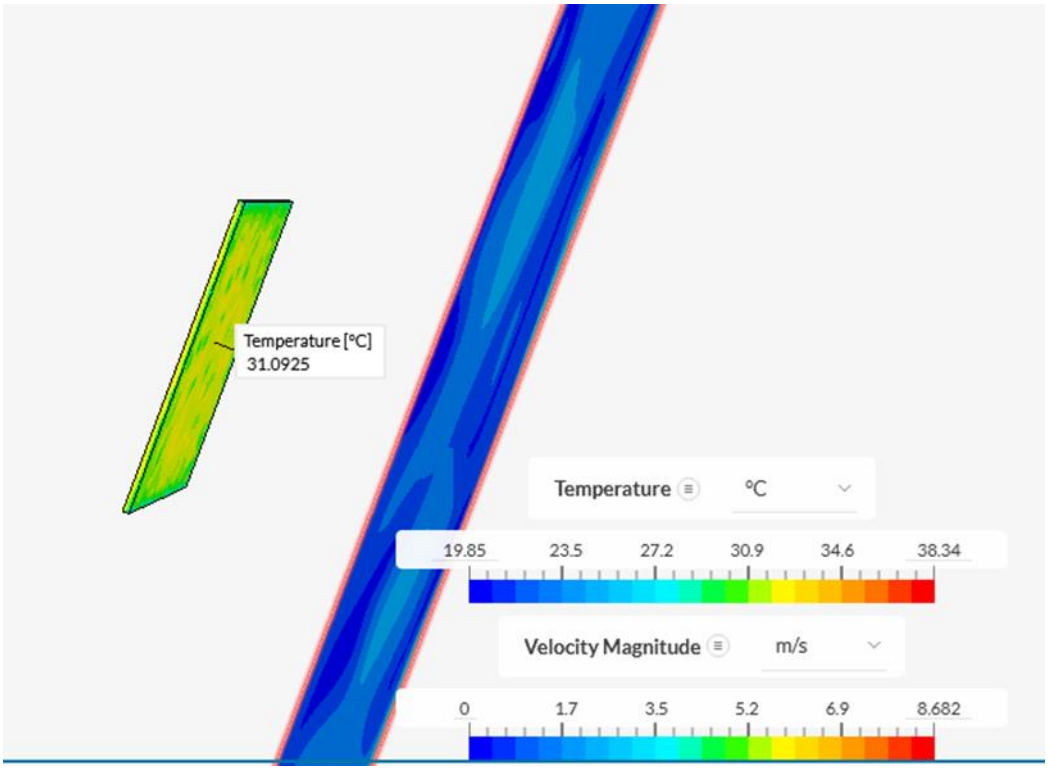

Figure 54: Outer side Temperature of the Hull plate (The blue surface represent the sea water temperature)

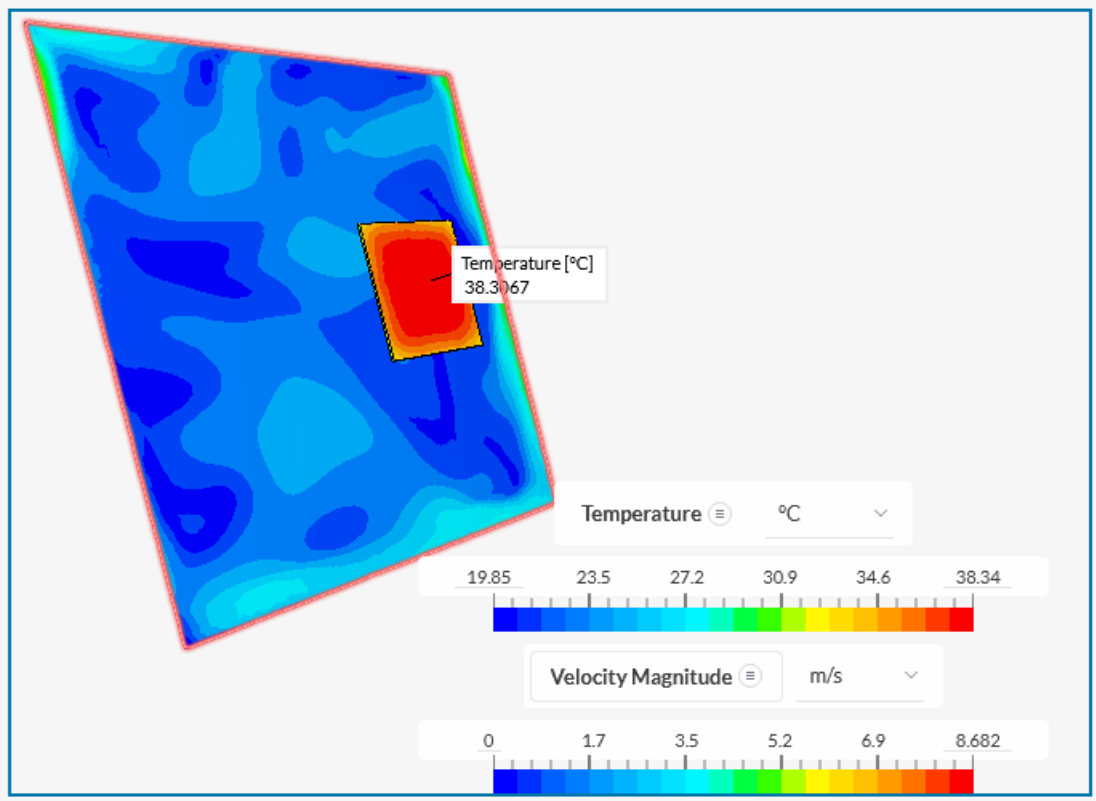

Figure 55: : Outer side Temperature of the Hull plate (The blue surface represent the sea water temperature)

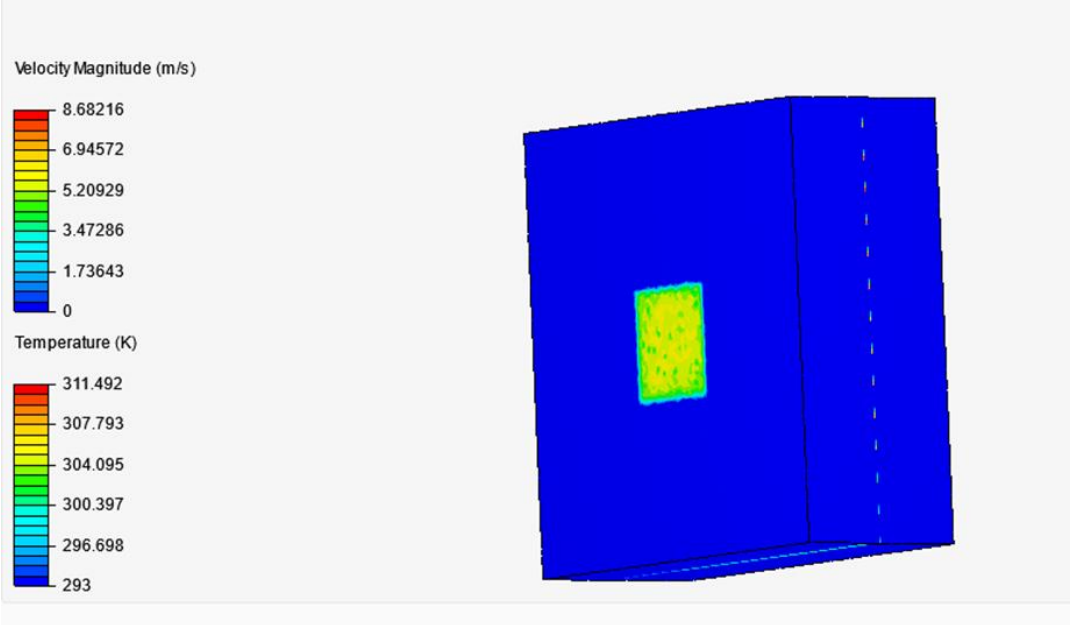

Figure 56: Depiction of the Hull plate against the Sea Water

CHAPTER 5: Statistical approach and hypothesis testing of the application.

5.1 The need for a statistical approach

The use of theoretical Statistics and statistic software such as the MINITAB® plays a critical role to determine how a number of parameters that change from year to year affect the installation and use of the TEG Network System on a vessel, especially when it refers to the decision to retrofit the system on an existing vessel. Parameters such as:

- the actual and expected yearly utilization of the vessel,
- the average temperature of the Seas the vessel is expected to sail more often,
- the cost of fossil fuel forecast[85],
- the austerity of the future international legislation regarding the reduction of the eco-footprint of the vessel[86],

are but a few to introduce nonlinearities and uncertainties in the System evaluation. As this research refers to a completely innovative technology and there is no previous experience whatsoever, the statistical examination of how all the above issues affect the decision to install such a system on a Vessel has to be checked.

The various Hypotheses Testing results will be discussed in the conclusions of this Research Thesis and hopefully, will give the motive to other Researchers to further improve System efficiency and remove or reduce its drawbacks.

As already mentioned in the modeling chapter, the cost for the development and testing of an experimental application of this technology even at a pilot scale is enormous and is

out of the scope of this Ph.D. thesis. Furthermore, the application on a real vessel would have to be approved by the Ship's Insurers and/or the manufactures of the machinery and equipment involved. Hence, the need for Hypothesis Testing -for several hypotheses becomes imperative.

5.2. Types of Hypotheses and Test Statistics[87]

5.2.1 Introduction

The method of hypothesis testing uses tests of significance to ascertain the significance level at which, the hypothesis would accept a statement as true. These statements are frequently tied to the mean or variance of a specific distribution. Knowing how to utilize each test correctly (and when to employ which test) is just as crucial as being familiar with the mathematical ideas that went into their derivation. Here, the objective is to concentrate on the latter ability. In order to achieve this, we will look at each statistical test that is often covered in an introductory course in mathematical statistics, emphasizing the circumstances in which one may use each test, the kinds of hypotheses that each test can test, and the proper technique to employ each test. To do this, it is necessary to first comprehend how to carry out a statistical significance test (by following the instructions in [MM]), after which we will demonstrate how to modify each test to fit inside this broad framework. The alternative hypothesis, which is the first thing we come up with, is the one to be tested. This hypothesis typically results from an effort to support an underlying premise (for example, attempting to show that petrol engines fail rate, on average, is higher than diesels). Using the same example, our null hypothesis would be that petrol engines do not, on average fail more often than diesels. This is done by conducting tests against the null hypothesis, which is the negation of the alternative hypothesis. The likelihood that we reject the null hypothesis when it is true is set as the probability level,

which will serve as our significance level. The rationale is to conduct a study on the relevant parameter after presuming the null hypothesis is correct. We can certainly conclude that the null hypothesis is false and adopt the alternative hypothesis if the investigation produces results that would be improbable if the null hypothesis were true (for example, results that would only occur with probability.01). Now that the hypotheses and the significance level are determined, the data is collected. Tests of hypotheses are conducted after data collection in the following 3 stages:

1. Establish a crucial region of size using the sample distribution of an applicable test statistic.
2. Use the sample data to calculate the test statistic's value.
3. Determine whether the test statistic value falls inside the critical zone; if it does, the null is rejected in favor of the alternative hypothesis; if it does not, the null is not rejected.

In this work the hypothesis trial will be based on these three procedures for each test, selecting the appropriate sample distribution for each test and the appropriate test statistic (the third step is done by simply comparing values).

5.2.2 Types of Hypotheses

- **Terms and Concepts**

One-tailed and two-tailed hypotheses are the two main categories of hypotheses that can be examined. In each scenario, the vital region will be built differently. The main distinction between the research problems and the null and alternative hypotheses is that the research problems are straightforward inquiries that cannot be tested. However, it is possible to examine these two theories.

Before the research's data collecting and interpretation phases, the null hypothesis and alternative hypothesis must be appropriately segmented. Well-fragmented hypothese show that the researcher has sufficient expertise in that field, enabling them to move the investigation further by employing a system that is much more systematic. It provides

guidance for the researcher's data collecting and interpretation. It provides guidance for the researcher's data collecting and interpretation.

Only when they explicitly describe the predicted relationship between the variables or when they are in line with the body of existing knowledge are the null hypothesis and alternative hypothesis useful. They ought to be stated as briefly and plainly as possible. If -and only, if- they have explanatory power, they are beneficial.

The null hypothesis and alternative hypothesis are significant because they roughly describe the phenomenon, which is their goal. The intention is to offer a relational statement that will be explicitly tested in a research study to the researcher or inquiry. The goal is to offer a structure for reporting the study's conclusions. The idea is to act as a tool for the theory to work. The objective, which is distinct from the investigator's beliefs and choices, is to demonstrate whether or not the test is supported. They also give the research orientation.

Typically, H0 is used to represent the null hypothesis. It states exactly the opposite of what a researcher or experimenter anticipates or forecasts. It clarifies the claim that there is no precise or meaningful link between the variables.

A common designation for the alternative hypothesis is H1. It makes a claim that implies or recommends what an analyst or researcher might anticipate as a possible consequence or conclusion. Directional alternative hypothesis and non-directional alternative hypothesis have been separated into two types. H0 is a common abbreviation for the null hypothesis. It reveals the exact opposite of what a researcher or experimenter anticipates or predicts. It defines the claim that the variables don't actually or precisely relate to one another.

Usually abbreviated as H1, the alternative hypothesis. It makes a claim that implies or advises a prospective result or conclusion that a researcher or investigator may anticipate. The two categories that have been assigned to it are non-directional alternative hypothesis and directional alternative hypothesis.being specified[88].

In practice, it is more reasonable to always have the equals sign in the null hypothesis, as in H0: μ= 100.

HA: μ > 100

The set indicated by H0 or by HA should both include the true value of the population parameter. As a result, in the case above, we can assume that μ is at minimum 100. A one-sided (or one-tailed) test is a statistical analysis in which the alternative hypothesis states that the population parameter totally lies above or below the value stated in H0, for example, H0: = 100 HA: > 100

A two-sided (or two-tailed) test is an alternate hypothesis that states that the parameter can lie on either side of the value provided by H0, for example, H0: = 100 HA:μ <or> 100

Depending on the nature of the case examined, either a 1-tailed or 2-tailed test should be utilized. A 2-tailed test is most commonly used. Typically, a 1-tailed test necessitates some additional theory.

Consider the null hypothesis that men and women earn the same amount of money.

A two-tailed option would only claim that wages are not equal, meaning that males may or may not make more money than women. Men earning more than women would be a one-tailed solution. The latter is a stronger assertion and calls for more theory since, in addition to asserting that there is a difference, you further specify the nature of the difference. The latter is a stronger assertion and calls for more theory since, in addition to asserting that there is a difference, the nature of the difference has to be specified.

In practice, a 1-tailed test such as H0: μ = 100 HA: μ > 100 is tested the same way as

H0: μ # 100

HA: μ > 100

For example, if it is concluded that μ > 100, it also has to be concluded that μ > 90, μ > 80, etc.

II. The decision problem.

A. The accepted practice is to assume H0 is true when deciding between H0 and HA, much as a presumption of one state until proven other wise. It is tested whether there is sufficient evidence to reject H0 using probability theory.

B. H0 is only rejected when there is a slim likelihood that it is accurate. Errors could occur because decisions are based on chance rather than absolute knowledge.

C. Type I error: When the null hypothesis is correct, we reject it. The likelihood of a Type I error =α. In other words, α= P(rejecting H0 | H0 is true) = Probability of Type I error.
The usual choices for α are .05 or .01. Therefore, if =.05, there is a 5% risk that we will incorrectly reject the null hypothesis when it is true.

D. Type II error: When the null hypothesis is false, we accept it. Type II error probability is equal to ß. In other words, P(accepting H0 | H0 is untrue) = ß = Probability of Type II error.

E. TYPE I AND TYPE II ERROR EXAMPLES:

H0: $\mu = 100$ or

HA: $\mu <> 100$

As an example of hypothesis testing let us suppose that μ really does equal 100. If the researcher accepts HA instead. A type I error has occurred.
In case μ is really 105, yet the researcher accepts H0, a type II error has occurred.

The following tables help to illustrate the different types of error based on the assumption that 20º C of seawater temperature are critical for the effective a financially sustainable investment for the installation of the waste heat recovery on an existing vessel.

.

	The true situation is Sea Temp<20 C (Ho)	Sea Temp>20 C (Ho)
Sea Temp>20 C	Type I error	Correct decision
Sea Temp<20 C	Correct decision	Type II error

Figure 57:Summary of decision-making algorithm

F. Probabilities α and β are closely related. As one raises, the other reduces. Nonetheless, both decrease as N increases because sample data error is reduced.

G. In this section, Type I error will be discussed. However, it is crucial to be aware that Type II error is as significant. For example, a small sample size may commonly lead to Type II mistakes, which means it's possible that your (alternative) hypotheses are true but that you don't reject the null even though you should because of the small sample size.

III. Hypothesis testing procedures.

The following 5 steps are followed when testing hypotheses.

1. Specify H0 and HA - the null and alternative hypotheses.

Examples:

(a)	H_0:	E(X) = 10	(b)	H_0:	E(X) = 10	(c)	H_0:	E(X) = 10
	H_A:	E(X) <> 10		H_A:	E(X) < 10		H_A:	E(X) > 10

In (a) HA is suggested as not equal (larger or smaller) to 10 than, although alternative values in example (b) and (c) are smaller or greater than those mentioned in H0. Therefore, a one-tailed test is required for (b) and (c).
The proportion of successes, p, in the hypothesis is frequently used when working with binomially distributed variables. Thus, for instance, if N = 20 and X has a binomial distribution, the aforementioned hypotheses are equivalent to:

(a)	H_0:	p = .5	(b)	H_0:	p = .5	(c)	H_0:	p = .5
	H_A:	p <> .5		H_A:	p < .5		H_A:	p > .5

- Choose the proper test statistic. A test statistic is a fuzzy variable used to assess how well a given sample result matches a certain hypothesis under investigation. In other words, the test statistic indicates how probable it is that we would get the specified sample result if H0 is true. The test statistic is frequently a Z score. A suitable test statistic, for instance, when applying the normal approximation to the binomial distribution is:

$$z = \frac{\#\ of\ successes \pm .5 - Np_0}{\sqrt{Np_0 q_0}}$$

where p0 and q0 represent the null hypothesis' inferred or stated probabilities of failure and success respectively. Z has a N(0,1) distribution whenever the null hypothesis is correct. Note that it is occasionally suggested that a

continuity adjustment should be used as X is not continuous. To achieve this, when x < Np0, then 0.5 has to be added to x, and when x> Np0, 0.5 should be subtracted. It should be noticed that the value of z is decreased by the continuity correction. It should be noted that the value of z is reduced by the continuity correction. That is, if continuity is not corrected, the z-score will be too high. The correction for continuity frequently goes unnoticed in practice, — particularly when N is large, but it can be significant in circumstances with low N or near the border. In essence, what we are doing is comparing what we really observed with what the null hypotheses indicated would occur; specifically, number of successes represent the recorded empirical result, or what actually occurred, and Np0 represents the outcome that the null hypothesis anticipated would occur.

Obviously, these numbers will not be exactly identical due to sample variability; for instance, the null hypothesis may have suggested 15 successes while the actual number was 17. However, if the discrepancy between the observed and predicted values becomes too large, we will draw the conclusion that the values stated in the null hypotheses are likely incorrect and the null should be rejected.

5.3. A real vessel's trip case probability study.

In order to establish the necessary base for the statistical approach to the subject a case study should be examined. Towards this, firstly a typical voyage of a modern vessel from China to the USA will be considered in terms of fuel-saving by the recovery of waste heat

carried by the exhaust gases produced by the vessel's main engine and the use of them in a system of TEG arrays attached to the ship's hull under the waterline. We will assume that the ship is sailing full of cargo at the MCR of its engine.
Then a 6 months study of the trips the Vessel did, was conducted utilizing Microsoft Excel® and MINITAB® statistic software:

This case study deals with the Bulk Carrier "Desert Challenger"[89] a fairly newbuilt (2017) Bulk Carrier of 61000 Tons DWT, IMO: 9699842. The ship's main Engine is a HYUNDAI – B&W 7G50ME-B9.3(TIER II) power system, having a nominal power rating of 12.040KW @ 100 rpm supplying the propeller shaft with 1149820 Nm of torque giving the fully loaded ship a maximum speed of 18 Knots. The ship's Power Supply System (hereafter "PSS") is powered by a set of three HYUNDAI HIMSEN / 5H21/32 generators each having a nominal Power of 910KW @ 900RPM. Two of the three generators cover approximately 120% of the Ship's full load requirements under normal operational conditions. No shaft generator is installed. Other thermal engines and ancillaries installed is the CMB-VS-1.6+0.5 +2x0.135/7 Composite Marine Boiler made by SAACKE, and the Maxi NG 150 SL WS Incinerator made by HYUNDAI ATLAS. The ship's emergency Generator will not be discussed here as it does not affect the research. The vessel departed at midnight on May 20th, 2020 from FUZHU (CN) port, (Latitude / Longitude: 26.000305° / 119.43515°), to arrive at SAN FRANCISCO (USA) port (Latitude / Longitude: 37.77395° / -122.3963°) approximately 22 days later on the 16:00 hrs of June 10th, 2020. The ship, having an average speed of 10,9 Kn covered the distance of 5668 NM in some 520 hrs.
During the voyage, the average sea temperature was measured on the same hour of each astronomical day and was duly logged. The average temperature of the inner side of the vessel's wet sheets was similarly observed and logged, at the same time as the sea

temperature and always at the same point having average installation characteristics see Table 10 and graphically in the folwing Figure.

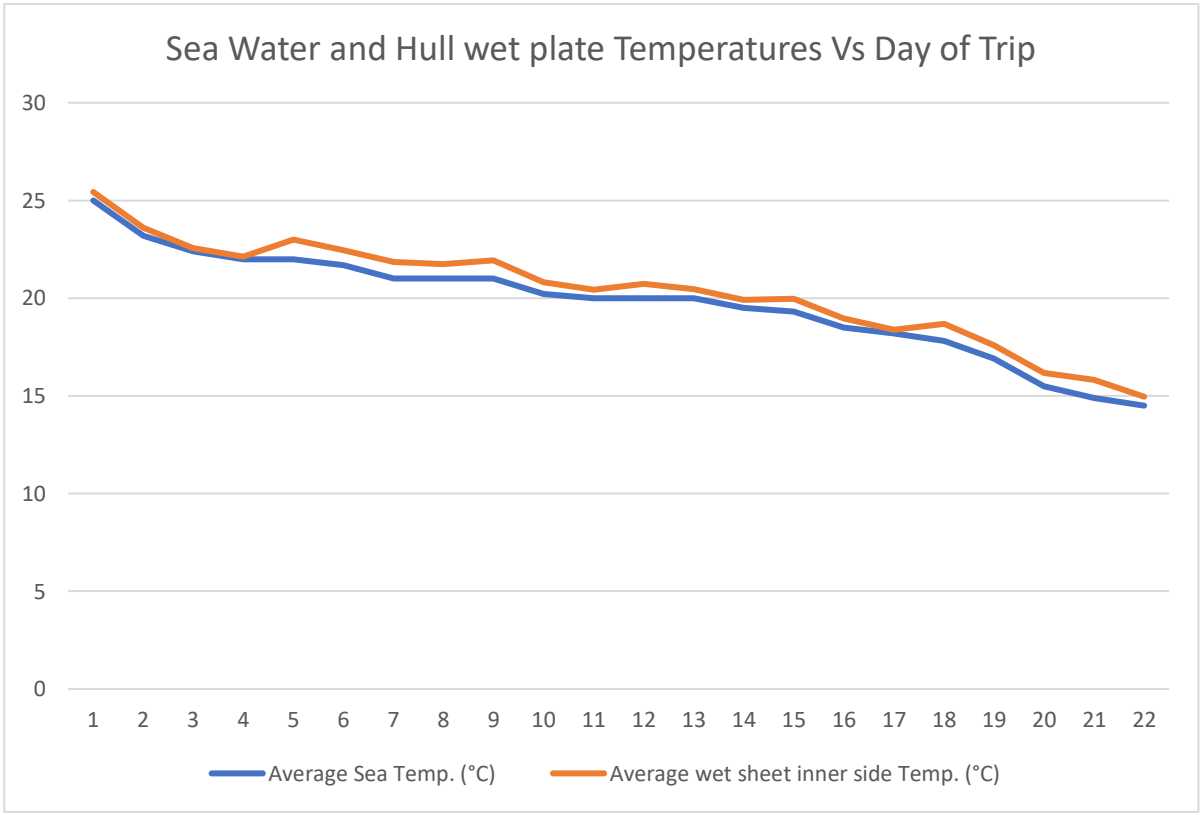

Figure 58: Sea Water and Hull plate temperature fluctuations Vs Days of Journey

The overall installed electrical power of the vessel is approx. 1520 KW and is covered by the continuous functioning of the two out of three Generation Sets installed. Although the power consumed when the ship is steaming at sea is far less than the totally installed, for the calculation of the worst-case scenario, we will consider full power was needed during the duration of the voyage.

As soon as the ship's main engine started and the engine's exhaust gases reached the nominal temperature, the system of TEG arrays became operative, starting the production of auxiliary power and supplying the vessel's grid.

The nominal specific oil consumption of each of the three installed Hyundai-Himsen generators 5H21/32 @ 900 rpm is 190 g/KWh[90]. Hence, if as assumed for the worst-case scenario each Genset works at full load for 24 hours, it will supply:

$$E_{d(KWh)} = P_{Gs(KW)} \times 24_{(h)} = 910 \times 24 = 21840 KWh$$

Consuming typically per day:

$$C_{d(Kg)} = \frac{S_{foc(g/KWh)} \cdot E_{d(KWh)}}{1000} = \frac{190_{(g/KWh)} \cdot 21840_{(KWh)}}{1000} = 4149,6 Kg$$

Therefore the daily fuel oil consumption of both the commissioned Gensets and for a day at sea will be:

$$4149,6_{(Kg)} \cdot 2 = 8299,2 Kg$$

Now let us assume that there is one (1) and only array of TEGs installed on the ship's hull, consisting of 270 Seebeck chips[91]. Feeding the data to the model and running the simulation (for a near matched load) tables 10 and 11 are completed. Table 11's contents will be discussed thoroughly in Conclusions.

Table 10: Actual Trip Data

Date	Trip Day	Average Speed (KN)	Distance covered (NM)	Average Sea Temp. (°C)	Average wet sheet inner side Temp. (°C)	Δθ (°C)
20/5/2020	1	10,9	261,6	25	25,43	204,57
21/5/2020	2	10,9	523,2	23,2	23,59	206,41
22/5/2020	3	10,9	784,8	22,4	22,57	207,43
23/5/2020	4	10,9	1046,4	22	22,12	207,88
24/5/2020	5	10,9	1308	22	22,99	207,01
25/5/2020	6	10,9	1569,6	21,7	22,46	207,54
26/5/2020	7	10,9	1831,2	21	21,84	208,16
27/5/2020	8	10,9	2092,8	21	21,75	208,25
28/5/2020	9	10,9	2354,4	21	21,94	208,06
29/5/2020	10	10,9	2616	20,2	20,81	209,19
30/5/2020	11	10,9	2877,6	20	20,44	209,56
31/5/2020	12	10,9	3139,2	20	20,74	209,26
1/6/2020	13	10,9	3400,8	20	20,46	209,54
2/6/2020	14	10,9	3662,4	19,5	19,92	210,08
3/6/2020	15	10,9	3924	19,3	19,96	210,04
4/6/2020	16	10,9	4185,6	18,5	18,96	211,04
5/6/2020	17	10,9	4447,2	18,2	18,38	211,62
6/6/2020	18	10,9	4708,8	17,8	18,69	211,31
7/6/2020	19	10,9	4970,4	16,9	17,59	212,41
8/6/2020	20	10,9	5232	15,5	16,16	213,84
9/6/2020	21	10,9	5493,6	14,9	15,44	214,56
10/6/2020	22	10,9	5668	14,5	14,96	215,04

Observing the simulation results, one could make the following remarks:

The minimum power supplied per chip was 14,24W when the ship sailed in the warmer waters of the China Sea, to rise up to 14,97W when she finished her journey at the colder waters of the North Pacific. Hence the total power supplied by the 1 m^2 array would be 3844,54 W to 4041,38W, thus supplying the ship with 92,27 KWh to 96,39KWh per day. Adding up the energy quantities supplied by the array to the vessel's grid the whole 22 days of the journey, the amount sums up to 2080,38 KWh/m^2.

Considering that the nominal specific oil consumption of each of the three installed Hyundai-Himsen generators 5H21/32 @ 900 rpm is 190 g/KWh, as indicated in the Engine's manual, that would require:

$$Q_{req(Kg)} = 2080,38_{(KWh)} \cdot 0,190_{(Kgr/KWh)} = 395,27_{(Kg)}$$

of fuel oil to be consumed by the Genset to produce the energy supplied by solely 1m^2 of TEG array consisting of 270 TEG chips. Having the above in mind and inverting the estimation we can reasonably assume that for the total removal of a whole Genset there will be required:

$$A_{(m^2)} = \frac{P_{Gs(KW)}}{aveP_{Array(KW/m^2)}} = \frac{910}{3,94} \approx 231m^2$$

of arrays to completely eliminate the use of one full Genset. It has to be kept in mind at all times that the above calculation refers to the specific trip of the particular ship[92].

As shown clearly in Fig. 26 (Desert Challenger, General Arrangement Plan, Bow Section) and Fig. 27: (Desert Challenger, Typical Web Section Plan) the necessary space between scantling elements is well enough to accommodate a TEG array system of that magnitude and in fact a much larger one. This by own means is a first approach to the feasibility study for the retrofitting of the System to an existing vessel. When the System is to be

fitted to a new vessel during its shipbuilding procedure, a suitable design to accommodate the system should be applied.

With distinctive exceptions such as icebreakers, modern vessels are drawn in such a way to be perfectly capable to travel in every part of the world, limited only by their size[93]. Hence, the TEG array system installed on a vessel will have to work under various seawater temperatures. The model presented above is capable of predicting the fuel-saving capacity of the array system in every trip provided the sea-water temperature is known[94], while the SCADA monitoring system will maintain efficiency by combining the connection method (series-parallel) of array modules so the overall internal resistance of the System to be as close to the matched load as possible.

Table 11: Trip, Temperature and Recovered Power data

Date	Trip Day	Average Speed (KN)	Distance covered (NM)	Average Sea Temp. (°C)	Average wet sheet inner side Temp. (°C)	Δθ (°C)	Voltage of each chip on matched load (V)	Typical chip power supplied (W)	Power supplied per $1m^2$ array of 270 chips (W)	Energy suplied (KWh)
20/5/2020	1	10,9	261,6	25	25,43	204,57	2,66	14,24	3844,54	92,27
21/5/2020	2	10,9	523,2	23,2	23,59	206,41	2,68	14,37	3879,20	93,10
22/5/2020	3	10,9	784,8	22,4	22,57	207,43	2,70	14,44	3898,31	93,56
23/5/2020	4	10,9	1046,4	22	22,12	207,88	2,70	14,47	3906,81	93,76
24/5/2020	5	10,9	1308	22	22,99	207,01	2,69	14,41	3890,53	93,37
25/5/2020	6	10,9	1569,6	21,7	22,46	207,54	2,70	14,45	3900,40	93,61
26/5/2020	7	10,9	1831,2	21	21,84	208,16	2,71	14,49	3912,06	93,89
27/5/2020	8	10,9	2092,8	21	21,75	208,25	2,71	14,50	3913,80	93,93
28/5/2020	9	10,9	2354,4	21	21,94	208,06	2,70	14,48	3910,12	93,84
29/5/2020	10	10,9	2616	20,2	20,81	209,19	2,72	14,56	3931,33	94,35
30/5/2020	11	10,9	2877,6	20	20,44	209,56	2,72	14,59	3938,44	94,52
31/5/2020	12	10,9	3139,2	20	20,74	209,26	2,72	14,57	3932,66	94,38
1/6/2020	13	10,9	3400,8	20	20,46	209,54	2,72	14,59	3938,05	94,51
2/6/2020	14	10,9	3662,4	19,5	19,92	210,08	2,73	14,62	3948,18	94,76
3/6/2020	15	10,9	3924	19,3	19,96	210,04	2,73	14,62	3947,38	94,74
4/6/2020	16	10,9	4185,6	18,5	18,96	211,04	2,74	14,69	3966,26	95,19
5/6/2020	17	10,9	4447,2	18,2	18,38	211,62	2,75	14,73	3977,08	95,45
6/6/2020	18	10,9	4708,8	17,8	18,69	211,31	2,75	14,71	3971,29	95,31
7/6/2020	19	10,9	4970,4	16,9	17,59	212,41	2,76	14,78	3991,84	95,80
8/6/2020	20	10,9	5232	15,5	16,16	213,84	2,78	14,88	4018,73	96,45
9/6/2020	21	10,9	5493,6	14,9	15,62	214,38	2,79	14,92	4028,86	96,69
10/6/2020	22	10,9	5668	14,5	14,96	215,04	2,80	14,97	4041,38	96,99

Trip Day	Date		Average Speed (KN)	Distance covered (NM)	Average Sea Temp. (°C)	Average wet sheet inner side Temp. (°C)	Δθ (°C)	Voltage of each chip on matched load (V)	Typical chip power supplied (W)	Power supplied per $1m^2$ array of 270 chips (W)	Energy suplied (KWh)
1	20/5/2020	Trip #1: Fuchu (CN) to San Francisco (USA)	10,9	261,6	25	25,43	204,57	2,66	14,24	3844,54	92,27
2	21/5/2020		10,9	523,2	23,2	23,59	206,41	2,68	14,37	3879,20	93,10
3	22/5/2020		10,9	784,8	22,4	22,57	207,43	2,70	14,44	3898,31	93,56
4	23/5/2020		10,9	1046,4	22	22,12	207,88	2,70	14,47	3906,81	93,76
5	24/5/2020		10,9	1308	22	22,99	207,01	2,69	14,41	3890,53	93,37
6	25/5/2020		10,9	1569,6	21,7	22,46	207,54	2,70	14,45	3900,40	93,61
7	26/5/2020		10,9	1831,2	21	21,84	208,16	2,71	14,49	3912,06	93,89
8	27/5/2020		10,9	2092,8	21	21,75	208,25	2,71	14,50	3913,80	93,93
9	28/5/2020		10,9	2354,4	21	21,94	208,06	2,70	14,48	3910,12	93,84
10	29/5/2020		10,9	2616	20,2	20,81	209,19	2,72	14,56	3931,33	94,35
11	30/5/2020		10,9	2877,6	20	20,44	209,56	2,72	14,59	3938,44	94,52
12	31/5/2020		10,9	3139,2	20	20,74	209,26	2,72	14,57	3932,66	94,38
13	1/6/2020		10,9	3400,8	20	20,46	209,54	2,72	14,59	3938,05	94,51
14	2/6/2020		10,9	3662,4	19,5	19,92	210,08	2,73	14,62	3948,18	94,76
15	3/6/2020		10,9	3924	19,3	19,96	210,04	2,73	14,62	3947,38	94,74
16	4/6/2020		10,9	4185,6	18,5	18,96	211,04	2,74	14,69	3966,26	95,19
17	5/6/2020		10,9	4447,2	18,2	18,38	211,62	2,75	14,73	3977,08	95,45
18	6/6/2020		10,9	4708,8	17,8	18,69	211,31	2,75	14,71	3971,29	95,31
19	7/6/2020		10,9	4970,4	16,9	17,59	212,41	2,76	14,78	3991,84	95,80
20	8/6/2020		10,9	5232	15,5	16,16	213,84	2,78	14,88	4018,73	96,45
21	9/6/2020		10,9	5493,6	14,9	15,75	214,25	2,79	14,91	4026,59	96,64
22	10/6/2020		10,9	5668	14,5	14,96	215,04	2,80	14,97	4041,38	96,99
23	11/6/2020		Days in harbour or at roads - main engines are off								
24	12/6/2020										
25	13/6/2020										
26	14/6/2020										

27	15/6/2020	Trip #1: San Francisco (USA) to Miura, (JPMIR)	10,9	261,6	14,02	15,41	214,587	2,79	14,94	4032,84	96,79
28	16/6/2020		10,9	523,2	14,6	17,36	212,638	2,76	14,80	3996,22	95,91
29	17/6/2020		10,9	784,8	14,5	17,35	212,647	2,76	14,80	3996,38	95,91
30	18/6/2020		10,9	1046,4	15,2	16,49	213,506	2,78	14,86	4012,52	96,30
31	19/6/2020		10,9	1308	15,3	17,53	212,467	2,76	14,79	3993,01	95,83
32	20/6/2020		10,9	1569,6	15,9	18,70	211,296	2,75	14,71	3970,99	95,30
33	21/6/2020		10,9	1831,2	16	17,92	212,081	2,76	14,76	3985,75	95,66
34	22/6/2020		10,9	2092,8	16	17,69	212,306	2,76	14,78	3989,96	95,76
35	23/6/2020		10,9	2354,4	16,1	17,21	212,790	2,77	14,81	3999,07	95,98
36	24/6/2020		10,9	2616	16	17,54	212,459	2,76	14,79	3992,85	95,83
37	25/6/2020		10,9	2877,6	16,9	18,59	211,413	2,75	14,72	3973,20	95,36
38	26/6/2020		10,9	3139,2	17,3	19,39	210,613	2,74	14,66	3958,16	95,00
39	27/6/2020		10,9	3400,8	18	19,96	210,044	2,73	14,62	3947,46	94,74
40	28/6/2020		10,9	3662,4	18,1	20,13	209,874	2,73	14,61	3944,27	94,66
41	29/6/2020		10,9	3924	19	21,80	208,198	2,71	14,49	3912,76	93,91
42	30/6/2020		10,9	4185,6	19,6	20,83	209,170	2,72	14,56	3931,05	94,35
43	1/7/2020		10,9	4447,2	20,8	23,13	206,865	2,69	14,40	3887,72	93,31
44	2/7/2020		10,9	4534,4	21	23,16	206,835	2,69	14,40	3887,16	93,29
45	3/7/2020	**Days in harbour or at roads - main engines are off**									
46	4/7/2020										
47	5/7/2020										
48	6/7/2020										
49	7/7/2020										
50	8/7/2020										
51	9/7/2020										

52	10/7/2020	Trip #2: Miura, (JPMIR) to Singapore Port, SGSIN	10,9	261,6	22	25,60	204,40	2,66	14,23	3841,32	92,19
53	11/7/2020		10,9	523,2	22,7	26,11	203,89	2,65	14,19	3831,79	91,96
54	12/7/2020		10,9	784,8	23	26,22	203,78	2,65	14,18	3829,75	91,91
55	13/7/2020		10,9	1046,4	23	25,50	204,50	2,66	14,23	3843,30	92,24
56	14/7/2020		10,9	1308	24,2	27,60	202,40	2,63	14,09	3803,86	91,29
57	15/7/2020		10,9	1569,6	23	26,24	203,76	2,65	14,18	3829,33	91,90
58	16/7/2020		10,9	1831,2	24,9	26,81	203,19	2,64	14,14	3818,70	91,65
59	17/7/2020		10,9	2092,8	25,1	26,39	203,61	2,65	14,17	3826,54	91,84
60	18/7/2020		10,9	2354,4	26	28,35	201,65	2,62	14,04	3789,66	90,95
61	19/7/2020		10,9	2616	28,4	31,48	198,52	2,58	13,82	3730,85	89,54
62	20/7/2020		10,9	2869	29	31,57	198,43	2,58	13,81	3729,13	89,50
63	21/7/2020	Days in harbour or at roads - main engines are off									
64	22/7/2020										
65	23/7/2020										
66	24/7/2020										
67	25/7/2020										
68	26/7/2020										
69	27/7/2020										
70	28/7/2020	Trip #3: Singapore Port, SGSIN to Cape Town, ZACPT	10,9	261,6	28,5	31,36	198,64	2,58	13,83	3733,09	89,59
71	29/7/2020		10,9	261,6	28	30,84	199,16	2,59	13,86	3742,84	89,83
72	30/7/2020		10,9	261,6	26,2	30,19	199,81	2,60	13,91	3755,11	90,12
73	31/7/2020		10,9	261,6	25,9	29,53	200,47	2,61	13,95	3767,45	90,42
74	1/8/2020		10,9	261,6	24,5	27,82	202,18	2,63	14,07	3799,62	91,19
75	2/8/2020		10,9	261,6	24	27,32	202,68	2,63	14,11	3809,02	91,42
76	3/8/2020		10,9	261,6	24,3	26,47	203,53	2,65	14,17	3825,05	91,80
77	4/8/2020		10,9	261,6	23	25,27	204,73	2,66	14,25	3847,59	92,34
78	5/8/2020		10,9	261,6	22,8	24,34	205,66	2,67	14,32	3865,05	92,76
79	6/8/2020		10,9	261,6	21,4	22,96	207,04	2,69	14,41	3890,94	93,38
80	7/8/2020		10,9	261,6	20,9	22,20	207,80	2,70	14,46	3905,35	93,73
81	8/8/2020		10,9	523,2	20,2	21,64	208,36	2,71	14,50	3915,88	93,98
82	9/8/2020		10,9	784,8	20,8	23,31	206,69	2,69	14,39	3884,39	93,23
83	10/8/2020		10,9	1046,4	19,4	22,46	207,54	2,70	14,45	3900,44	93,61
84	11/8/2020		10,9	1308	18	19,49	210,51	2,74	14,65	3956,17	94,95
85	12/8/2020		10,9	1569,6	17,2	20,03	209,97	2,73	14,62	3946,09	94,71
86	13/8/2020		10,9	1831,2	16	17,66	212,34	2,76	14,78	3990,63	95,78
87	14/8/2020		10,9	2092,8	15,3	18,20	211,80	2,75	14,74	3980,44	95,53
88	15/8/2020	Days in harbour or at roads - main engines are off									
89	16/8/2020										
90	17/8/2020										
91	18/8/2020										

92	19/8/2020	Trip #4: Cape Town, ZACPT to Hoek van Holland Rotterdam NLRTM	10,9	261,6	17,0	19,4	210,58	2,74	14,66	3957,51	94,98
93	20/8/2020		10,9	523,2	17,8	19,7	210,26	2,73	14,64	3951,58	94,84
94	21/8/2020		10,9	784,8	18,7	22,1	207,86	2,70	14,47	3906,41	93,75
95	22/8/2020		10,9	1046,4	19,5	22,7	207,31	2,70	14,43	3896,09	93,51
96	23/8/2020		10,9	1308	20,4	22,3	207,68	2,70	14,46	3902,98	93,67
97	24/8/2020		10,9	1569,6	21,2	22,8	207,19	2,69	14,42	3893,90	93,45
98	25/8/2020		10,9	1831,2	22,1	24,3	205,68	2,67	14,32	3865,36	92,77
99	26/8/2020		10,9	2092,8	22,9	24,6	205,36	2,67	14,29	3859,50	92,63
100	27/8/2020		10,9	2354,4	23,8	25,9	204,12	2,65	14,21	3836,20	92,07
101	28/8/2020		10,9	2616	24,6	27,0	202,97	2,64	14,13	3814,52	91,55
102	29/8/2020		10,9	2877,6	25,5	28,2	201,80	2,62	14,05	3792,54	91,02
103	30/8/2020		10,9	3139,2	26,3	29,0	200,98	2,61	13,99	3777,14	90,65
104	31/8/2020		10,9	3400,8	27,2	30,5	199,51	2,59	13,89	3749,54	89,99
105	1/9/2020		10,9	3662,4	28,0	30,7	199,27	2,59	13,87	3744,97	89,88
106	2/9/2020		10,9	3924	27,6	30,5	199,48	2,59	13,89	3749,01	89,98
107	3/9/2020		10,9	4185,6	27,2	29,9	200,12	2,60	13,93	3761,02	90,26
108	4/9/2020		10,9	4447,2	26,8	29,4	200,62	2,61	13,96	3770,44	90,49
109	5/9/2020		10,9	4708,8	26,4	27,9	202,09	2,63	14,07	3798,04	91,15
110	6/9/2020		10,9	4970,4	26,0	28,3	201,66	2,62	14,04	3789,95	90,96
111	7/9/2020		10,9	5232	25,6	27,4	202,65	2,63	14,11	3808,44	91,40
112	8/9/2020		10,9	5493,6	25,2	28,0	201,99	2,63	14,06	3796,17	91,11
113	9/9/2020		10,9	5755,2	24,7	27,4	202,65	2,63	14,11	3808,45	91,40
114	10/9/2020		10,9	6016,8	24,3	27,0	203,00	2,64	14,13	3815,08	91,56
115	11/9/2020		10,9	6278,4	23,9	27,0	202,97	2,64	14,13	3814,60	91,55
116	12/9/2020		10,9	6540	23,5	26,2	203,82	2,65	14,19	3830,47	91,93
117	13/9/2020		10,9	6801,6	23,1	24,5	205,49	2,67	14,30	3861,95	92,69
118	14/9/2020		10,9	7063,2	22,7	24,8	205,24	2,67	14,29	3857,11	92,57
119	15/9/2020		10,9	7324,8	22,3	25,0	204,97	2,66	14,27	3852,16	92,45
120	16/9/2020		10,9	7586,4	21,9	25,5	204,53	2,66	14,24	3843,92	92,25
121	17/9/2020		10,9	7848	21,5	23,3	206,70	2,69	14,39	3884,65	93,23
122	18/9/2020		10,9	8109,6	21,1	22,9	207,12	2,69	14,42	3892,50	93,42
123	19/9/2020		10,9	8371,2	20,7	24,4	205,59	2,67	14,31	3863,78	92,73
124	20/9/2020		10,9	8632,8	20,3	22,3	207,74	2,70	14,46	3904,19	93,70
125	21/9/2020		10,9	8894,4	19,9	21,6	208,38	2,71	14,50	3916,22	93,99
126	22/9/2020		10,9	9156	19,5	21,6	208,36	2,71	14,50	3915,89	93,98
127	23/9/2020		10,9	9417,6	19,0	21,8	208,24	2,71	14,49	3913,56	93,93
128	24/9/2020		10,9	9679,2	18,6	21,6	208,40	2,71	14,51	3916,66	94,00
129	25/9/2020		10,9	9940,8	18,2	20,0	210,05	2,73	14,62	3947,53	94,74
130	26/9/2020		10,9	10202,4	17,8	21,3	208,70	2,71	14,53	3922,24	94,13
131	27/9/2020		10,9	10464	17,4	20,4	209,60	2,72	14,59	3939,14	94,54
132	28/9/2020		10,9	10725,6	17,0	20,5	209,45	2,72	14,58	3936,32	94,47
133	29/9/2020	Days in harbour or at roads - main engines are off									
134	30/9/2020										
135	1/10/2020										
136	2/10/2020										
137	3/10/2020										
138	4/10/2020										
139	5/10/2020										
140	6/10/2020										

141	7/10/2020	**Trip #4:Hoek van Holland Rotterdam NLRTM to Halifax CA**	10	240	15,8	18,43	211,57	2,75	14,73	3976,06	95,43
142	8/10/2020		10	480	15,8	18,86	211,14	2,74	14,70	3968,12	95,23
143	9/10/2020		10	720	15,9	17,30	212,70	2,77	14,80	3997,29	95,93
144	10/10/2020		10	960	15,9	18,34	211,66	2,75	14,73	3977,78	95,47
145	11/10/2020		10	1200	15,9	19,40	210,60	2,74	14,66	3957,89	94,99
146	12/10/2020		10	1440	16,0	17,46	212,54	2,76	14,79	3994,33	95,86
147	13/10/2020		10	1680	16,0	17,65	212,35	2,76	14,78	3990,85	95,78
148	14/10/2020		10	1920	16,0	18,57	211,43	2,75	14,72	3973,57	95,37
149	15/10/2020		10	2160	16,1	19,46	210,54	2,74	14,65	3956,76	94,96
150	16/10/2020		10	2400	16,1	18,30	211,70	2,75	14,74	3978,52	95,48
151	17/10/2020		10	2640	16,1	19,69	210,31	2,73	14,64	3952,41	94,86
152	18/10/2020		10	2880	16,2	18,91	211,09	2,74	14,69	3967,07	95,21
153	19/10/2020	**Days in harbour or at roads - main engines are off**									
154	20/10/2020										
155	21/10/2020										
156	22/10/2020										
157	23/10/2020										
158	24/10/2020										

159	25/10/2020	Trip #4: Halifax CA to Montevideo URMV	10,5	252	16,1	17,6	212,40	2,76	14,78	3991,75	95,80
160	26/10/2020		10,5	504	16,1	18,0	211,99	2,76	14,76	3983,98	95,62
161	27/10/2020		10,5	756	16,2	18,2	211,81	2,75	14,74	3980,71	95,54
162	28/10/2020		10,5	1008	16,3	19,1	210,86	2,74	14,68	3962,78	95,11
163	29/10/2020		10,5	1260	16,4	17,7	212,28	2,76	14,78	3989,47	95,75
164	30/10/2020		10,5	1512	16,4	17,6	212,37	2,76	14,78	3991,10	95,79
165	31/10/2020		10,5	1764	16,5	20,4	209,56	2,72	14,59	3938,46	94,52
166	1/11/2020		10,5	2016	16,6	20,5	209,47	2,72	14,58	3936,75	94,48
167	2/11/2020		10,5	2268	16,6	20,6	209,43	2,72	14,58	3936,02	94,46
168	3/11/2020		10,5	2520	16,7	18,1	211,86	2,75	14,75	3981,61	95,56
169	4/11/2020		10,5	2772	16,8	18,2	211,76	2,75	14,74	3979,76	95,51
170	5/11/2020		10,5	3024	16,9	19,2	210,75	2,74	14,67	3960,79	95,06
171	6/11/2020		10,5	3276	16,9	18,7	211,25	2,75	14,70	3970,14	95,28
172	7/11/2020		10,5	3528	17,0	20,9	209,11	2,72	14,56	3929,89	94,32
173	8/11/2020		10,5	3780	17,1	19,1	210,95	2,74	14,68	3964,48	95,15
174	9/11/2020		10,5	4032	17,1	19,5	210,54	2,74	14,65	3956,84	94,96
175	10/11/2020		10,5	4284	17,2	20,9	209,07	2,72	14,55	3929,10	94,30
176	11/11/2020		10,5	4536	17,3	20,9	209,08	2,72	14,55	3929,40	94,31
177	12/11/2020		10,5	4788	17,4	19,7	210,34	2,73	14,64	3953,08	94,87
178	13/11/2020		10,5	5040	17,4	20,7	209,29	2,72	14,57	3933,35	94,40
179	14/11/2020		10,5	5292	17,5	20,9	209,14	2,72	14,56	3930,56	94,33
180	15/11/2020		10,5	5544	17,6	20,5	209,49	2,72	14,58	3936,97	94,49
181	16/11/2020		10,5	5618	17,6	21,4	208,62	2,71	14,52	3920,68	94,10
182	17/11/2020	Days in harbour or at roads - main engines are off									
183	18/11/2020										
184	19/11/2020										
185	20/11/2020										
186	21/11/2020										
187	22/11/2020										
188	23/11/2020										
189	24/11/2020										

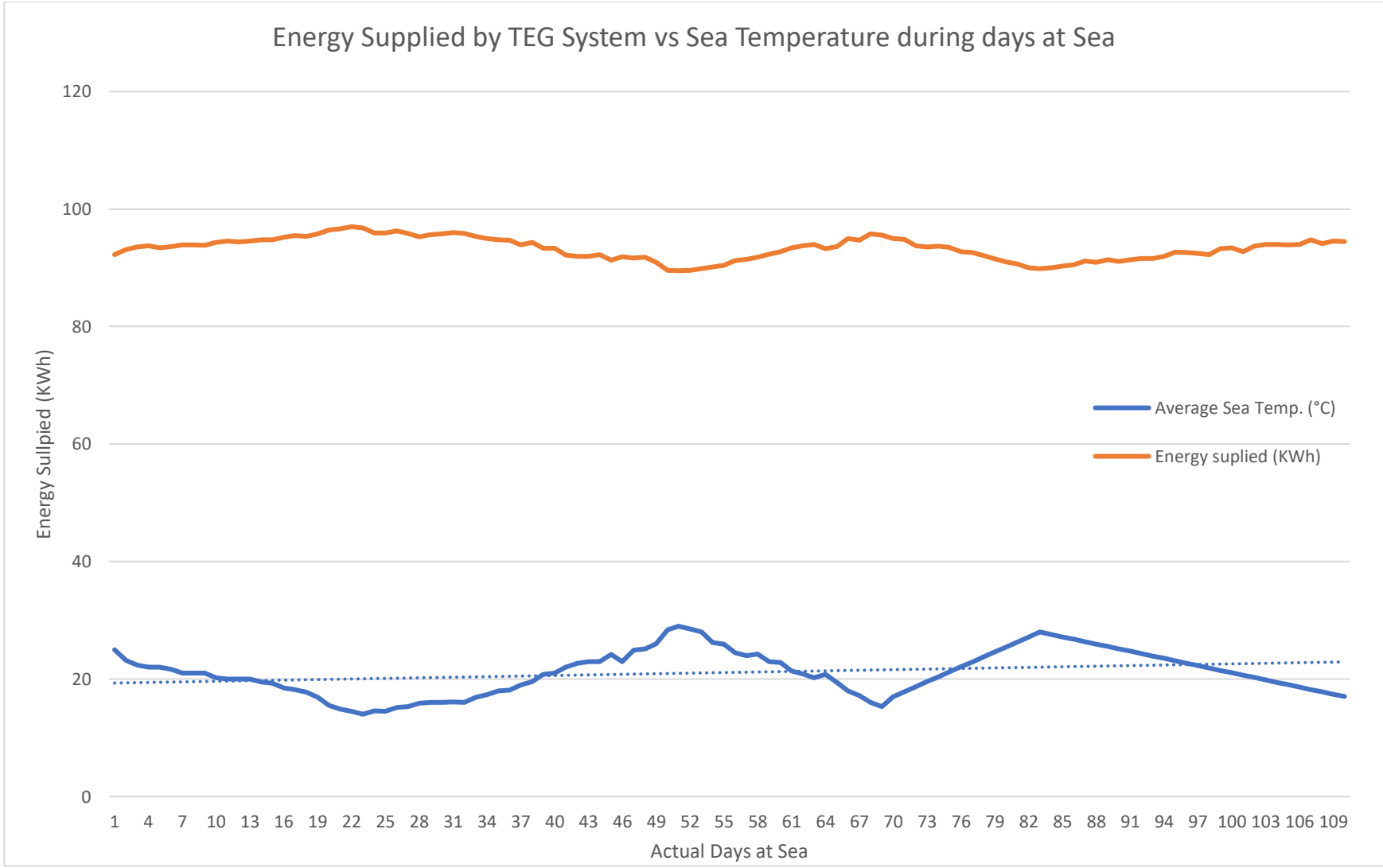

Figure 59: Energy supplied by the System to the Ship during a 109 days at sea Itinerary

Model estimated results for six months (109 days at sea):

Total Energy Capability per m^2, for six months period (109 days at Sea): **13589,33 KWh.**

Total quantity of Fuel saved per 6 months trip per m^2 of TEG arrays: **2582 Kg** (Calculation based on the Hyundai-Himsen H21/32 @ 900rpm, fuel consumption 190 g/KWh, charged in nominal power).

5.4 Statistically Critical Hypotheses Testing

Based on the data presented in the above tables several hypotheses critical for the decision of the worth of the investment for the System installation could be tested.

- SEA TEMPERATURE FLUCTUATION

As shown in the theoretical part of this dissertation as well as from the model results, becomes clear that the power output of the system depends mainly on the ΔT – temperature difference between the cold and hot side of the TEG elements. As the hot part side temperature remains roughly steady to that of the temperature of the exhaust gases, the critical factor on which the power output greatly depends on is the temperature of the inner side of the wet plate being almost a linear function of the seawater temperature itself. Figure 59 shows clearly the direct linking of the seawater temperature to the power output of the System.

Assuming that:

a. the key seawater temperature is 20^{o} C below of which the system's efficiency is particularly high as Figure 59 implies and,
b. the ports called by the Vessel in these 6 months consist a typical set of trips of the specific type and capacity vessel, it would be interesting to know what is

the possibility of the vessel traveling to warmer waters in the years to come, hence when sailing in warmer waters, one is to expect lower power output from the system. Towards this, a Hypothesis Testing at a 0,05 level of significance (95% possibility) should be run. To test this Hypothesis the initial H_0 should be defined as the "mean temperature of the seawater" $\mu_0 \leq$ **20° C.** Hence, the alternative hypothesis H_1 would be $\mu >$ **20° C.**

- Hypothesis testing can be done easily by introducing the data from the tables to the Data Analysis function of Microsoft Excel® . The testing will be the "two samples assuming unequal variances"[95]. The outcome of the analysis is presented in the following table.

Table 12: t-Test for Hypothesis testing for the possibility of Sea Temperatures higher than 20 C

t-Test, two samples assuming unequal variances

	Average Sea Temp. (°C)
Mean	20.55302
Variance	22.6638
Observations	145
Hypothesized Mean Difference	20
Degrees of freedom	144
tStat	1.398797
P(T<=t) one-tail	0.082012
t critical one-tail	1.655504
P(T<=t) two-tail	0.164024
t t Critical two-tail	1.976575

As the t statistic (1,398) is lower than the t Critical (1,655) we cannot reject the Initial Hypothesis H_o, being 95% sure that the expected mean seawater temperature will be less than or equal to 20° C for future typical trips of the vessel. Hence, we cannot reject the hypothesis that the average power supplied by the system to the ship's grid will be pretty near to the one estimated on the previous page.

CHAPTER 6: Conclusions and future research directions

By the time of writing this dissertation, being the 5th year of my research, several subjects have been made clear; the most important of them being the realization that all the critical parameters of the basic idea kept changing radically and fast, monitored by a vast bibliography. Keeping track of these changes by a simple scientific observer would be a difficult task, let alone by a researcher intended to use them. The bibliography related to the subject and used in the research turns to be equally vast, with the data (both manufactural and operational) originating from the case study ship only, being enormous in number and severity. The impossibility of creating a near real-life hands-on model and installing it on the case study ship was known from the beginning, due to financial and insurance reasons[96]. However, the lack of disposition of large laboratories (e.g. NTUA and L.C. Salamis) due to the Covid 19 pandemic, was impossible to be foreseen. Hence more parameters had to be evaluated by models and simulations and more issues creating uncertainties had to be statistically investigated.

Yet, the objective of this research, namely the feasibility of using large-scale TEG arrays attached to the vessel's inner hull plates below the waterline, seems more reachable than ever. Showing that this is feasible, beyond any scientifically reasonable doubt is the conclusion of this research and at the same time it has shown the necessity of a specific real world vessel experiment where the system will be installed or retrofitted. This, being clearly out of the scope of this feasibility study, would definitely lead to the utmost quested issue: Reduce of fossil oil usage and consequently of the ecological impact of Merchant Marine to the environment.

This research has come to the conclusion that significant waste power recovery can be achieved by means of Seebeck Elements. The quantity of the energy estimated by the

mathematical model built and the FEA simulations run has shown that a minimum of 92 KWh are saved per m^2 (approx. 270 elements) for each working day. That saves approximately 17,5 Kg of Diesel oil, otherwise burnt to produce the same amount of energy. In a real life 6 months (109 days at sea) journey between the usual destinations of the specific vessel, and in a typical range of seawater temperatures, the model predicted a total energy capability per m^2 of 13589,33 KWh, which reflects to a total quantity of Fuel 2582 Kg (Calculation based on the Hyundai-Himsen H21/32 @ 900rpm, fuel consumption 190 g/KWh, charged in nominal power). Nevertheless this refers to an optimum case where the sea temperatures do not exceed the 20^o C, yet the energy recovery would drop linearly should the vessel sailed in warmer seas, hence the temperature gradient would be smaller. And the estimation of the probability of sailing to warmers seas (with seawater temperature higher than 20^o C), was the subject of the statistical analysis in this research.

A number of drawback issues have to be considered in each case study concerning each individual vessel, as declared right from the introduction:

- The built-up of back-pressure and the effective design of the ducting system to minimize it, or keep it below the limits set by the Diesel Engine manufacturer. The simulations run and presented in this Thesis have clearly shown that the parallel configuration of the ducting system leads to far smaller back-pressure built-up while the temperature drop is significantly lower compared to the in series configuration. The latter is not due to less waste heat recovery but due to the fact that the in series configuration involves a longer ducting system. Nevertheless, as already stated, the decision on the configuration of the ducting system is going to be the subject of a separate analysis for each vessel case.
- .The continuous monitoring of the exhaust gas temperature[97] inside the duct system, in order to keep it always over the dew point. That would elaborate a number of temperature and PH sensors along the ducting network. The installation of an automatic flushing system in case of emergency, and a preventing flushing routine are necessary in order to prevent extensive or

premature wear in the ducting system. The flushing solution (calcium-, magnesium-, potassium-, or sodium-based sorbents, ammonia, or plain seawater) could be possibly supplied by the vessel's scrubber system.

- Electrical considerations would include the alteration from DC to AC and matching the load. As the vast majority of the electrical loads in a modern vessel require AC power supply the DC power supplied by the TEG arrays have to be inverted to AC, by means of suitable inverters. This, taken into consideration the efficiency of modern inverters, would decrease the overall efficiency of the system by some lower class, single-digit percentage. Matching the load might be somewhat more difficult, as the efficiency of the system depends a lot heavier on the matched load according to the maximum power transfer theorem, as described thoroughly in this thesis. Nevertheless, a suitable algorithm (executed by a PLC system) could be developed to continuously monitor the load and make the necessary modifications in the connection of the array modules so as the System to operate always close to the optimum point[98].

The environmental impact is also predicted to be considerable. Each m^2 of arrays installed, would save fuel burnt to produce 68 Kg of CO_2 per day, otherwise emitted into the atmosphere. As decarbonization[99] and desulphurization[100] of marine fuels are two of the main goals of the international sustainability efforts, it is obvious that every possible GHG emission omitted is of paramount importance. Even a "back of the envelope calculation" would suggest that given the number of the vessels at sea nowadays, an enormous amount of GHG would be saved, if the specific technology would be widely applied in marine practices.

A significant point that should be taken into account is the lifetime of the Seebeck elements themselves. In general the Seebeck as well as the Peltier modules, are considered very robust due to their solid-state structure. Although at the time of preparing this dissertation there were no thorough scientific publications on the subject,

there are several business-oriented studies indicating that the lifetime expectancy of the elements is estimated to be several decades and is affected by the maximum temperature applied to the hot side and the thermal cycling of the module[101]. Considering recycling, Bismuth, a metal, and Tellurium, a metalloid, being the main critical components of contemporary Seebeck elements, are important minerals with the bismuth being twice as abundant as gold, and Tellurium's abundancy being comparable to that of platinum (about 1 μg/kg). Hence Bismuth is rare and Tellurium is one of the rarest stable solid elements[102]. The above considerations make both these materials worth and necessary for recycling, though there are no widely accepted techniques applied to TEG recycling at the time of this research.

Following the creation and discovery of new TE materials, recycling of this class of materials received little attention for many decades. This was primarily due to two factors:

(i) a lack of concerns regarding the supply of the specific raw materials, and (ii) the fact that TE modules' useful lives were still many decades away from coming to an end. As the demand for TE materials grew over the past two decades, additional studies were conducted to address the economic and environmental problems related to the creation of new TE materials and the disposal of old TE materials.

As the subject's importance grows together with the continuous expansion of the use of Seebeck elements, several important articles have been published on that issue[103].

All the above issues could form a mainframe of the subjects of future research. As environmental issues become more important by the day, the significance of avoiding enormous amounts of GHG emissions to the atmosphere is imperative. At the time of completion of this dissertation there were more than 55000 vessels in the world[104], while a very serious war conflict was affecting dramatically the market of fossil fuels and making the cost of shipping to rise unexpectedly[105]. These factors make further research of alternative ways of saving fuel by waste heat recovery, not just necessary but inevitable.

Finally, the research depicted in this dissertation has clearly shown in numbers, that the beneficiary results of the use of Seebeck elements in self-propelled sea vessels using this newly proposed efficient cooling technology are significant in both financial and environmental terms. This could turn the whole effort of reducing the total operational costs of Marine Transport and environmental impact into a win-win case, for the benefit of the operators and the sustainability of life on the planet.

APPENDIX

1. SIMULINK MATLAB CODE

a. The .rtw code:

```
/*
 * HeatTransfer1v2A.c
 *
 * Academic License - for use in teaching, academic research, and meeting
 * course requirements at degree granting institutions only.  Not for
 * government, commercial, or other organizational use.
 *
 * Code generation for model "HeatTransfer1v2A".
 *
 * Model version              : 1.44
 * Simulink Coder version : 9.5 (R2021a) 14-Nov-2020
 * C source code generated on : Sun Oct  3 13:48:06 2021
 *
 * Target selection: grt.tlc
 *  Note:  GRT  includes  extra  infrastructure  and  instrumentation  for
prototyping
 * Embedded hardware selection: Intel->x86-64 (Windows64)
 * Code generation objective: Execution efficiency
 * Validation result: Not run
 */

#include "HeatTransfer1v2A.h"
#include "HeatTransfer1v2A_private.h"

/* Real-time model */
static RT_MODEL_HeatTransfer1v2A_T HeatTransfer1v2A_M_;
RT_MODEL_HeatTransfer1v2A_T       *const       HeatTransfer1v2A_M       =
&HeatTransfer1v2A_M_;

/* Model step function */
void HeatTransfer1v2A_step(void)
{
  /* Update absolute time for base rate */
  /* The "clockTick0" counts the number of times the code of this task has
   * been executed. The absolute time is the multiplication of "clockTick0"
   * and "Timing.stepSize0". Size of "clockTick0" ensures timer will not
   * overflow during the application lifespan selected.
```

```
   */
  HeatTransfer1v2A_M->Timing.t[0] =
    ((time_T)(++HeatTransfer1v2A_M->Timing.clockTick0)) *
    HeatTransfer1v2A_M->Timing.stepSize0;

  {
    /* Update absolute timer for sample time: [6.0s, 0.0s] */
    /* The "clockTick1" counts the number of times the code of this task has
     * been executed. The resolution of this integer timer is 6.0, which is
the step size
     * of the task. Size of "clockTick1" ensures timer will not overflow
during the
     * application lifespan selected.
     */
    HeatTransfer1v2A_M->Timing.clockTick1++;
  }
}

/* Model initialize function */
void HeatTransfer1v2A_initialize(void)
{
  /* Registration code */

  /* initialize real-time model */
  (void) memset((void *)HeatTransfer1v2A_M, 0,
                sizeof(RT_MODEL_HeatTransfer1v2A_T));

  {
    /* Setup solver object */
    rtsiSetSimTimeStepPtr(&HeatTransfer1v2A_M->solverInfo,
                          &HeatTransfer1v2A_M->Timing.simTimeStep);
    rtsiSetTPtr(&HeatTransfer1v2A_M->solverInfo,
&rtmGetTPtr(HeatTransfer1v2A_M));
    rtsiSetStepSizePtr(&HeatTransfer1v2A_M->solverInfo,
                       &HeatTransfer1v2A_M->Timing.stepSize0);
    rtsiSetErrorStatusPtr(&HeatTransfer1v2A_M->solverInfo,
(&rtmGetErrorStatus
      (HeatTransfer1v2A_M)));
    rtsiSetRTModelPtr(&HeatTransfer1v2A_M->solverInfo, HeatTransfer1v2A_M);
  }

  rtsiSetSimTimeStep(&HeatTransfer1v2A_M->solverInfo, MAJOR_TIME_STEP);
  rtsiSetSolverName(&HeatTransfer1v2A_M->solverInfo,"FixedStepDiscrete");
  rtmSetTPtr(HeatTransfer1v2A_M, &HeatTransfer1v2A_M->Timing.tArray[0]);
  HeatTransfer1v2A_M->Timing.stepSize0 = 6.0;
}

/* Model terminate function */
void HeatTransfer1v2A_terminate(void)
{
  /* (no terminate code required) */
}
```

b. The p macros code:

```
/*
 * HeatTransfer1v2A_private.h
 *
 * Academic License - for use in teaching, academic research, and meeting
 * course requirements at degree granting institutions only.  Not for
 * government, commercial, or other organizational use.
 *
 * Code generation for model "HeatTransfer1v2A".
 *
 * Model version              : 1.44
 * Simulink Coder version : 9.5 (R2021a) 14-Nov-2020
 * C source code generated on : Sun Oct  3 13:48:06 2021
 *
 * Target selection: grt.tlc
 *  Note:  GRT  includes  extra  infrastructure  and  instrumentation  for
prototyping
 * Embedded hardware selection: Intel->x86-64 (Windows64)
 * Code generation objective: Execution efficiency
 * Validation result: Not run
 */

#ifndef RTW_HEADER_HeatTransfer1v2A_private_h_
#define RTW_HEADER_HeatTransfer1v2A_private_h_
#include "rtwtypes.h"
#include "multiword_types.h"

/* Private macros used by the generated code to access rtModel */
#ifndef rtmIsMajorTimeStep
#define  rtmIsMajorTimeStep(rtm)            (((rtm)->Timing.simTimeStep)  ==
MAJOR_TIME_STEP)
#endif

#ifndef rtmIsMinorTimeStep
#define  rtmIsMinorTimeStep(rtm)            (((rtm)->Timing.simTimeStep)  ==
MINOR_TIME_STEP)
#endif

#ifndef rtmSetTPtr
#define rtmSetTPtr(rtm, val)           ((rtm)->Timing.t = (val))
#endif
#endif                             /* RTW_HEADER_HeatTransfer1v2A_private_h_
*/
```

c. Multiwording

```
/*
 * multiword_types.h
 *
 * Academic License - for use in teaching, academic research, and meeting
 * course requirements at degree granting institutions only.  Not for
 * government, commercial, or other organizational use.
 *
 * Code generation for model "HeatTransfer1v2A".
 *
 * Model version              : 1.44
 * Simulink Coder version : 9.5 (R2021a) 14-Nov-2020
 * C source code generated on : Sun Oct  3 13:48:06 2021
 *
```

```
 * Target selection: grt.tlc
 *  Note:  GRT  includes  extra  infrastructure  and  instrumentation  for
prototyping
 * Embedded hardware selection: Intel->x86-64 (Windows64)
 * Code generation objective: Execution efficiency
 * Validation result: Not run
 */

#ifndef MULTIWORD_TYPES_H
#define MULTIWORD_TYPES_H
#include "rtwtypes.h"

/*
 * MultiWord supporting definitions
 */
typedef long long longlong_T;

/*
 * MultiWord types
 */
typedef struct {
  uint64_T chunks[2];
} int128m_T;

typedef struct {
  int128m_T re;
  int128m_T im;
} cint128m_T;

typedef struct {
  uint64_T chunks[2];
} uint128m_T;

typedef struct {
  uint128m_T re;
  uint128m_T im;
} cuint128m_T;

typedef struct {
  uint64_T chunks[3];
} int192m_T;

typedef struct {
  int192m_T re;
  int192m_T im;
} cint192m_T;

typedef struct {
  uint64_T chunks[3];
} uint192m_T;

typedef struct {
  uint192m_T re;
  uint192m_T im;
} cuint192m_T;

typedef struct {
  uint64_T chunks[4];
```

```
} int256m_T;

typedef struct {
  int256m_T re;
  int256m_T im;
} cint256m_T;

typedef struct {
  uint64_T chunks[4];
} uint256m_T;

typedef struct {
  uint256m_T re;
  uint256m_T im;
} cuint256m_T;

typedef struct {
  uint64_T chunks[5];
} int320m_T;

typedef struct {
  int320m_T re;
  int320m_T im;
} cint320m_T;

typedef struct {
  uint64_T chunks[5];
} uint320m_T;

typedef struct {
  uint320m_T re;
  uint320m_T im;
} cuint320m_T;

typedef struct {
  uint64_T chunks[6];
} int384m_T;

typedef struct {
  int384m_T re;
  int384m_T im;
} cint384m_T;

typedef struct {
  uint64_T chunks[6];
} uint384m_T;

typedef struct {
  uint384m_T re;
  uint384m_T im;
} cuint384m_T;

typedef struct {
  uint64_T chunks[7];
} int448m_T;

typedef struct {
  int448m_T re;
```

```
  int448m_T im;
} cint448m_T;

typedef struct {
  uint64_T chunks[7];
} uint448m_T;

typedef struct {
  uint448m_T re;
  uint448m_T im;
} cuint448m_T;

typedef struct {
  uint64_T chunks[8];
} int512m_T;

typedef struct {
  int512m_T re;
  int512m_T im;
} cint512m_T;

typedef struct {
  uint64_T chunks[8];
} uint512m_T;

typedef struct {
  uint512m_T re;
  uint512m_T im;
} cuint512m_T;

typedef struct {
  uint64_T chunks[9];
} int576m_T;

typedef struct {
  int576m_T re;
  int576m_T im;
} cint576m_T;

typedef struct {
  uint64_T chunks[9];
} uint576m_T;

typedef struct {
  uint576m_T re;
  uint576m_T im;
} cuint576m_T;

typedef struct {
  uint64_T chunks[10];
} int640m_T;

typedef struct {
  int640m_T re;
  int640m_T im;
} cint640m_T;

typedef struct {
```

```
  uint64_T chunks[10];
} uint640m_T;

typedef struct {
  uint640m_T re;
  uint640m_T im;
} cuint640m_T;

typedef struct {
  uint64_T chunks[11];
} int704m_T;

typedef struct {
  int704m_T re;
  int704m_T im;
} cint704m_T;

typedef struct {
  uint64_T chunks[11];
} uint704m_T;

typedef struct {
  uint704m_T re;
  uint704m_T im;
} cuint704m_T;

typedef struct {
  uint64_T chunks[12];
} int768m_T;

typedef struct {
  int768m_T re;
  int768m_T im;
} cint768m_T;

typedef struct {
  uint64_T chunks[12];
} uint768m_T;

typedef struct {
  uint768m_T re;
  uint768m_T im;
} cuint768m_T;

typedef struct {
  uint64_T chunks[13];
} int832m_T;

typedef struct {
  int832m_T re;
  int832m_T im;
} cint832m_T;

typedef struct {
  uint64_T chunks[13];
} uint832m_T;

typedef struct {
```

```
  uint832m_T re;
  uint832m_T im;
} cuint832m_T;

typedef struct {
  uint64_T chunks[14];
} int896m_T;

typedef struct {
  int896m_T re;
  int896m_T im;
} cint896m_T;

typedef struct {
  uint64_T chunks[14];
} uint896m_T;

typedef struct {
  uint896m_T re;
  uint896m_T im;
} cuint896m_T;

typedef struct {
  uint64_T chunks[15];
} int960m_T;

typedef struct {
  int960m_T re;
  int960m_T im;
} cint960m_T;

typedef struct {
  uint64_T chunks[15];
} uint960m_T;

typedef struct {
  uint960m_T re;
  uint960m_T im;
} cuint960m_T;

typedef struct {
  uint64_T chunks[16];
} int1024m_T;

typedef struct {
  int1024m_T re;
  int1024m_T im;
} cint1024m_T;

typedef struct {
  uint64_T chunks[16];
} uint1024m_T;

typedef struct {
  uint1024m_T re;
  uint1024m_T im;
} cuint1024m_T;
```

```
typedef struct {
  uint64_T chunks[17];
} int1088m_T;

typedef struct {
  int1088m_T re;
  int1088m_T im;
} cint1088m_T;

typedef struct {
  uint64_T chunks[17];
} uint1088m_T;

typedef struct {
  uint1088m_T re;
  uint1088m_T im;
} cuint1088m_T;

typedef struct {
  uint64_T chunks[18];
} int1152m_T;

typedef struct {
  int1152m_T re;
  int1152m_T im;
} cint1152m_T;

typedef struct {
  uint64_T chunks[18];
} uint1152m_T;

typedef struct {
  uint1152m_T re;
  uint1152m_T im;
} cuint1152m_T;

typedef struct {
  uint64_T chunks[19];
} int1216m_T;

typedef struct {
  int1216m_T re;
  int1216m_T im;
} cint1216m_T;

typedef struct {
  uint64_T chunks[19];
} uint1216m_T;

typedef struct {
  uint1216m_T re;
  uint1216m_T im;
} cuint1216m_T;

typedef struct {
  uint64_T chunks[20];
} int1280m_T;
```

```
typedef struct {
  int1280m_T re;
  int1280m_T im;
} cint1280m_T;

typedef struct {
  uint64_T chunks[20];
} uint1280m_T;

typedef struct {
  uint1280m_T re;
  uint1280m_T im;
} cuint1280m_T;

typedef struct {
  uint64_T chunks[21];
} int1344m_T;

typedef struct {
  int1344m_T re;
  int1344m_T im;
} cint1344m_T;

typedef struct {
  uint64_T chunks[21];
} uint1344m_T;

typedef struct {
  uint1344m_T re;
  uint1344m_T im;
} cuint1344m_T;

typedef struct {
  uint64_T chunks[22];
} int1408m_T;

typedef struct {
  int1408m_T re;
  int1408m_T im;
} cint1408m_T;

typedef struct {
  uint64_T chunks[22];
} uint1408m_T;

typedef struct {
  uint1408m_T re;
  uint1408m_T im;
} cuint1408m_T;

typedef struct {
  uint64_T chunks[23];
} int1472m_T;

typedef struct {
  int1472m_T re;
  int1472m_T im;
} cint1472m_T;
```

```
typedef struct {
  uint64_T chunks[23];
} uint1472m_T;

typedef struct {
  uint1472m_T re;
  uint1472m_T im;
} cuint1472m_T;

typedef struct {
  uint64_T chunks[24];
} int1536m_T;

typedef struct {
  int1536m_T re;
  int1536m_T im;
} cint1536m_T;

typedef struct {
  uint64_T chunks[24];
} uint1536m_T;

typedef struct {
  uint1536m_T re;
  uint1536m_T im;
} cuint1536m_T;

typedef struct {
  uint64_T chunks[25];
} int1600m_T;

typedef struct {
  int1600m_T re;
  int1600m_T im;
} cint1600m_T;

typedef struct {
  uint64_T chunks[25];
} uint1600m_T;

typedef struct {
  uint1600m_T re;
  uint1600m_T im;
} cuint1600m_T;

typedef struct {
  uint64_T chunks[26];
} int1664m_T;

typedef struct {
  int1664m_T re;
  int1664m_T im;
} cint1664m_T;

typedef struct {
  uint64_T chunks[26];
} uint1664m_T;
```

```
typedef struct {
  uint1664m_T re;
  uint1664m_T im;
} cuint1664m_T;

typedef struct {
  uint64_T chunks[27];
} int1728m_T;

typedef struct {
  int1728m_T re;
  int1728m_T im;
} cint1728m_T;

typedef struct {
  uint64_T chunks[27];
} uint1728m_T;

typedef struct {
  uint1728m_T re;
  uint1728m_T im;
} cuint1728m_T;

typedef struct {
  uint64_T chunks[28];
} int1792m_T;

typedef struct {
  int1792m_T re;
  int1792m_T im;
} cint1792m_T;

typedef struct {
  uint64_T chunks[28];
} uint1792m_T;

typedef struct {
  uint1792m_T re;
  uint1792m_T im;
} cuint1792m_T;

typedef struct {
  uint64_T chunks[29];
} int1856m_T;

typedef struct {
  int1856m_T re;
  int1856m_T im;
} cint1856m_T;

typedef struct {
  uint64_T chunks[29];
} uint1856m_T;

typedef struct {
  uint1856m_T re;
  uint1856m_T im;
```

```
} cuint1856m_T;

typedef struct {
  uint64_T chunks[30];
} int1920m_T;

typedef struct {
  int1920m_T re;
  int1920m_T im;
} cint1920m_T;

typedef struct {
  uint64_T chunks[30];
} uint1920m_T;

typedef struct {
  uint1920m_T re;
  uint1920m_T im;
} cuint1920m_T;

typedef struct {
  uint64_T chunks[31];
} int1984m_T;

typedef struct {
  int1984m_T re;
  int1984m_T im;
} cint1984m_T;

typedef struct {
  uint64_T chunks[31];
} uint1984m_T;

typedef struct {
  uint1984m_T re;
  uint1984m_T im;
} cuint1984m_T;

typedef struct {
  uint64_T chunks[32];
} int2048m_T;

typedef struct {
  int2048m_T re;
  int2048m_T im;
} cint2048m_T;

typedef struct {
  uint64_T chunks[32];
} uint2048m_T;

typedef struct {
  uint2048m_T re;
  uint2048m_T im;
} cuint2048m_T;

#endif                                 /* MULTIWORD_TYPES_H */
```

d. The rt header modelling

```
/*
 *  rtmodel.h:
 *
 * Academic License - for use in teaching, academic research, and meeting
 * course requirements at degree granting institutions only.  Not for
 * government, commercial, or other organizational use.
 *
 * Code generation for model "HeatTransfer1v2A".
 *
 * Model version              : 1.44
 * Simulink Coder version : 9.5 (R2021a) 14-Nov-2020
 * C source code generated on : Sun Oct  3 13:48:06 2021
 *
 * Target selection: grt.tlc
 *  Note:  GRT  includes  extra  infrastructure  and  instrumentation  for
prototyping
 * Embedded hardware selection: Intel->x86-64 (Windows64)
 * Code generation objective: Execution efficiency
 * Validation result: Not run
 */

#ifndef RTW_HEADER_rtmodel_h_
#define RTW_HEADER_rtmodel_h_

/*
 *  Includes the appropriate headers when we are using rtModel
 */
#include "HeatTransfer1v2A.h"
#define GRTINTERFACE                   0

/* Macros generated for backwards compatibility  */
#ifndef rtmGetStopRequested
#define rtmGetStopRequested(rtm)       ((void*) 0)
#endif
#endif                                 /* RTW_HEADER_rtmodel_h_ */
```

e. The rtw types

```
/*
 * rtwtypes.h
 *
 * Academic License - for use in teaching, academic research, and meeting
 * course requirements at degree-granting institutions only.  Not for
 * government, commercial, or other organizational use.
 *
 * Code generation for model "HeatTransfer1v2A".
 *
 * Model version              : 1.44
 * Simulink Coder version : 9.5 (R2021a) 14-Nov-2020
 * C source code generated on : Sun Oct  3 13:48:06 2021
 *
 * Target selection: grt.tlc
```

```
 *  Note:  GRT  includes  extra  infrastructure  and  instrumentation  for
prototyping
 * Embedded hardware selection: Intel->x86-64 (Windows64)
 * Code generation objective: Execution efficiency
 * Validation result: Not run
 */

#ifndef RTWTYPES_H
#define RTWTYPES_H
#include "tmwtypes.h"
#ifndef POINTER_T
#define POINTER_T

typedef void * pointer_T;

#endif

/* Logical type definitions */
#if (!defined(__cplusplus))
#ifndef false
#define false                          (0U)
#endif

#ifndef true
#define true                           (1U)
#endif
#endif

#ifndef INT64_T
#define INT64_T

typedef long long int64_T;

#define MAX_int64_T                    ((int64_T)(9223372036854775807LL))
#define MIN_int64_T                      ((int64_T)(-9223372036854775807LL-
1LL))
#endif

#ifndef UINT64_T
#define UINT64_T

typedef unsigned long long uint64_T;

#define MAX_uint64_T                   ((uint64_T)(0xFFFFFFFFFFFFFFFFULL))
#endif

/*=======================================================================
==*
 *       Additional       complex       number       type       definitions
*

*=======================================================================
=*/
#ifndef CINT64_T
#define CINT64_T

typedef struct {
  int64_T re;
```

```
  int64_T im;
} cint64_T;

#endif

#ifndef CUINT64_T
#define CUINT64_T

typedef struct {
  uint64_T re;
  uint64_T im;
} cuint64_T;

#endif
#endif                                                  /* RTWTYPES_H */
```

2. Index of key words and phrases

3. List of Abbreviations and Acronyms

ABC	Atlantic Bulk Carriers
CAD	Computer Aided Design
CFD	Computational fluid dynamics
ECA	Emissions Control Area
EGB	Exhaust Gas Boiler
FEA	Finite Elements Analysis
GHG	Green House Gas
HFO	Heavy Fuel Oil
IMO	International Maritime Organization
LED	Light Emitting Diode
LNG	Liquified Natural Gas
MCR	Maximum Continuous Rating
MDO	Marine Diesel Oil
MFO	Marine Fuel Oil
MGO	Marine Gas Oil
SCADA	Supervisory Control And Data Acquisition
TEG	Thermo Electric Generators
VLCC	Very Large Crude Carrier.

4. Table of figures

5. List of Tables

6. BIBLIOGRAPHY

1. "Electrotechnical Applications on ships and floating structures", Ioannis Prousalidis, 1st edition in the Greek language, Symmetria Editions, Athens 2012, ISBN: 9789602663615.
2. "Electrotechnics and Electronic Technology", Evangelos Christoforou, 1st edition in Greek language, Kallipos Editions, Athens 2015, ISBN: . 978-960-603-501-2.
3. "Engineering Heat Transfer", James R. Welty, Oregon 1974, John Wiley &Sons Inc. ISBN: 0-471-93340-06.
4. "Enhanced Thermoelectric Performance and Anomalous Seebeck Effects in Topological Insulators",Yong Xu, Zhongxue Gan, and Shou-Cheng Zhang, Phys. Rev. Lett. 112, 226801. Published 2 June 2014
5. "Exploitation of Waste Heat of Marine Diesel Engines using Seebeck Elements" Yiannis Armenakis, International Journal of Innovative Research in Science, Engineering and Technology, Volume 11, Issue 7, July 2022, DOI:10.15680/IJIRSET.2022.1107002.
6. "Fluid Mechanics for Engineers: A Graduate Textbook", Meinhard T. Schobeiri, 3rd edition, Texas 2010, Springer Editions, ISBN: 9783642115936.
7. "Fluid Mechanics Vol.1", Angelos Papaioannou, 2nd edition in Greek language, G. Gelbesis Editions, Athens 2002, ISBN: 9608028124.
8. "Fluid Mechanics Vol.2", Angelos Papaioannou, 2nd edition in Greek language, G. Gelbesis Editions, Athens 2002, ISBN: 9608028132 .
9. "Fundamentals of Classical Thermodynamics", Gordon J. Van Wylen, Richard E. Sonntag, 2nd Edition, New York 1978, John Wiley & Sons, Inc., ISBN: 9780471041887
10. "Hybrid Renewable Energy Systems and Microgrids" Edited by: Ersan Kabalci (Chapter 2: Centralized power generation), 2021 Elsevier Inc. (Via the CUT Library), ISBN: 978-0-12-821724-5
11. "Hybrid Technologies for Power Generation-A volume in Hybrid Energy Systems" (Chapter 14: Modeling hybrid energy systems for marine applications: Hybrid electric ships), Edited by: Massimiliano Lo Faro, Orazio Barbera and Giosué Giacoppo, 2022 Elsevier Inc. ISBN 978-0-12-823793-9, (Via the CUT library).
12. "Modern Engineering Statistics", Thomas P. Ryan, 1st Edition, John Wiley & Sons, Inc., ISBN-10: 0470081872.
13. "Modern Physics for Semiconductor Science", Charles C. Coleman, 1st edition, Wiley-VCH, New York 2007, ISBN: 3527407014 (borrowed).

14. “Nanostructured Thermoelectrics: The New Paradigm?," M. G. Kanatzidis, Chemistry of Materials, vol. 22, pp. 648-659, Feb 9 2010.
15. “New Technologies for Emission Control in Marine Diesel Engines”, Masaaki Okubo and Takuya Kuwahara, (Chapter 4: Operation examples of emission control systems), 2019 Elsevier Inc. (Via the CUT Library), ISBN: 978-0-12-812307-2,
16. “Precise measurement of absolute Seebeck coefficient from Thomson effect using ac-dc technique”, Y. Amagai, T. Shimazaki, K. Okawa, H. Fujiki, T. Kawae, and N.-H. Kaneko, AIP Advances 9, 065312 (2019); https://doi.org/10.1063/1.5095485
17. “Programmable Logic Controllers and Applications for Marine Engineers and ETOs”, Alexandr Yakimchuk, Witherbys Editions, Livingston Scotland, UK, 2020, ISBN: 9781856098120
18. “Rethinking Thermoelectric Effects In Seebeck And Peltier Elements: Toward A Unifying Paradigm”, Michael Spry, 1st Edition, 2013, Scotts Valley, California, ISBN:1492328278.
19. “Seebeck-driven transverse thermoelectric generation” .Zhou, W., Yamamoto, K., Miura, A. *et al. Nat. Mater.* **20**, 463–467 (2021). https://doi.org/10.1038/s41563-020-00884-2
20. “Semiconductor Devices”, Kanaan Kano, 1st Edition 1997, Prentice Hall, ISBN: 0023619384 (borrowed).
21. “Ship Construction”, George J Bruce, D J Eyres, 7th Edition, Butterworth-Heinemann Editions, Oxford UK 2012, ISBN-10: 008097239X.
22. “Shipboard Electrical Power Systems”, Mukund R. Patel, 2nd Edition 2021, CRC Press, ISBN 9780367430351.
23. “Shipboard Power Systems Design and Verification Fundamentals”, Mohammed M. Islam, 2018, Wiley-IEEE Standards Association, IEEE Library book number 8390724.
24. “Statistics for Engineers and Scientists”, William Navidi, 4th edition 2014, New York, McGraw Hill, ISBNQ: 0073401331.
25. “Sustainable Energy Systems on Ships-Novel Technologies for Low Carbon Shipping”, Edited by: Francesco Baldi, Andrea Coraddu and Maria E. Mondejar, 2022, (Chapter 4: Waste heat recovery on ships), https://doi.org/10.1016/C2020-0-01975-4 , ISBN :978-0-12-824471-5 (Elsevier, via the CUT Library).
26. “Synthesis and Characterization of Bismuth Telluride-Based Nanostructured Thermoelectric Composite Materials”, Keshavarz Khorasgani, M. (2014). (PhD thesis, École Polytechnique de Montréal). Retrieved from https://publications.polymtl.ca/1372/
27. “Thermodynamics and an Introduction to Thermostatistics”, Herbert B. Callen, 1st Edition, New York 1990, John Wiley & Sons, Inc., ISBN: 9780471862567.

28. “Thermodynamics: An Engineering Approach” Yunus A. Cengel, Michael A. Boles, September 22, 2006 by McGraw-Hill, ISBN:9780073305370.
29. “Thermoelectric Generation Based on Spin Seebeck Effects," K. Uchida et al., in Proceedings of the IEEE, vol. 104, no. 10, pp. 1946-1973, Oct. 2016, doi: 10.1109/JPROC.2016.2535167.
30. “Treatise on Thermodynamics”, Max Plank, 3rd edition, (translated from the 7th German Edition), Dover Publicatons Inc.New York, ISBN: 0-486-60219-2.

7. REFERENCES

[1] Colgan, Jeff D. "Fueling the Fire: Pathways from Oil to War." *International Security*, vol. 38, no. 2, 2013, pp. 147–180. *JSTOR*, www.jstor.org/stable/24480933. Accessed 25 Oct. 2020. Also, https://energypost.eu/twenty-first-century-energy-wars-oil-gas-fuelling-global-conflicts/ Accessed 25 Oct.2020.

[2].M. Baleynaud, Feng Huang, Jie Zheng, Jean-Michel Baleynaud, Jun Lu. Heat recovery potentials and technologies in industrial zones. Journal of the Energy Institute, Maney Publishing, 2016, 90 (6),pp.951-961. 10.1016/j.joei.2016.07.012. hal-02152487

[3] Liu, X., Meng, J. & Guo, Z. Entropy generation extremum and entransy dissipation extremum for heat exchanger optimization. *Chin. Sci. Bull.* **54,** 943–947 (2009). https://doi.org/10.1007/s11434-009-0130-6

[4] Saha, Gopi Mohan, "The technical and economical aspects of marine engine selection" (1996). World Maritime University Dissertations. 1052. https://commons.wmu.se/all_dissertations/1052 also, https://www.wartsila.com/sustainability/innovating-for-sustainable-societies/improving-efficiency Accessed 20 Oct.2020.

[5] Including but not limited to fuel and lubricating oil preheating, water evaporator preheating, usage water heating etc.

[6] Korczewski Z.: Exhaust gas temperature measurements in diagnostic examination of marine turbocharged engines. Part I and II. Diagnostic and operating tolerances. Polish Maritime Research, (In English, and in printing).

[7] Wood C..: Materials for thermoelectric energy conversion. Downloaded from https://iopscience.iop.org/article/10.1088/0034-4885/51/4/001/meta on May 20, 2019.

[8] Polozine Alexandre, Sirotinskaya Susanna Schaeffer Lirio, History of Development of Thermoelectric Materials for Electric Power Generation and Criteria of their Quality, The ResearchGate Materials Research 17(5):1260-1267 September 2014

[9] Armenakis Yiannis P., Chatzis Soterios, "Waste heat recovery and electrical power production on vessels by means of TEG arrays attached on the hull plates below the waterline" As tresented in the ESTS 2019 International Conference, Washington USA, 15/08/2019.

[10] Initial experiments held in Hellenic Government/Mnistry of Education/Salamis Lab Centre Sept.2017 to March 2020.

[11] "Size" at this point, referrs to the power transfer potential of the whole installation, which is actualy a measure of the total length of the network itself times its average cross sectional area.

[12] For all four bulleted subjects please referr to note 9 above.

[13] Weidenkaff, Anke: Thermoelectricity for future sustainable energy technologies, The Researchgate The European Physical Journal Conferences January 2017

[14] Mikerov, Alexander , "From history of electrical engineering V: Electron discovery and its properties estimation", 2016 IEEE NW Russia Young Researchers in Electrical and Electronic Engineering Conference (EIConRusNW), St Petersburg, Russia: IEEE, pp. 3–7

[15] Polozine, Alexandre et al. "History of Development of Thermoelectric Materials for Electric Power Generation and Criteria of their Quality" *Materials Research*. 2014; 17(5): 1260-1267

[16] As above p. 4/8

[17] Thorough theoretical presentations of the Seebeck, Peltier, Thomson and Joule effects are.widely available in the International Bibliography. Nevertheless, as the subject of this study is the feasibility of the implementation of practical TEG chips to ships heat waste recovery systems, the extended theoretical discussion of the TEG phaenomenae -although presented- is out of the scope of this dissertation. Still they will be further explained in the mathematical modeling part of this dissertation.

[18] L. D. Hicks and M. S. Dresselhaus, "Thermoelectric figure of merit of a one-dimensional conductor", Phys. Rev. B 47, (1993),

[19] Goupil, Christophe; Ouerdane, Henni; Zabrocki, Knud; Seifert, Wolfgang; Hinsche, Nicki F.; Müller, Eckhard (2016). "Thermodynamics and thermoelectricity". In Goupil, Christophe (ed.). Continuum Theory and Modeling of Thermoelectric Elements. New York, New York, USA: Wiley-VCH.

[20] As (9) above, pages 2 & 3.

[21] Bos JW. *Thermoelectric materials: efficiencies found innanocomposites*. London: Royal Society of Chemistry; 2014. Available from: <http://www.rsc.org/Education/EiC/issues/2012March/thermoelectric-materials-nanoparticles.asp>. Access on:24/05/2020.

[22] McCormick. *Thermoelectric Material the Best at ConvertingHeat Waste to Electricity*. Evanston: McCormick School of Engineering and Applied Science; 2012. Available at: <http://www.mccormick.northwestern.edu/news/articles/2012/09/vinayak-dravid-thermoelectric-materialworld-record.html>. As the particular essay was based on facts and figures dated back in 2012 and having in mind the evolution ot TEG technolgy it is reasonable to expect a rise in efficiency to more than 25 % within the current decade.

[23] Hasan U. Zaman et al. Conversion of wasted heat energy into electrical energy using TEG, 2016 IEEE Annual Computing and Communication Workshop and Conference p 1-5

[24] Freer Robert Powell, Anthony V. Realising the potential of thermoelectric technology: a Roadmap *Journal of. Materetrial Chemistry. C*, 2020,8, 441-463

[25] Though TEC and TEG modules share the same physics principle, in practical manufacturing terms, they differ significantly. Lapping, Max. temperature and soldering material and techniques are different. See https://tecteg.com/thermoelectric-power-module-selection-purchase/

[26] As (9) above, page 4

[27] As this dissertation was being written a new more efficient model of an "of the shelf" TEG element was commercially available. TEG1-12610-5.1 by Tecteg Co. https://tecteg.com/wp-content/uploads/2014/09/1.pdf

[28] https://www.ics-shipping.org/shipping-facts/shipping-and-world-trade as well as Environmental Assessment Source Book Volume II page. 185, World Bank Technical Paper (No 140)

[29] https://www.marineinsight.com/marine-electrical/electrical-propulsion-system-in-ships/ (visited 05/08/2020)

[30] Mukund, Patel P. Shipboard Propulsion, Power Electronics, and Ocean Energy, CRC Press, 2012, pages 179-293

[31] As energy cannot be consumed or produced in anyway, the terms "Power Production" and "Power Consumption" despite the fact that they have prevailed in the international literature as well as in everyday life, they are incorrect in absolute scientific terms. In this work these terms wherever mentioned are meant with their conventional and not strict scientific meaning.

[32] https://www.f-cca.com/downloads/2018-Cruise-Industry-Overview-and-Statistics.pdf (visited 12/08/2020)

[33] Warships of the Hellenic Navy (RHN at the time) supplied power to Ithaka and Kephalonia basic shore resque services for several days during the 1953 Earthquakes.

[34] https://www.ee.co.za/article/power-ships-real-solution-south-africas-short-term-energy-needs.html (visited 15/11/2020)

[35] Options For Establishing Shore Powerfor Cruiseshipsin Port Of Copenahgen Nordhavn, Published by City & Port Development, CMP and the City of Copenhagen, May 2015

[36] MGO stands for "Marine Gas Oil". Marine gas oil describes marine fuels that consist exclusively of distillates. Distillates are all those components of crude oil that evaporate in fractional distillation and are then condensed from the gas phase into liquid fractions. Marine gasoil usually consists of a blend of various distillates. Marine gasoil is similar to diesel fuel, but has a higher density. Unlike heavy fuel oil (HFO), marine gasoil does not have to be heated during storage. For further reading: https://www.marquard-bahls.com/en/news-info/glossary/detail/term/marine-gasoil-mgo.html .

[37] Giernalczyk A.,, Górski Z., Analysis Of Trends In Energy Demand For Main Propulsion, Electric Power And Auxiliary Boilers Capacity Of General Cargo And Container Ships, Translated into English, 2008 Journal of Polish CIMAC Volume: 4, Issue: 1, pp 23-28

[38] Prenc R. et Al. Advantages of using a DC power system on board ship, University of Rijeka, Faculty of Maritime Studies Press, ISSN 0554-6397UDK: 621.311 629.5.064.5 06/08/2016,

[39] Kyunghwa Kim et Al. DC-grid system for ships: a study of benefits and technical considerations Journal of International Maritime Safety, Environmental Affairs, and Shipping Volume 2, 2018 - Issue 1

[40] Hyundai Himsen Engine, IMO Tier III Engine product manual, 2016, p.24

[41] Note 25 above.

[42] https://www.marineinsight.com/environment/the-green-source-of-power-shaft-generator/ (visited 20.09.20)

[43] Prousalidis J. Gkika K. et Al, Shaft-Generators in Ships: Techno-Economic Sensitivity Analysis Study, 2016 International Conference on Mathematics and Computers in Sciences and in Industry p. 5, DOI: 10.1109/MCSI.2016.015

[44] https://www.wartsila.com/marine/build/power-systems/shaft-generator-systems/shaft-generator (visited 20.09.20)

[45] Behrendt, Cezary, "Conditions of waste heat recovery in marine waste heat recovery systems" p.3, Researchgate , April 2019

[46] As above, p.5

[47] Thermo Effciency System for Reduction of Fuel Consumption and CO_2 Emission, Publication of MAN Diesel & Turbo, Kopenhagen, 2015, p.16

[48] https://www.imo.org/en/MediaCentre/PressBriefings/pages/02-IMO-2020.aspx

[49] See Chapter 2, par. 2.2

[50] Text within quotes is verbatim derived from https://www.marineinsight.com/main-engine/exhaust-gas-system-of-main-engine-on-ship/ (visited 22.11.20)

[51] Silencer is used to reduce the noise level in the exhaust gas manifold and it is generally placed after the EGB. This is necessary in order to decrease high noise levels in the accommodation, which is now moderated under Maritime Labor Convention.

[52] Politakis, George. "ILO Maritime Labour Convention, 2006, Abstract". International Foundation for the Law of the Sea. Archived from the original on 12 December 2013.

[53] HYUNDAI-B&W 7G50ME-B9.3(TIER II) marine engine is the main propulsion system of the M/V Desert Challenger, which is the case study of this research.

[54] Available at https://marine.man-es.com/applications/projectguides/2stroke/content/printed/G50ME-B9_3.pdf chapter 6.03

[55]https://marine.mandieselturbo.com/docs/librariesprovider6/technical-papers/exhaust-gas-emission-control-today-and-tomorrow.pdf?sfvrsn=22

[56] Report on Research for CO2 Emission from Ships 2000 (SFOC, Japan) Interim Report by Transport Policy Council (MLIT, JapanCommon Guideline for CalculationMethod of CO2 Emission in Logiostics(issued in 2006 by METI and MLIT)

[57] As 47,above, p.5

[58] Perry, R.H., 1984. “Perry's Chemical Engineers' Handbook”, McGraw-Hill, New York, 6th edition

Reid, R.C., J.M. Prausnitz and B.E. Poling, 1987. “The Properties of Gases and Liquids”, McGraw-Hill, New York, 4th edition

[59] Hyundai Himsen Engine, IMO Tier III Engine product manual, 2016, p.20

[60] Thi Minh Hao Dong And Xuan Phuong Nguyen (2019) Exhaust Gas Recovery From Marine Diesel Engine In Order To Reduce The Toxic Emission And Save Energy: A Mini Review. *Journal Of Mechanical Engineering Research And Developments*, 42(5) : 143-147.

[61] Yunus A. Gensel-Afshin Ghajar “Heat and Mass Transfer-Foundamentals and Applications” 9th Greek edition, p.466, Tziolas Editions.

[62] Engine manufacturers are usually very conservative on their back pressure limits. For example, diesel generator set engines from Caterpillar, Cummins, John Deere and DDC/MTU ranging in size from 15 to over 1000 kW have back pressure limits ranging from 6.7 to 10.2 kPa. However, Marine diesel engines backpressure limints are bigger. https://dieselnet.com/tech/diesel_exh_pres.php#emi

[63] Totally eliminating backpressure is theoretically impossible due to the first law of fluid mechanics. Still in practical terms several techniques are applied when designing a fluid network so as to minimize the pressure drop and backpressure.

[64] ssumption quite natural if we consider the existance of exhaust pressure balancer in the exhaust system of Marine engines

[65] Muh Ichsanudin, “fundamentals of fluid mechanics” Chapter 8 Pipe & Duct Flow, www.academia.edu., literally.

[66] James R. Welty “Fundamental Hydrodynamics” Bethnam Green Editions, 1986, p34.

[67] MAN B&W G50ME-B9.3-TII Project Guide, p.15.07

[68] Yunus A. Gensel-Afshin Ghajar “Heat and Mass Transfer-Foundamentals and Applications” 9th Greek edition, p.487, Tziolas Editions.

[69] In certain occasions the back pressure built by the duct network might be such as to impose additional means to drag the gases through. Such means could be auxiliary Bernoulli hoses, connection with downstream ducting of existing fans, etc.

[70] Flue gas desulphurization in compliance with IMO 2020 is becoming more sought after nowadays. Sulphur dioxide (SO_2) is mainly produced by burning fossil fuels. It is one of the most harmful pollutants which appear as the result of human activity. Sulfur dioxide affects health and causes acid rain, both at the local and regional levels. It harms nature and the environment. It is therefore no wonder that the International Maritime Organisation, or IMO, came with new regulations from 2020 onwards to cap Sulphur pollution through marine fuels., iaw https://www.europiren.com/reagent-for-flue-gases-desulfurization/ , literally.

[71] Luján, José Manuel et al., “Turbine and exhaust ports thermal insulation impact on the engine efficiency and aftertreatment inlet temperature”, p.4 etr on, Applied Energy,Volume 240, 2019.

[72] See notes 43 and 44, above

[73] James R Welty "Engineering Heat Transfer" John Wiley and Sons Inc. Editions, 1974, p.194

[74] As above, p.262

[75] Dittus F.W. and Boelter L.M.K.University of California Publications, Eng. 2 , p. 443

[76] Yunus A. Gensel-Afshin Ghajar "Heat and Mass Transfer-Foundamentals and Applications" 9th Greek edition, p.385, Tziolas Editions.

[77] Khayet et al., 2004

[78] The installation of new mechanical, electrical or electronic equipment on a vessel, demands globally a "Marine Type Approval" of the equipment by an accredited ships register for several safety, security and insurance reasons. Hence the case study is done on a study basis as installing the equipment on an actual ship would not be allowed without its prior marine approval issue.

[79] Karami, Nabil et al. "New modeling approach and validation of a thermoelectric generator" IEEE Cnference of Ind. Electronics, June 2017, with the necessary corrections to mistaken expressions and equations.

[80] Champier D. et al. Prototype combined heater/thermoelectric power generator for remote applications. Journal of Electronic Materials, pages 1–12, 2013.

[81] In calculus, Rolle's theorem or Rolle's lemma essentially states that any real-valued differentiable function that attains equal values at two distinct points must have at least one stationary point somewhere between them—that is, a point where the first derivative (the slope of the tangent line to the graph of the function) is zero. https://www.wolframcloud.com/objects/demonstrations/RollesTheorem-source.nb

[82] https://www.sciencedirect.com/topics/engineering/maximum-power-transfer-theorem

[83] It is perfectly normal to assume that there is no wind of significant velocity in the interior of the vessel where the duct system would be installed.

[84] Conditions of temperature and pressure in the interior of the vessel in general. However, in certain occasions (e.g. inside an engine room) temperatures of 40° C are not uncommon, something the studier should take under consideration at the stage of the installation design.

[85] John Wiley & Sons Ltd, "Marine fuels: Price impact of new 2020 low sulfur regulations negated by refineries and Covid-19" published in Oil and Energy Trends. 2020;45:3–15

[86] The tendency to stricter rules and legislation in order to reduce the environmental impact of shipping is the subject of a continuously increasing number of researches: i.e. Walker, Tony et Al. "Environmental Effects of Marine Transportation" Research Gate , September 2018, and https://www.eli.org/sites/default/files/eli-pubs/marine-litter-legislation-toolkit-policymakers.pdf firsty visited on December 6, 2019.

[87] Taken from Author's lecture notes of the Statistics II Class, El.Eng. Dept. QMW UoL, based on "Testing Statistical Hypothses" by E.L. , Lehmann, Springer Verlag,2007 (first ed. 1957).

[88] Massey Adam, Miller Steven J. "Tests of Hypotheses Using Statistics" Mathematics Department Brown University Providence, RI USA

[89] Under the operational management of Atlantic Bulk Carriers Management Ltd (www.abcml.com).

[90] HYUNDAI-HIMSEN genset technical manual, page 29

[91] As the subject to be discussed hereafter will be power generation and energy supply the connection method (parallel or in series) will be indifferent.

[92] As stated in the theoretical approach and as introduced in the model, the lower the average seawater temperature is, the better the performance of the TEG Chips.

[93] Merchant ships are broadly classified on the basis of their sizes and areas of operation. The classification of the ship is decided right at the design stage on the basis of route of operation and purpose of the ship. The ship's dimensions play an important part in determining the areas of operation of any type of merchant vessel. https://www.marineinsight.com/types-of-ships/the-ultimate-guide-to-ship-sizes/

[94] Seawater temperature is being monitored and logged daily around the globe nowadays by several organizations. Furthermore, by use of sensors of various parameters like Wave, surface and Water Column currents and the help of statistical models a rather accurate prediction of the seawater temperature can be achieved as well. https://www.seatemperature.org/

[95] In fact we need to have a one sample t test, however there is now such an option available in Excel. Therefore we will have to "trick" or "fool" Excel by running a two sample test the one of them being a set of "0".

[96] The International insurance policy and current Marine Insurance practices prohibit the installation of new equipment on vessels without prior "type approval" from the Register of Shipping to which the vessel is registered. Ref.: Par. 4 of the Directive 2009/20/EC of the European Parliament and of the Council of 23 April 2009 on the insurance of ship owners for maritime claims.

[97] The monitoring should include also several other physical and chemical parameters e.g. the pressure drop of the gases, the PH, and the total salinity.

[98] This is the subject of a new undergoing research by the Author.

[99] Serra, P.; Fancello, G. Towards the IMO's GHG Goals: A Critical Overview of the Perspectives and Challenges of the Main Options for Decarbonizing International Shipping. *Sustainability* **2020**, *12*, 3220. https://doi.org/10.3390/su12083220

[100] Thalis P.V. Zis, Kevin Cullinane, The desulphurisation of shipping: Past, present and the future under a global cap, Transportation Research Part D: Transport and Environment, Volume 82, 2020, 102316, ISSN 1361-9209, https://doi.org/10.1016/j.trd.2020.102316.

[101] https://thermal.ferrotec.com/technology/thermoelectric-reference-guide/thermalref10/ visited on August 17, 2022.

[102] Ayres, Robert ; Ayres, Leslie (2002). "A handbook of industrial ecology". Edward Elgar Publishing. p. 396. ISBN 1-84064-506-7.

[103] Bahrami, A., Schierning, G., Nielsch, K., "Waste Recycling in Thermoelectric Materials". *Adv. Energy Mater*. 2020, 10, 1904159. https://doi.org/10.1002/aenm.201904159

[104] https://www.statista.com/statistics/264024/number-of-merchant-ships-worldwide-by-type/. Visited on October 21, 2022

[105] https://unctad.org/news/war-ukraine-raises-global-shipping-costs-stifles-trade. Visited on October 21, 2022